Examining the role yeast initiator tRNA sequence and structure plays in communicating start codon recognition

By Antonio Michael Muñoz

A dissertation submitted to Johns Hopkins University in conformity with the requirements for the degree of Doctor of Philosophy

Baltimore, Maryland
October 2014

Abstract

Translation initiation accuracy in the cell is of paramount importance, as beginning polypeptide synthesis at the wrong location can lead to the production of toxic proteins. In vivo, altering elements in various regions of $tRNA_i$ results in either decreased (Sui^- phenotype) or increased (Ssu^- phenotype) fidelity of start codon recognition. We have characterized the behaviors of mutant initiator tRNAs as they may affect the transition between the scanning-competent P_{out}/Open state of the PIC and the scanning-arrested P_{in}/Closed state. Single mutations in the acceptor stem produce both Sui^- phenotypes and defects in forming the eIF2-GTP-Met-$tRNA_i$ ternary complex (TC). Sui^- mutations also reduce off rates, consistent with their stabilizing the closed state of the PIC and decreasing fidelity. The Sui^- acceptor stem mutation G70A also dramatically reduces the TC binding rate, but this is completely rescued by an Ssu^- mutation in the N-terminal tail of eIF1A. Anticodon stem mutants conferring the Ssu^- phenotype exhibit defects in the affinity of TC for the 40S subunit. Other Sui^- mutations in the T loop and ASL display slightly slowed rates of association, indicating a distinct mechanism in blocking rearrangement to the P_{in}/Closed state. We demonstrate that the initiator tRNA sequence and structure are finely tuned to allow accurate start codon recognition by the preinitiation complex, highlighting the role of tRNA as an active player in translation.

Over the course of this study a new protocol for purifying yeast ribosomes was established wherein a monolithic anion exchange column was employed as

an initial separation and concentration step. This method results in an increase in yield, while also decreasing preparation variability and reducing reagent usage.

Lastly, additional experiments were performed to understand the roles and interplay of factors eIF5, eIF1, and eIF1A. This work furthered the understanding of how the C-terminal tail (CTT) of eIF1A comes into closer proximity with the N-terminal domain of eIF5 and also linking this event to eIF1 dissociation, the rate of movement of the eIF1A-CTT and eIF5-NTD towards each other, and phosphate release from eIF2.

Advisor: Jon R. Lorsch

Second Reader: Rachel Green

Acknowledgements:

I would like to extend an enormous thanks to all of those who have helped me during my journey through graduate school. It has been a wonderful experience and I wish to extend good luck to all that I have met along the way.

I thank my advisor Jon, my collaborators at the NIH Drs. Hinnebusch and Dong, all lab members past and present, the faculty and administration at Johns Hopkins Biophysics at both campuses, and the NIH and Turock award for funding.

For my advisor, Jon, thank you for your continued support and the wonderful and unique opportunities and teachings you provided me these last 5 years. I truly could not have had a better environment to complete a Ph.D. I wish you the best of luck with your new position at the NIGMS and hope that many of your ideas become reality for the future generations of graduate students.

To members of the lab past and present: Thank you for your help and support of an occasionally too optimistic graduate student. Sarahs and Julie, I wouldn't have joined the lab had it not been for you. Vaishnavi, I thank you for your thoughtful discussions, and the crosswords. I miss them. Thank you for all of the experimental/presentation/life support Jagpreet, Sarah and Colin.

Thank you to all of my friends and colleagues in and around Hopkins for the many wonderful memories of happy hours; intermural sports including water polo, dodge ball and soccer; and general hangouts. It was these events and our many wonderfully interesting (albeit sometimes derailed) conversations that help keep the sanity.

To my family, thank you all for your continued support of my endeavors. I love you all very much and it makes my life so much easier knowing that I have all of the support and love from my closest family and friends. For my best friend and brother Steven, thank you for always being exactly that, my best friend.

And to my wonderful wife, I love you Janna with all of my heart. Thank you for all of your help and support through everything. You are a truly amazing person and your love and strength pushes me to be a better person in everyway. You are such an inspiration to me each day. With love, Tony.

Table of Contents

List of Tables

List of Figures

Chapter 1

Translation initiation and the role of $tRNA_i$

Antonio M. Munoz

Department of Biophysics and Biophysical Chemistry, Johns Hopkins University School of Medicine, Baltimore, MD 21205, USA
Current address: Laboratory on the Mechanism and Regulation of Protein Synthesis, NICHD, NIH, Bethesda, Maryland 20892

Introduction

One of the most highly regulated pathways in gene expression is translation initiation, the process by which the ribosome, with its associated factors and mRNA message are brought together to begin creating the appropriate polypeptide product. This process is pivotal because an incorrect start point for translation could lead to toxic protein production, in addition to the great energy and resources wasted by the cell up to that point in the gene expression process.

In eukaryotes, 12 different translation initiation factors (eIFs), representing at least 24 polypeptides, are required to come together along with the initiator methionyl tRNA, mRNA and the two ribosomal subunits in order to begin protein synthesis. This process is described in detail in Figure 1.1 (Dong et al. 2014). Briefly, a ternary complex (TC) is formed by the binding of tRNA to initiation factor eIF2, which also binds to a GTP molecule. This TC binds to the small ribosomal subunit (40S), along with factors eIF1, eIF1A, eIF3, and eIF5 to form a 43S preinitiation complex (PIC). Another set of factors (the eIF4 factors) is thought to bind to the 5' cap of the mRNA and along with eIF3 is involved in recruiting the mRNA to the 43S complex. The PIC then scans along the mRNA searching for the start codon. There are thought to be at least two conformational states of the PIC: 1) the P_{out}/Open state of the PIC, in which the complex is capable of scanning the mRNA for the start codon and the tRNA is thought to not be fully engaged in the ribosomal P site, and 2) the scanning-arrested P_{in}/Closed state that exists after start codon recognition (Hinnebusch and Lorsch 2012). Upon recognition of the start codon by base pairing with the anticodon of the tRNA, downstream steps are triggered, including eIF1 and P_i release and the conformational change to the closed state

Fig. 1.1. Model of the canonical eukaryotic translation initiation pathway by the scanning mechanism. This series of discrete steps starts with assembly of the 43S preinitiation complex (PIC), which is depicted both as a single step via the multifactor complex (MFC) and as two separate steps in which eukaryotic initiation factors (eIFs) eIF1, -1A, and -3 bind first, followed by the ternary complex (TC) and eIF5. The 43S PIC is then loaded onto an activated messenger RNA (mRNA)-protein complex near the 5' cap. Subsequent scanning of the mRNA is accompanied by GTP hydrolysis by the TC without release of phosphate (Pi) from eIF2-GDP. Recognition of the start codon triggers downstream steps in the pathway; including eIF1 dissociation, Pi release from eIF2; and conversion to the closed, scanning-arrested conformation of the PIC. eIF5B in its GTP-bound form promotes joining of the 60S subunit to the PIC, accompanied by release of eIF5B/GDP and eIF1A to form the 80S initiation complex (IC), ready for the elongation phase of protein synthesis. eIF2/GDP, released after subunit joining, is then recycled back to eIF2/GTP by the exchange factor eIF2B; this reaction is impeded by eIF2α phosphorylation. GTP appears as a green ball and GDP as a red ball; and eIF4E is shown as a brown crescent interacting with the m7G cap on mRNA. Abbreviations: Met-tRNAi, methionyl initiator transfer RNA; PABP, poly(A)-binding protein. Modified from (Dong et al. 2014).

Fig. 1.1.

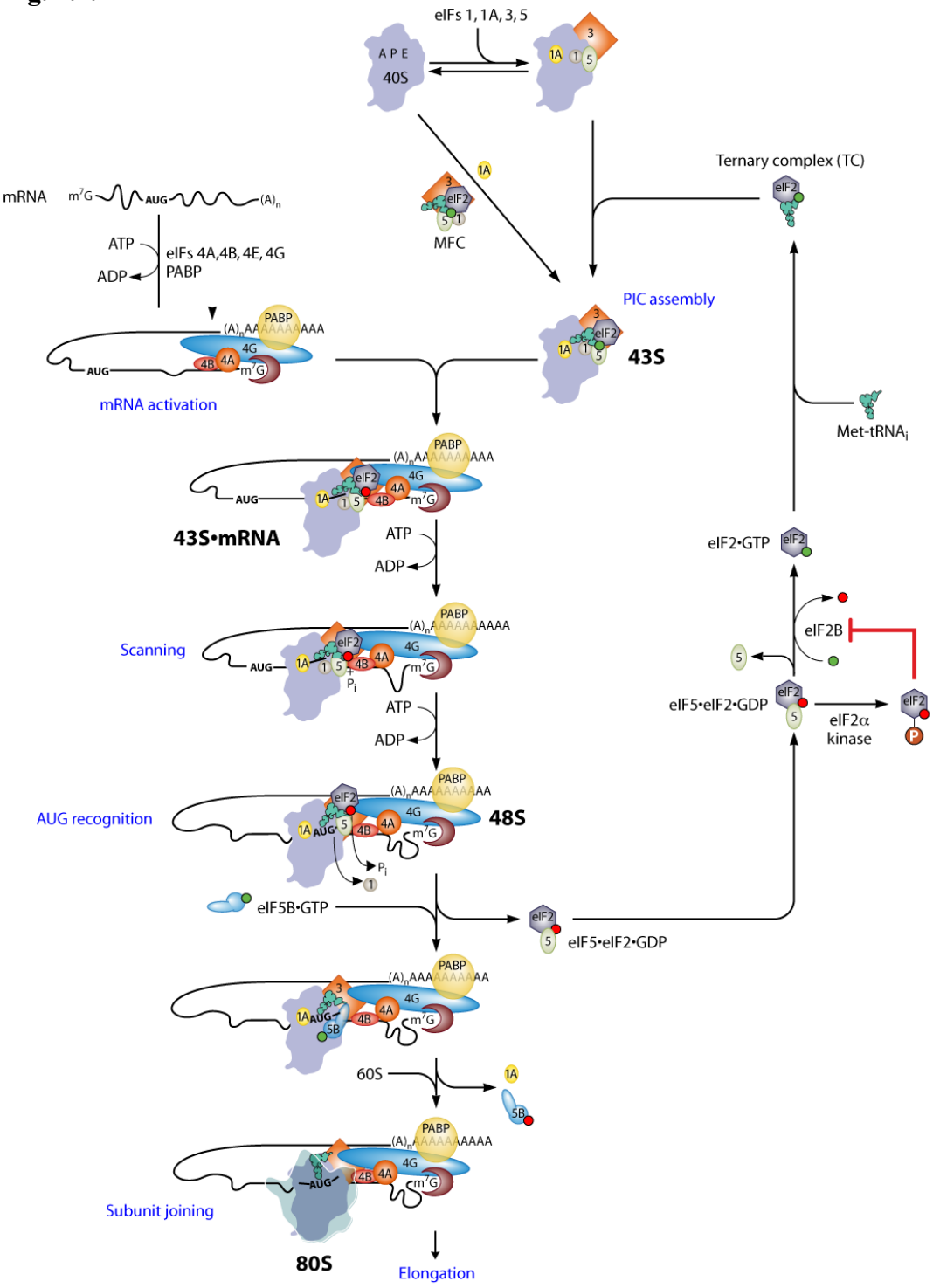
eIFs 1, 1A, 3, 5
A P E
40S
3
1A
1
5
Ternary complex (TC)
eIF2
1A
3
eIF2
5
1
MFC
mRNA
m7G
AUG
(A)n
ATP
ADP
eIFs 4A,4B, 4E, 4G
PABP
PIC assembly
43S
PABP
(A)nAAAAAAAAA
4G
4A
4B
m7G
AUG
mRNA activation
Met-tRNAi
43S•mRNA
ATP
ADP
eIF2•GTP
eIF2B
Scanning
Pi
eIF5•eIF2•GDP
eIF2α
kinase
48S
AUG recognition
eIF5B•GTP
5B
60S
Subunit joining
80S
Elongation

of the PIC. This allows for release of eIF2•GDP, and joining of the 60S ribosomal subunit to form the elongation-competent 80S ribosome.

This thesis work focused on the role the initiator tRNA plays in regulating start codon recognition and transmitting that signal throughout the PIC. My work provided evidence that the body of the initiator tRNA ($tRNA_i$) plays a role in transmitting the start codon recognition signal within the PIC during translation initiation.

Identity Elements Distinguish Between Initiator and Elongator tRNAs

An understanding of the unique role initiator tRNA plays is key to this work, and the ability to distinguish initiator and elongator forms of $tRNA^{Met}$ is critical for cell viability. Transfer RNAs adopt a cloverleaf secondary structure formed by the presence of various stem and loop regions, with the acceptor stem, to which the amino acid is attached, oriented at the top (Figure 1.2). Following sequentially 5' to 3' the three loop regions that make up the clover are the D-loop, anticodon stem loop, and T-loop. These D and T-loops interact to help form the L shape of the tRNA tertiary structure. Despite this common conserved structure of tRNAs the translational apparatus must be able to distinguish the initiator tRNA from elongator tRNAs so that only the former is used in the initiation process.

Initiator tRNA must be both discriminated against by elongation factors and also selected for by initiation factors to bind the P site of the ribosome in a unique manner. These actions may be accomplished through sequence and modification differences between the initiator and elongator forms of tRNA (reviewed in detail by (Kolitz et al. 2009)). Identity elements at various sequence positions, conserved in tRNAs

Figure 1.2. Secondary structure of yeast initiator and elongator Met-tRNA with identity elements highlighted. The identity elements of the two forms of yeast Met-tRNA are shown. Initiator elements include base pair A1:U72 in the acceptor stem, lack of residue 17, G:C pairs in the anticodon stem, and A54 in the T loop.

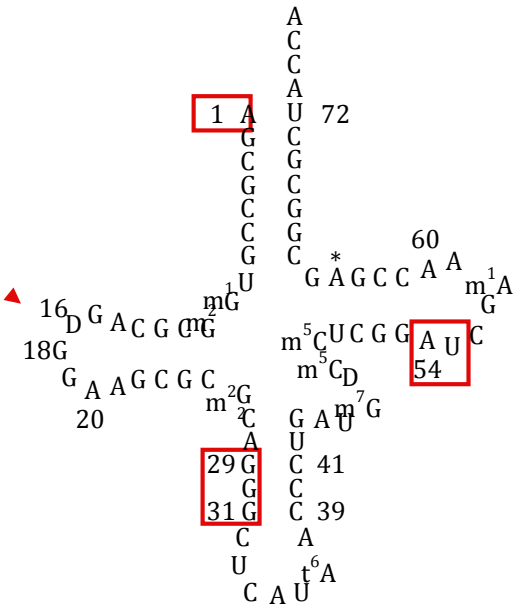

S. cerevisiae initiator tRNA^{Met}

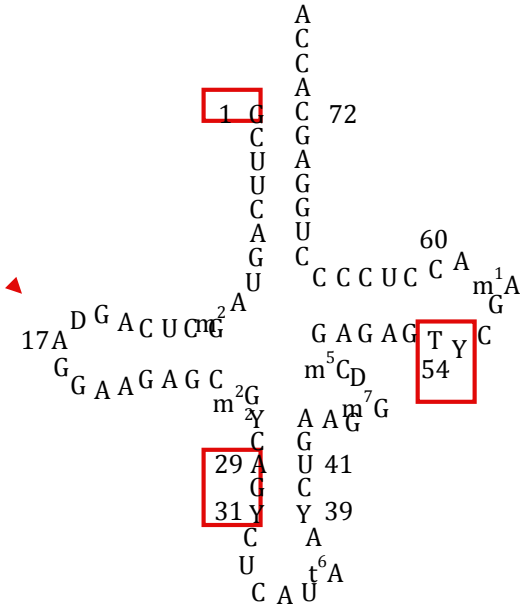

S. cerevisiae elongator tRNA^{Met}

throughout all domains of life, allow for the specific recognition of tRNAs during distinct stages of translation (Marck and Grosjean 2002). In eukaryotic elongation the factor 1A (eEF1A) is responsible for bringing the aminoacylated tRNAs to the A site analogous to eIF2 function delivering Met-$tRNA_i$ to the P site of the ribosome. Despite the similarity in function, elongator tRNAs (which generally contain a G1:C72 pair in the acceptor stem) bind eEF1A two orders of magnitude tighter than their initiator counterparts (Dreher et al. 1999) that contain an A1:U72 pair throughout the eukaryotic and archaeal kingdoms. The identity of the 1:72 base pair was likewise shown to be important for initiator tRNA binding to eIF2, as a 16-fold decrease in binding affinity was seen when the human initiator tRNA was mutated to the elongator-specific G1:C72 (Farruggio et al. 1996). Thus, the 1:72 base pair in the acceptor stem of the tRNA is important both for discrimination by the elongation machinery, and also for binding to eIF2. Other identity elements that distinguish initiator and elongator tRNAs include the lack of A17 and presence of A20 in $tRNA_i$. The 20 position in elongator tRNAs and in E. coli initiator tRNA is generally dihydrouridine, but the A20 in eukaryotic initiators is important for hydrogen bonding with the T loop residues G57, A59, and A60 (Basavappa and Sigler 1991) to bring together the T and D loops and produce the tertiary L shape structure of tRNA. The T loop residue A54 is known to be critical to initiator function (Pawel-Rammingen et al. 1992). In vivo work determined that substituting the A54 with U in *Saccharomyces cerevisiae* initiator tRNA, which reestablishes base pairing at 54:60, is lethal. Also, a double substitution of A54U and A60C conferred slow growth even when expressed on a high copy vector in an initiator tRNA null strain of yeast. This indicates initiator tRNA has a specific sequence requirement at A54 U60 for proper translation

function. Using S1 cleavage reactions the anticodon stem base pairs, G29-31:C39-41, have been implicated in determining the unique structural differences between the anticodon loop of initiator and elongator tRNAs (Seong and rajbhandary 1987; Wrede et al. 1979). These specific identities may contribute to the ability of initiator to bind the P site specifically. This idea was supported by data showing an increase in the off rate of deacylated bacterial elongator tRNAs from 70S ribosomes relative to deacylated or aminoacylated initiator tRNA or peptidyl elongator tRNAs, even in the presence of mutations to the ribosomal RNA, indicating the initiator tRNA exhibits an inherent ability to bind to the P site (Shoji et al. 2009). Seong and RajBhandaray highlighted the importance of the G:C pairs in initiator tRNA for P site binding, as changing their identities reduced their ability to bind the ribosomal P site and reduced the rate and extent of protein synthesis in *E.coli* , (1987). Lowered translational efficiency has also been observed upon mutation of the anticodon stem G:C pairs in human $tRNA_i$ (Drabkin et al. 1993).

In addition to RNA sequence elements that allow for discrimination between initiator and elongator tRNA, the amino acid attached to the tRNA may also play a role in determining when initiator tRNA associates with eIF2. Methionylated Initiator tRNA binds eIF2 in the GTP-bound form with high affinity (9 nM), and has a ~10 fold lower affinity for the GDP-bound eIF2 complex, as observed using in vitro filter binding assays (Kapp and Lorsch 2004). These results indicate that the GTP-bound form of eIF2 is important for delivery of the tRNA to the ribosome and the GDP form is crucial to dissociation, subsequent to codon selection and GTP hydrolysis. In contrast, deacylated initiator tRNA binds both the GTP and GDP-bound forms with the same affinity (130

nM), much weaker than the methionylated-tRNA binding to the GTP-bound eIF2. Thus, the methionyl moiety itself is crucial for binding eIF2 and translation. Other studies have shown that various *E. coli* tRNAs bind the ribosome with similar affinities, despite differences in primary sequence (as determined by measuring association and dissociation of tRNAs from the 70S). However, chimeric swapping experiments of residues that varied in different isoacceptors resulted in large decreases or increases in affinity. The interplay between amino acid and tRNA body has also been observed in binding to EF-Tu and eEF1A and this may be a common strategy of ensuring the correct tRNA is used (Fahlman et al. 2004; Olejniczak et al. 2005). These findings indicate that the specific charged amino acid on the tRNA is utilized in addition to and in conjunction with sequence elements to impart specificity in translation, and begins to suggest cooperation throughout the tRNA structure in this function.

Role of the tRNA body in communicating long-range signals across the ribosome

Several lines of evidence suggest that the three-dimensional structure of the tRNA is important for transmitting signals across the ribosome. Structural studies of the initiator tRNA have pinpointed a unique D and T loop interaction responsible for the characteristic L-shape of the tRNA body (Basavappa and Sigler 1991). Maintenance of the 18:55 and 19:56 interactions is critical for several steps in the translation elongation cycle as shown by translocation rate and ternary complex affinity measurements of tRNAs harboring substitutions at these residues. Mutations to one or both base pairs decreases the rate of translocation and the affinity for the EF-Tu•GTP•aa-tRNA complex, whereas introduction of compensatory mutations that maintain pairing fully rescue the

effects, indicating that the results are due to the disruption of local tRNA structure (Pan et al. 2006; 2008)(Pan et al. 2006, 2008). Further evidence of an active role of the tRNA body was established through in vitro work by (Cochella and Green 2005)(2005). They demonstrated that a special nonsense suppressor $tRNA^{Trp}$ (the Hirsch suppressor) containing the D loop mutation G24A (far from the anticodon) increased rates of GTPase activation of EF-Tu and accommodation of mutant tRNA independent of the ordinarily required cognate codon-anticodon pairing. This specific increase in forward rate constants in a codon-independent manner provides evidence that the tRNA structure itself plays an active role in communicating signals across the ribosome. Finally, a functional interaction between distal elements in the initiator tRNA anticodon stem and T loop was also reported (Kapp et al. 2006). In vitro work demonstrated that mutation of the two conserved G:C base pairs in the anticodon stem (29:41 and 31:39) resulted in higher affinity binding to the 43S complex than WT tRNA in the absence of mRNA, but, surprisingly, conferred weaker affinity in the presence of an mRNA containing an AUG start codon. However, when these anticodon stem mutations were combined with mutations in the T loop (U54 and C60), wild type levels of binding were restored (Fig. 1.3). These results indicated that the conserved G:C basepairs in the anticodon stem are required for thermodynamic coupling between start codon recognition and the conformational change that gates downstream events in initiation. Since the effects of mutating these anticodon stem pairs were compensated for by changes in the T loop, this further suggested communication across the ribosome through the body of the tRNA.

Figure 1.3. Start codon recognition is decoupled by mutations in the anticodon stem and rescued by additional mutations to the initiator tRNA in the T loop.
Measurements are shown of the binding constants for Ternay complex, containing wild type (WT) or mutant tRNA, for the 40S subunit and initiation factors eIF1 and eIF1A. WT binds in the absence of mRNA with a K_d of 60 nM while a much tighter binding event (<1nM) occurs in the prescence of a model mRNA containing an AUG start codon. The double mutation G31U:C39U changes the binding constants to 12 and 20 nM respectively for no mRNA and AUG containing message. A quadruple mutant of G31U:C39U paired with A54U and A60C results in recovery of WT binding levels. Data from Kapp et al. 2006.

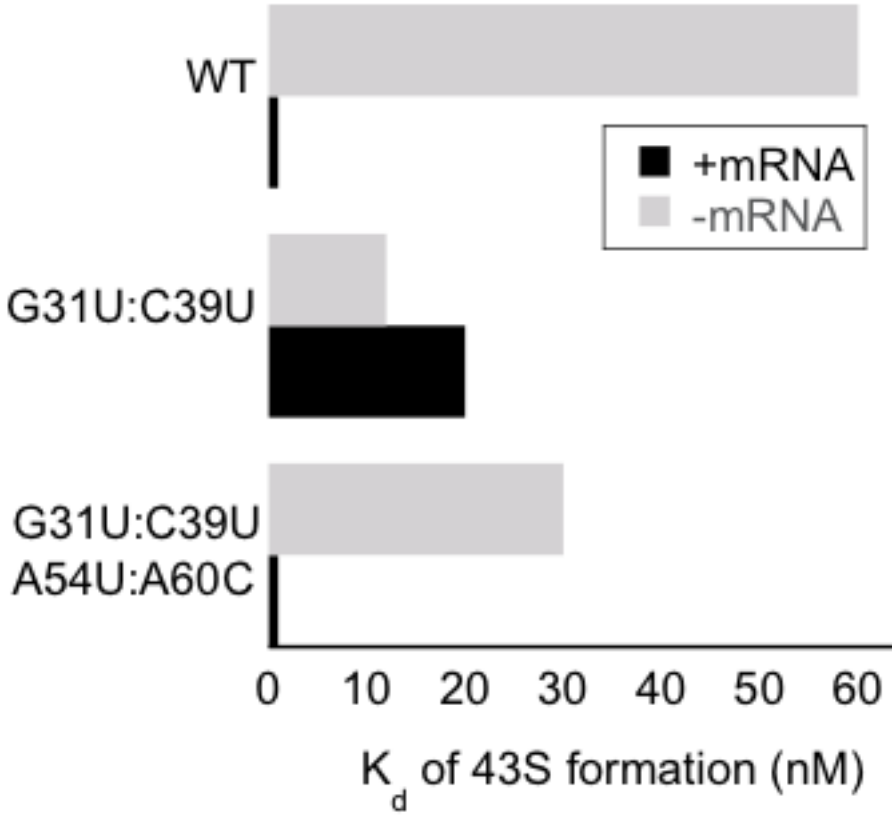

Structures of Translation Initiation Complexes

In consideration of the initiator tRNA as an active player in start codon recognition signal communication, an understanding of the placement and movement of tRNA and initiation factors within the PIC is warranted. Ribosomes consist of a large and small subunit with three tRNA-binding sites: Acceptor (A), Peptidyl (P), and Exit (E). During translation elongation, tRNAs move from the A site to the P site and from the P site to the E site following peptidyl transfer, and the E-site tRNA eventually dissociates from the ribosome. Initiator tRNA is the only tRNA thought to bind directly to the P site during translation, and in eukaryotes, is delivered by eIF2 to form a 43S preinitiation complex. This 43S complex is formed by the cooperative binding of TC to the 40S ribosomal subunit along with eIF1 and eIF1A, and is enhanced by interactions with additional factors eIF3 and eIF5. Biochemical and genetic studies of mammalian and yeast translation systems have indicated the existence of at least two states of the pre-initiation complex (Maag et al. 2005; Pestova et al. 1998). The open, scanning-competent form undergoes a conformational change to a closed, scanning-arrested form. The tRNA adopts two different states as well. A P_{out} form, where the tRNA is loosely associated in the P site of the ribosome, and a P_{in} state where the tRNA is fully accommodated in the P site upon start codon recognition (Maag et al. 2005). Movement of tRNA into the P_{in} state is accompanied by movements of eIF1A and the release of eIF1, a gate-keeper of this transition. Recent studies of several eukaryotic preinitiation complexes have provided structural information regarding these and other functional states.

Studies of the *Tetrahymena* system using crystallography show a potential clash of the eIF1 and anticodon stem of the tRNA that would prohibit the $tRNA_i$ from properly

entering the P site (Rabl et al. 2011). eIF1 is positioned also on top of h44 within the region of the tRNA ASL binding in the P site. Here helix 44 is rearranged in closer proximity to the eIF1A binding site (Weisser et al. 2013). Cryo-EM structures of the ribosomal complex with eIF1, eIF1A or both factors showed a change in the conformational state of the complex upon binding of both factors (Passmore et al. 2007). These changes involved opening of the apo 40S structure at the latch, the interaction that forms between the head and body of the ribosome, allowing for a clear mRNA entry channel upon binding of the eIF1 and eIF1A factors. It is this open structure that was shown to facilitate TC recruitment to the PIC via in vitro kinetics. A P_{out} state for the tRNA is observed in a crystal structure of the rabbit 40S subunit with eIFs 1 and 1A bound along with mRNA, a different state than those seen post codon recognition. Movement of the tRNA towards the E site is blocked in this complex by rRNA helices h24 and h29 that contact the ASL and position it within the P site (Lomakin and Steitz 2013). Its positioning also prevents tRNA accommodation in the A site. The overlaid structures would sterically clash between the basic loop (R38-K42) of eIF1 and the ASL. A second clash would also occur at P77-G80 and the D stem. This indicated that the tRNA is mobile within the P site during translation initiation and that eIF1 blocks access to full accommodation in the P site.

The tails of eIF1A are thought to move in coordination with steps in translation initiation. (Maag et al. 2006)showed increased fluorescence anisotropy for C-terminally labeled eIF1A within the PIC when eIF5 bound. This effect indicates a reduction in mobility of the tail within the complex. Hydroxyl radical probing using eIF1A derivatized with the hydroxyl radical generating complex Fe^{2+}-BABE showed cleavages

in the P site (Yu et al. 2009), but a lack of electron density in the crystal structure of the mammalian PIC did not allow modeling. These findings taken together demonstrate a process by which eIF1 prevents tRNA binding fully within the P site until codon:anticodon pairing has been accomplished. At this time the eIF1 must be ejected from the P site to allow for complete placement of the tRNA and it is these actions that trigger the conformational change to the closed state.

New direct electron detectors have recently allowed for higher resolution images to be constructed from smaller numbers of particles using cryo-EM, allowing previously impossible visualization of dynamic complexes. In a recent study of 80S initiation complexes, eIF5B was seen to undergo a conformational change upon ribosome binding and interaction with the tRNA via its carboxy terminal domain (CTD) (Fernandez et al. 2013). This CTD of eIF5B makes multiple contacts with the conserved A1:U72 identity element in the acceptor stem, allowing it to couple eIF5B GTP hydrolysis to specific recognition of the initiator tRNA. Here the tRNA adopted a conformation where the acceptor stem sits outside the peptidyl transferase center with a bend near the conserved G:C basepairs in the anticodon stem, potentially stabilized by this initiator-specific feature. This distorted state prevents the 14xpressed end of the tRNA from entering the peptidyl transferase center prior to eIF5B GTP hydrolysis and release. Orientation of the tRNA 3' CCA end outside the peptidyl transferase center was also observed in a structure of a bacterial translation initiation complex where an intermediate P/I state was defined with the tRNA held in this position by the homologous IF2 CTD, indicating the possibility that this is a conserved quality control mechanism across domains (Simonetti et al. 2008).

The entirety of these structural studies demonstrates that the positioning and movement of the tRNA within the P site of the ribosome is crucial to translation initiation. The initiator tRNA is in fact playing an active role in communicating across the PIC during translation initiation specifically by coupling GTP hydrolysis to full accommodation of the tRNA into the P site, displacing eIF1, and triggering the conformational change to the closed state.

Mutational studies of initiator tRNA to determine the role in PIC communication

Mutations have been identified in initiation factors eIF1, -1A, -2, -3, -5, and -4G that allow increased translation of a reporter gene that initiates with a near-cognate start codon (one nucleotide changed from the cognate AUG start codon), resulting in a suppressor of initiation (decreased initiation fidelity), or Sui$^-$ phenotype. Suppressors of Sui$^-$ mutations (Ssu$^-$) confer enhanced fidelity of start codon recognition. Our efforts here were to further examine the effects that mutations to the tRNA can have on translation initiation and to understand the role of the initiator tRNA structure in sending the signal that the start codon has been located. In collaboration with Alan Hinnebusch's lab, we have characterized the behaviors of mutant initiator tRNAs in vivo and in vitro using a reconstituted yeast translation initiation system (Chapter 2 and (Dong et al. 2014)). In vivo, altering elements in various domains of $tRNA_i$ results in either decreased (Sui$^-$ phenotype) or increased (Ssu$^-$ phenotype) fidelity of start codon recognition. In vitro Thermodynamic studies of the formation of ternary complex were performed for each of these mutants. Subsequently, binding of those TCs to the 40S ribosomal subunit, to form the PIC, was probed thermodynamically using methods described in Figure 1.4. Kinetic

Figure 1.4. Methodologies employed to analyze the role of tRNAi structural identity in translation initiation. (A) tRNA radiolabeled at the 3' end is incubated with eIF2 and a non-hydrolyzable GTP analog GDPNP. After incubation these complexes are passed over two membranes on a vacuum manifold. The top (Nitrocellulose) membrane will capture complexes whereas labeled tRNA will bind to the bottom (Nytran Supercharge) membrane and free label will wash though both membranes. Counting these membranes gives a ratio of ternary complex formation. **(B)** Formation of the PIC was monitored through gel shift assays where complexes migrate more slowly on 4% PAGE gels than the free tRNA. Shown is an example gel measuring the Kd of PIC formation by measuring ratios of complexs containing labeled TC divided by the counts of free labeled tRNA.

A

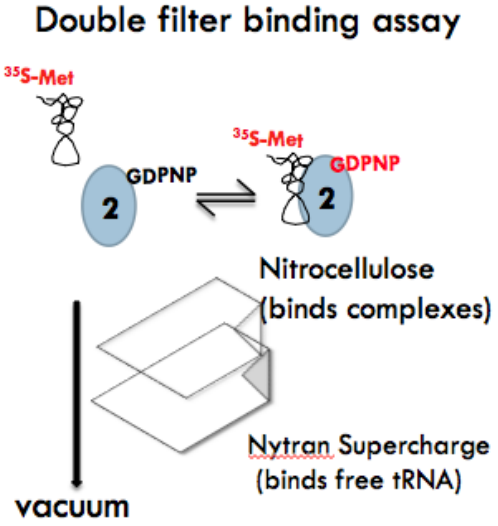

B

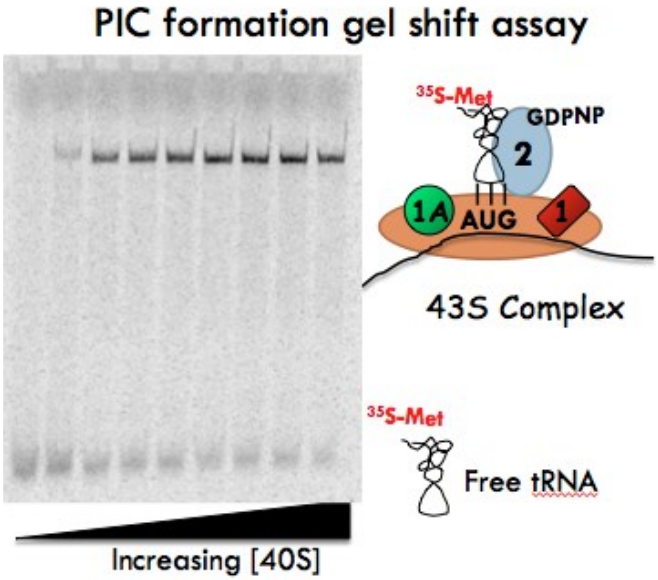

studies of formation and dissociation of the PIC were used to further the examination of the tRNA nucleotide mutations effects. Overall, our data indicate the identity elements tune the tRNA to have the proper energetic barriers and flexibility to make the required conformational transitions within the PIC upon start codon recognition.

In addition, large amounts of various protein factors and ribosomes were used for these in vitro experiments. Over the course of this study a new protocol for purifying yeast ribosomes was established wherein a monolithic anion exchange column was employed as an initial separation and concentration step. This method resulted in an increase in yield, while also decreasing preparation variability and reducing time and reagent usage. This work is detailed in Chapter 3.

Lastly, additional experiments performed to understand the roles and interplay of factors eIF5, eIF1, and eFI1A are described in Appendix A. This work furthered the understanding of the sequence of actions that occur upon start codon recognition. Specifically, I contributed to the knowledge of how the C-terminal tail (CTT) of eIF1A comes into closer proximity with the N-terminal domain of eIF5. Additional observations were made linking this event to eIF1 dissociation, the rate of movement of the eIF1A-CTT and eIF5-NTD towards each other, and phosphate release from eIF2 (Nanda et al. 2013).

This work has advanced our understanding of the molecular mechanisms underlying start codon recognition in eukaryotes. We demonstrate that the initiator tRNA sequence and structure are finely tuned to allow accurate start codon recognition by the preinitiation complex, highlighting the role of tRNA as an active player in translation. We also present an improved purification method for generating large quantities of

ribosomal subunits that will facilitate reproducibility in future in vitro studies of translation. Together these results form the basis for future studies to deconstruct the mechanisms of translation initiation in hopes of providing insight into the molecular basis underlying human diseases.

Chapter 2

Conserved residues in yeast initiator tRNA calibrate initiation accuracy by regulating preinitiation complex stability at the start codon

Jinsheng Dong[1*], Antonio M. Munoz[2,3*], Sarah E. Kolitz[2,4], Adesh K. Saini[1,5], Wen-ling Chiu[1], Hafsa Rahman[1], Jon R. Lorsch[2,3] and Alan G. Hinnebusch[1]

[1]Laboratory of Gene Regulation and Development, NICHD, NIH, Bethesda, Maryland 20892; [2]Department of Biophysics and Biophysical Chemistry, Johns Hopkins University School of Medicine, Baltimore, Maryland 21205

[3]Current address: Laboratory on the Mechanism and Regulation of Protein Synthesis, NICHD, NIH, Bethesda, Maryland 20892

[4]Current address: Immuneering Corporation, One Broadway, 14th Floor, Cambridge, MA, 02142

[5]Current address: Department of Biotechnology, Shoolini University of Biotechnology and Management Sciences, Solan, Himachal Pradesh-173212, India

[*]these authors contributed equally

Author Contribution: The results described in this chapter represent the work of multiple persons on the project. Antonio Munoz performed in vitro experiments to determine binding constants for ternary complex and preinitiation complex (PIC) formation with mutant and WT tRNAs, as well as association and dissociation kinetics for PIC assembly as part of this thesis work. The work by Antonio Munoz can be found in Tables 2.2-2.5 and Figures 2.4 and 2.7.

Abstract

Eukaryotic initiator tRNA ($tRNA_i$) contains several highly conserved unique sequence features, but their importance in accurate start codon selection was unknown. Here we show that conserved bases throughout $tRNA_i$, from the anticodon stem to acceptor stem, play key roles in ensuring the fidelity of start codon recognition in yeast cells. Substituting the conserved G31:C39 base pair in the anticodon stem with different pairs reduces accuracy (the Sui^- phenotype), whereas eliminating base pairing increases accuracy (the Ssu^- phenotype). The latter defect is fully suppressed by a Sui^- substitution of T-loop residue A54. These genetic data are paralleled by opposing effects of Sui^- and Ssu^- substitutions on the stability of Met-$tRNA_i$ binding (in the ternary complex with eIF2-GTP) to reconstituted preinitiation complexes (PICs). Disrupting the C3:G70 base pair in the acceptor stem produces a Sui^- phenotype and also reduces the rate of TC binding to 40S subunits in vitro and in vivo. Both defects are suppressed by an Ssu^- substitution in eIF1A that stabilizes the open/P_{OUT} conformation of the PIC that exists prior to start codon recognition. Our data indicate that these signature sequences of $tRNA_i$ regulate accuracy by distinct mechanisms, promoting the open/P_{OUT} conformation of the PIC (for C3:G70) or destabilizing the closed/P_{IN} state (for G31:C39 and A54) that is critical for start codon recognition.

Identification of the translation initiation codon in eukaryotic mRNA typically occurs by a scanning mechanism where the 40S ribosomal subunit recruits methionylated initiator tRNA (Met-tRNA$_i$) in a ternary complex (TC) with eIF2-GTP, the resulting 43S PIC attaches to the mRNA 5' end, and the leader sequence is inspected for complementarity with the anticodon of Met-tRNA$_i$ to identify the AUG start codon (Hinnebusch 2011). The GTP in TC is hydrolyzed in the scanning complex, dependent on eIF5, but P_i release is blocked by eIF1, which also impedes stable binding of Met-tRNA$_i$ in the P site. AUG recognition triggers dissociation of eIF1 from the 40S subunit (Maag et al. 2005), which allows interaction between eIF5 and the C-terminal tail (CTT) of eIF1A (Nanda et al. 2013), P_i release (Algire et al. 2005), and stable binding of TC to the P site (Passmore et al. 2007). Subsequent dissociation of eIF2-GDP and other eIFs enables eIF5B-catalyzed subunit joining and formation of an 80S initiation complex with Met-tRNA$_i$ base paired to AUG in the P site (Pestova et al. 2007).

Both eIF1 and scanning enhancer (SE) elements in the eIF1A CTT promote an open, scanning-conducive conformation of the PIC and metastable mode of TC binding (the P_{OUT} state) that allows inspection of P site triplets during scanning. A scanning inhibitor element (SI) in the eIF1A N-terminal tail (NTT) antagonizes SE function and promotes rearrangement to the closed state (Fekete et al. 2007), with dissociation of eIF1 (Cheung et al. 2007) and more stable binding of TC in the P_{IN} conformation (Saini et al. 2010) (Fig. 2.1A). Biochemical mapping experiments for the eIF1A CTT (Yu et al. 2009) and X-ray crystal structures of PICs containing eIF1, eIF1A or tRNA$_i$ (Rabl et al. 2011; Lomakin and Steitz 2013; Weisser et al. 2013) suggest that the eIF1A CTT and eIF1

physically obstruct Met-tRNA$_i$ binding in the P_{IN} state, thus favoring P_{OUT}, whereas the eIF1A NTT likely stabilizes TC binding in the P_{IN} state (Fig. 2.1A).

Genetic experiments have implicated eIFs 1, 1A, 5, and 2 in accurate AUG selection in living cells. Sui$^-$ (Suppressor of initiation codon) mutations in these factors enable initiation at the third, UUG codon in *his4-301* mRNA, lacking the wild-type (WT) AUG codon, to restore growth on medium lacking histidine (His$^+$/Sui$^-$ phenotype) (Yoon and Donahue 1992; Donahue 2000) (Saini et al. 2010). Most Sui$^-$ mutations in eIF1 weaken its 40S binding and likely enable eIF1 release at near-cognate triplets (Valasek et al. 2004; Cheung et al. 2007; Martin-Marcos et al. 2013). Sui$^-$ mutations in the eIF1A SE elements destabilize the open/P_{OUT} conformation, allowing transition from the open/P_{OUT} to closed/P_{IN} state at near-cognates, and also reduce the rate of TC loading (Saini et al. 2010), as TC binds most rapidly to the open conformation (Passmore et al. 2007) (Fig. 2.1B). Substitution of residues 17-21 in the eIF1A SI element stabilizes the open/P_{OUT} state, which reduces UUG initiation in Sui$^-$ mutants—the Ssu$^-$ (suppressor of Sui$^-$) phenotype (Fekete et al. 2007)—and also increases the rate of TC binding (Saini et al. 2010) while decreasing the rate of eIF1 dissociation (Cheung et al. 2007) (Fig. 2.1C).

tRNA$_i$ contains highly conserved sequences not present in elongator tRNAs (Fig. 2.1A) (RajBhandary and Chow 1995; Marck and Grosjean 2002), with important functions in initiation. The A1:U72 base pair of the acceptor stem enhances eIF2-GTP binding to Met-tRNA$_i$ (Farruggio et al. 1996; Kapp and Lorsch 2004) and TC binding to 40S PICs (Kapp et al. 2006), and is required for WT tRNA$_i$ function in yeast cells (von Pawel-Rammingen et al. 1992b; Astrom et al. 1993). The 3 consecutive G:C pairs in the anticodon stem-loop (ASL) promote P site binding of tRNA$_i$ in eubacteria

Figure 2.1. Model describing conformational rearrangements of the PIC during scanning and start codon recognition and mechanisms of Sui$^-$ and Ssu$^-$ substitutions in eIF1A (A) Assembly of the PIC, scanning and start codon selection in WT cells. (i) eIF1 and the scanning enhancer elements (SE) in the CTT of eIF1A stabilize an open conformation of the 40S subunit to which the TC rapidly loads. (ii) The 43S PIC in the open conformation scans the mRNA for the start codon with Met-tRNA$_i$ bound in the P_{OUT} state. The GAP domain in the N-terminal domain of eIF5 (5N) stimulates GTP hydrolysis by the TC to produce GDP·P_i, but release of P_i is blocked. The unstructured NTT of eIF2β (wavy line) interacts with eIF1 to stabilize eIF1·40S association and the open conformation. (iii) On AUG recognition the Met-tRNA$_i$ moves from the P_{OUT} to P_{IN} state, clashing with eIF1. Movement of eIF1 away from the P site disrupts its interaction with the eIF2β-NTT, and the latter interacts with the eIF5-CTD instead. eIF1 dissociates from the 40S subunit and the eIF1A SE elements move away from the P site. The eIF5-NTD dissociates from eIF2 and interacts with the 40S subunit and the eIF1A CTT, facilitating P_i release and blocking reassociation of eIF1 with the 40S subunit. The black arrows shown above between (ii) and (iii) summarize that eIF1 and the eIF1A SE elements promote P_{OUT} and block the transition to the P_{IN} state, whereas the scanning enhancer element (SI) in the NTT of eIF1A antagonizes the P_{OUT} state and stabilizes P_{IN}. (Adapted from (Hinnebusch and Lorsch 2012; Nanda et al. 2013)). **(B)** Substitution of the scanning enhancer elements (SE_1 and SE_2) in the eIF1A CTT with alanines (mutation SE*, shown as green asterisk) destabilizes the open conformation and P_{OUT} mode of TC binding and shifts the balance towards the closed/P_{IN} state (green dotted lines/arrows above and below between complexes (ii) and (iii)). This decreases the rate of TC loading

to the open complex, conferring the Gcd$^-$ phenotype (complex (i), dotted green arrow), but once TC binds and scanning commences, it allows an increased frequency of rearrangement from the open/P_{OUT} conformation (ii) to the closed/P_{IN} state at UUG codons (iii), increasing the ratio of initiation at UUG versus AUG codons and conferring the Sui$^-$ phenotype. **(C)** Substitution of the scanning inhibitor element in the eIF1A NTT (mutation 17-21, red asterisk) co-suppresses the Gcd$^-$ and Sui$^-$ phenotypes of the SE* substitution. 17-21 destabilizes the closed/P_{IN} state and shifts the equilibrium back towards the open/P_{OUT} conformation (red dotted lines between (ii) and (iii)). This rescues rapid TC loading to diminish the Gcd$^-$ phenotype (solid red line) and reduces transition to the closed/P_{IN} state at UUG codons (iii), suppressing the elevated UUG:AUG ratio and Sui$^-$ phenotype conferred by the SE* substitutions.

Figure 2.1.

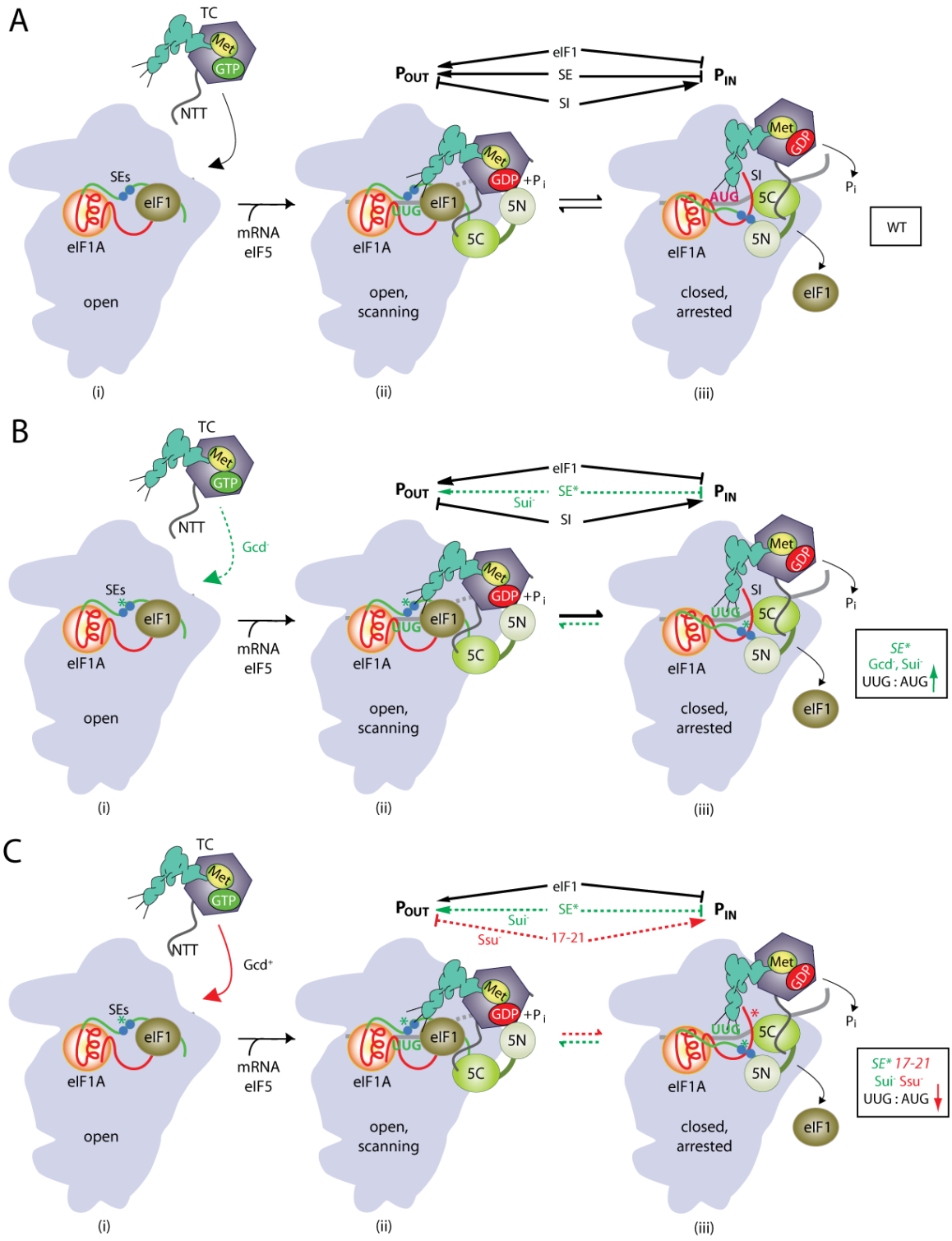
A
TC
Met
GTP
NTT
SEs
eIF1
eIF1A
open
mRNA
eIF5
eIF1
SE
SI
POUT
PIN
GDP
+Pi
5N
5C
UUG
open,
scanning
AUG
SI
Pi
WT
closed,
arrested
(i)
(ii)
(iii)
B
Gcd-
Sui-
SE*
SE*
Gcd-, Sui-
UUG : AUG
C
Gcd+
Ssu-
17-21
SE* 17-21
Sui- Ssu-
UUG : AUG

(Varshney et al. 1993; Mandal et al. 1996). They also confer efficient initiation in mammalian extracts (Drabkin et al. 1993) and enhance the stability of mammalian PICs reconstituted in vitro (Lomakin et al. 2006). In the reconstituted yeast system, the 1st (G29:C41) and 3rd (G31:C39) of these G:C pairs were found to be required for the stabilizing effect of AUG on the affinity of TC for 43S·mRNA PICs. The deleterious effect on TC binding of substituting G31:C39 with the corresponding U:U pair in elongator Met-tRNA ($tRNA_e^{Met}$) (Fig. 2.2A) was mitigated by replacing conserved T-loop residues A54 and A60, suggesting interplay between T-loop and ASL in AUG recognition by Met-$tRNA_i$ in the P site (Kapp et al. 2006). Surprisingly, however, G31:C39, G29:C41, A54 and A60 were altered to their $tRNA_e^{Met}$ identities without affecting yeast growth (von Pawel-Rammingen et al. 1992a), making it unclear whether the function of these residues identified in vitro are important in living cells for the efficiency or accuracy of initiation. To address this last question, we investigated whether substitutions in these and other conserved residues created by site-directed mutagenesis confer Sui^- or Ssu^- phenotypes in yeast cells. We also screened a library of substitutions produced by random mutagenesis for the Sui^- phenotype. Our findings demonstrate that the identities of the 3rd G:C pair of the ASL, T-loop residue A54, and the invariant C3:G70 pair in the acceptor stem are crucial for accurate AUG selection, and that these signature residues employ distinct molecular mechanisms to discriminate against near-cognate start codons.

RESULTS

Disrupting Watson-Crick pairing at G31:C39 in the ASL increases initiation accuracy.

We examined substitutions of $tRNA_i$ for Sui^- or Ssu^- phenotypes using a *his4-301* strain lacking all four genes (*IMT1-IMT4*) encoding the same WT $tRNA_i$ and harboring WT *IMT4* on a *URA3* plasmid. The latter was replaced with high-copy (hc) *LEU2* plasmids containing the mutant *IMT2* alleles of interest by counter-selection with 5-fluoroorotic acid (5-FOA) (Boeke et al. 1987). Sui^- phenotypes were recognized by the ability to grow on (-His) medium lacking histidine, whereas Ssu^- phenotypes were identified by the ability to suppress the dominant His^+/Sui^- phenotype conferred by the *SUI5* allele of eIF5 introduced on a plasmid. Adverse effects of the *IMT2* mutations on cell viability were quantified by measuring the efficiency of plating (EOP) on 5-FOA medium (von Pawel-Rammingen et al. 1992b) (Table 2.1). Viable mutants displaying significant reductions in EOP were characterized for slow growth phenotypes (Slg^-) by spotting serial dilutions on +His medium.

We began by analyzing replacements of the 1st and 3rd of the 3 consecutive G:C pairs in the ASL, unique to $tRNA_i$, with the A:U and U:U pairs found at these positions in $tRNA_e^{Met}$, generated by site-directed mutagenesis of *IMT2* (Fig. 2.2A). These replacements, G29A:C41U and G31U:C39U, have little effect on the EOP (Table 2.1) or cell growth rate (von Pawel-Rammingen et al. 1992b); nor do they increase growth on –His medium in the manner expected for Sui^- substitutions (data not shown). However, comparing expression of matched *HIS4-lacZ* reporters containing AUG or UUG start codons, revealed ~50% reduced UUG:AUG initiation ratios for both G31U:C39U and the

Figure 2.2. Loss of W:C pairing at 31:39 increases accuracy of start codon recognition. (A) Secondary structures of yeast initiator (left) and elongator (right) methionyl tRNAs. Arrows indicate substitutions analyzed below. **(B)** *his4-301* strains with the indicated *IMT2* alleles and harboring *HIS4-lacZ* fusions (shown schematically) with AUG or UUG start codons (on plasmids p367 and p391, respectively) were cultured in SD+His medium and β-galactosidase activities measured in WCEs. Ratios of mean activities from 3 three transformants are plotted with error bars indicating S.E.M.s. Asterisks indicate significant differences between mutant and WT as judged by a Student's t-test ($p<0.005$). **(C)** *his4-301* strains with the indicated *IMT2* alleles and harboring a sc *SUI5* plasmid or empty vector (Vec) were spotted on SD+His and incubated for 3d (+His) or 6d (-His) at 30°C. **(D)** UUG:AUG initiation ratios were determined as in (B) for strains harboring the indicated *IMT2* alleles and sc *SUI5,* except using *HIS4-lacZ* reporters on p367 (AUG) and p4957 (UUG). Asterisks indicate significant differences between mutant and WT or between two mutants (connected by a bracket) ($p<0.005$). **(E)** In vivo analysis of aminoacylation. Total RNA was extracted and resolved by electrophoresis under acidic conditions and subjected to Northern analysis using [^{32}P]-labeled oligonucleotides complementary to $tRNA_i$ (upper), or $tRNA_e^{Met}$ (lower), and signal intensities were quantified by phosphorimaging. For *in vitro* deacylation, an aliquot of each RNA was deacylated at pH 9.0. Normalized percentages of $tRNA_i$ aminoacylation were determined by calculating the ratio of signals: Met-$tRNA_i$/(Met-$tRNA_i$ + $tRNA_i$) for each non-deacylated sample, normalizing to the same ratio determined for $tRNA_e^{Met}$, and expressing the results as a fraction of the value determined for WT. **(F)** ASL structures and phenotypes for substitutions (in boldface) at

the 31:39 base pair. **(G)** Phenotypic analysis of strains with the indicated *IMT2* alleles and sc *SUI5* or empty vector conducted as in (C). **(H)** UUG:AUG initiation ratios determined as in (D) for strains harboring the indicated *IMT2* alleles and sc *SUI5*.

Figure 2.2.

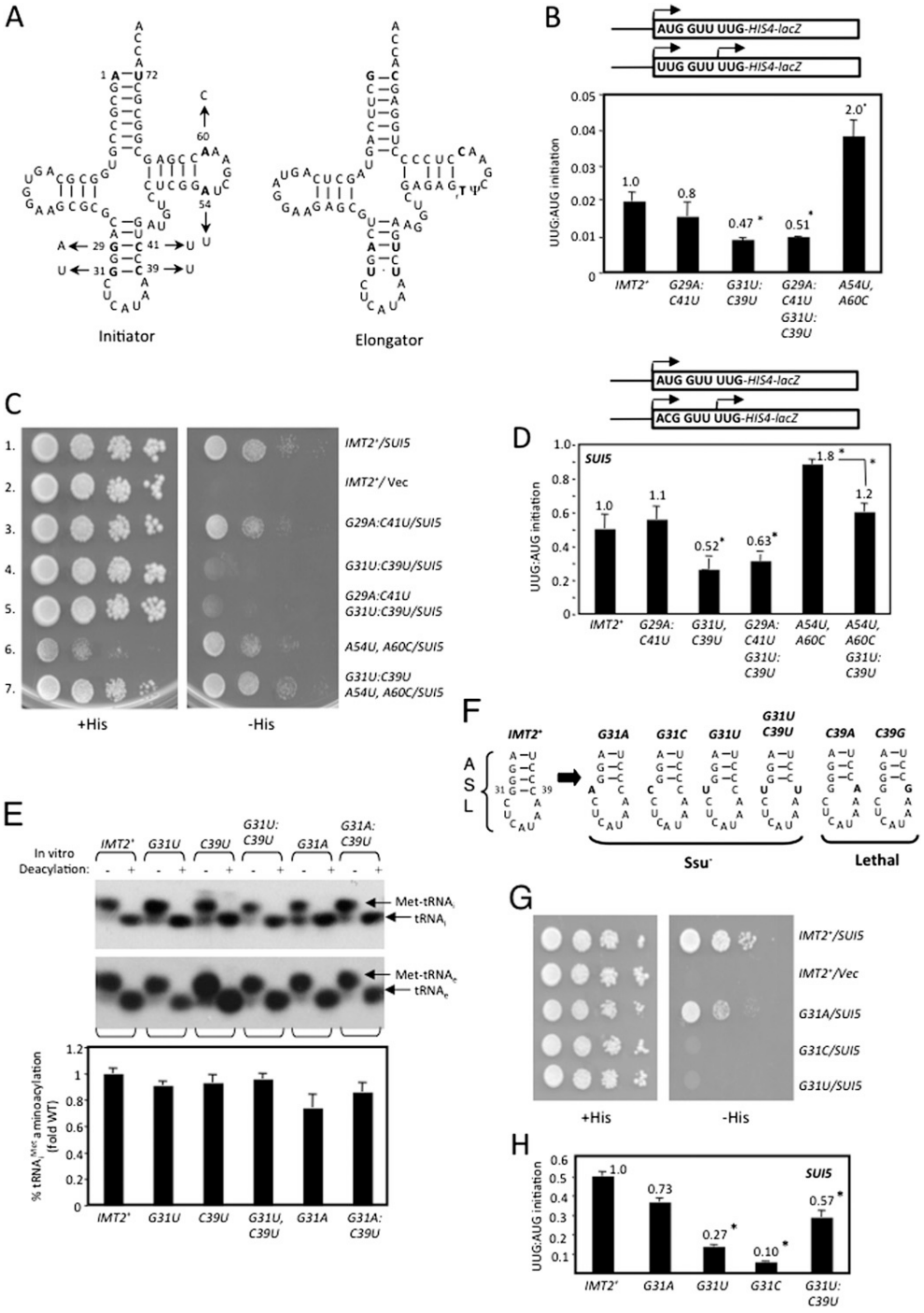

Table 2.1. Efficiency of plating (EOP) measurements of *IMT2* alleles

$tRNA_i$ Substitution	Normalized EOP[a]	Growth on +His[c]	Structural Element
None (WT)	1.0	4.0+	
A1G:U72C	0.15	3.5+	Acc stem
G70A	0.17	1.5+	Acc stem
C3U:G70A	0.72	nd	Acc stem
G70C	0.19	1.0+	Acc stem
C3G:G70C	0.49	nd	Acc stem
G70U	1.15	nd	Acc stem
C3A:G70U	0.99	nd	Acc stem
C3A	0.36	3.0+	Acc stem
C3G	0.22	3.0+	Acc stem
C3U	0.37	3.0+	Acc stem
G31A:C39U	0.96	nd	ASL
G31C:C39G	0.85	nd	ASL
G31U:C39A	1.15	nd	ASL
C39U	0.33	3.5+	ASL
C39A	$<3x10^{-5}$	lethal	ASL
C39G	$<3x10^{-5}$	lethal	ASL
G31A	0.23	1.2+	ASL
G31U	0.87	nd	ASL
G31C	0.63	nd	ASL
G31U:C39U	0.89	nd	ASL
G29A:C41U G31U:C39U	0.70	nd	ASL
G29A:C41U	0.68	nd	ASL
G29U:C41A	0.80	nd	ASL
G29C:C41G	0.85	nd	ASL
G30A:C40U	0.37	4.0+	ASL
G30U:C40A	0.33	3.0+	ASL
G30C:C40G	0.70	nd	ASL
G31U:C39U A54U, A60C	0.06	1.0+	ASL, T-loop
G29A	0.85	nd	ASL
G29C	$<10^{-6}$	lethal	ASL
G29U	0.87	nd	ASL
G30A	0.49	4.0+	ASL
G30C	$<10^{-6}$	lethal	ASL
G30U	$<10^{-6}$	lethal	ASL
C40A	$<10^{-6}$	lethal	ASL
C40G	$<10^{-6}$	lethal	ASL

Table 2.1 (cont'd). Efficiency of plating (EOP) measurements of *IMT2* alleles

$tRNA_i$ Substitution	Normalized EOP[a]	Growth on +His[c]	Structural Element
C40U	1.43	nd	ASL
C41A	$<10^{-6}$	lethal	ASL
C41G	$<10^{-6}$	lethal	ASL
C41U	0.95	nd	ASL
A54U	$<8x10^{-3}$[b]	lethal	T-loop
A54C	0.56	nd	T-loop
A54G	0.49	nd	T-loop
A60U	$<1.2x10^{-3}$[b]	lethal	T-loop
A60C	0.77	nd	T-loop
A60G	0.56	nd	T-loop
A54U, A60C	0.17	2.5+	T-loop
A54C, A60U	0.23	4.0+	T-loop
G70U, A54U, A60C	$<2.5x10^{-3}$	lethal	Acc Stem, T-loop
G70U, A54C, A60U	$<3.8x10^{-5}$	lethal	Acc Stem, T-loop
G70U, A54C	$<1.2x10^{-5}$	lethal	Acc Stem, T-loop

[a]Transformants of strain HD666 (harboring *IMT4*$^+$on hc *URA3* plasmid p2996) containing the indicated *IMT2* alleles on hc *LEU2* vector Yep351 were cultured to saturation in SC-Leu,-Ura and serial dilutions were plated on YEPD medium and SC-Leu containing 1 mg/mL 5-FOA. The EOP was calculated as the ratio of colonies formed on 5-FOA medium to those formed on YEPD medium. The absolute EOP value for transformants containing WT *IMT2*$^+$ on Yep351 (p1777) ranged from $1.1x10^{-2}$ to $1.6x10^{-2}$ and the EOP value for each mutant was normalized to that observed for p1777.

[b]EOP with *IMT2* allele on lc *LEU2* plasmid pSA03 (von Pawel-Rammingen et al. 1992a).

[c]Qualitative assessment of the rate of colony formation by transformants harboring the indicated *IMT2* alleles on hc *LEU2* vector Yep351 (derived by plasmid shuffling from HD666) relative to strain HD1726 (containing WT *IMT2*$^+$ on Yep351). Mutants harboring *IMT2* alleles that conferred an EOP of <0.4 were spotted on SD+His+Ura medium and incubated for 3d at 30°C and relative growth was scored qualitatively as shown in Fig. 2.S3. nd, not determined; Acc, acceptor.

G29A:C41U,G31U:C39U double substitution (Fig. 2.2B), suggesting that G31U:C39U increases initiation accuracy. This possibility is supported by the fact that G31U:C39U and the double substitution, but not G29A:C41U alone, are Ssu$^-$, suppressing the His$^+$ phenotype of *SUI5* (Fig. 2.2C, rows 1, 4,5) and reducing by ~50% the elevated UUG:AUG ratio conferred by *SUI5* (Fig. 2.2D). (These last measurements involved a *HIS4-lacZ* UUG reporter that mimics *his4-301* in containing an ACG at codon-1 and UUG at codon-3.) Thus, converting G31:C39 to U31:U39 increases the requirement for an AUG start codon. Consistent with previous findings (von Pawel-Rammingen et al. 1992b), Northern analysis of total RNA under acidic conditions shows that G31U:C39U does not diminish $tRNA_i$ abundance nor the proportion aminoacylated in vivo (Fig. 2.2E, lanes 7-8 vs. 1-2). (Unless otherwise stated, none of the $tRNA_i$ variants we analyzed significantly reduce $tRNA_i$ abundance or aminoacylation; Fig. 2.6A).

Interestingly, any of the 3 possible substitutions of G31, which disrupt Watson-Crick pairing (W:C) at 31:39 (Fig. 2.2F), resembled G31U:C39U in conferring Ssu$^-$ phenotypes, diminishing the His$^+$ phenotype (Fig. 2.2G) and, at least for G31U and G31C, substantially lowering the elevated UUG:AUG ratio (Fig. 2.2H) in *SUI5* cells. The weaker Ssu$^-$ phenotype of G31A might be attributable to the fact that it introduces an A:C wobble pair at 31:39. Although G31A evokes a 20-30% reduction in the proportion of $tRNA_i$ aminoacylated in vivo (Fig. 2.2E), this is unlikely to contribute to its Ssu$^-$ phenotype because a strain lacking two of four *IMT* genes (*IMT3* and *IMT4*), with substantially reduced levels of $tRNA_i$ and TC (Dever et al. 1995), displays essentially WT UUG:AUG initiation (data not shown). C39A and C39G, which also disrupt W:C pairing at 31:39, are lethal (Table 2.1 and Fig. 2.2F). These findings are consistent with

the possibility that W:C pairing at 31:39 is important for efficient start codon recognition, such that viable Ssu$^-$ substitutions disrupting 31:39 increase the requirement for AUG and thereby diminish UUG initiation. In this view, the lethal substitutions would substantially reduce recognition of AUG as well as near-cognates.

We also examined the effects of disrupting W:C pairing at G29:C41 and G30:C40. As summarized in Fig. 2.3F, 7 of 8 single base substitutions that introduce purine:purine or pyrimidine:pyrimidine pairs at positions 29:41 or 30:40 are lethal. By contrast, substitutions that generate A:C or G:U wobble replacements are viable and either have no effect on initiation accuracy (G29A, G30A, and C40U) or moderately increase accuracy and confer a weak Ssu$^-$ phenotype (C41U) (Table 2.1).

Thus, the integrity of all three G:C base pairs in the ASL stem is critical in vivo, as substitutions that generate purine:purine pairs at any of these positions are lethal, and pyrimidine:pyrimidine pairs are either lethal (1st and 2nd base pairs) or confer marked hyperaccuracy (Ssu$^-$) phenotypes (3rd base pair). By contrast, most wobble replacements have little or no effect on initiation accuracy.

W:C substitutions of 31:39 in the ASL strongly decrease initiation accuracy.

We next analyzed the effects of double substitutions that replace the conserved G:C base pairs with other W:C pairs (Fig. 2.3A). Remarkably, all three W:C replacements of G31:C39, as well as C39U that produces a wobble G:U at this position, substantially reduce initiation accuracy, conferring His$^+$/Sui$^-$ phenotypes (Fig. 2.3B) and increasing the UUG:AUG ratio 6- to 7-fold for the W:C substitutions and ~2.5-fold for the G:U replacement (Fig. 2.3C). By contrast, W:C substitutions of the 1st G:C pair did not

Figure 2.3. W:C replacements at 31:39 and A54 substitutions in the T-loop reduce the accuracy of start codon recognition. (A) ASL structures and phenotypes (in order of severity: $Sui^{-} > Sui^{-/+} > Sui^{+/-}$) for W:C substitutions of G:C pairs. **(B &D)** *his4-301* strains with the indicated *IMT2* alleles were replica-plated to +His medium (0.3 mM His) or 0.5% His (1.5 μM His) and incubated for 3d (+His) or 7-10 d (0.5% His). **(C, E & G)** UUG:AUG initiation ratios were determined as in Fig. 1B for strains with the indicated *IMT2* alleles. **(F)** Phenotypes of substitutions that disrupt W:C pairing at positions 29:41 and 30:40. **(H)** Structures of the T-loop with substitutions at A54 or A60 and the associated phenotypes.

Figure 2.3.

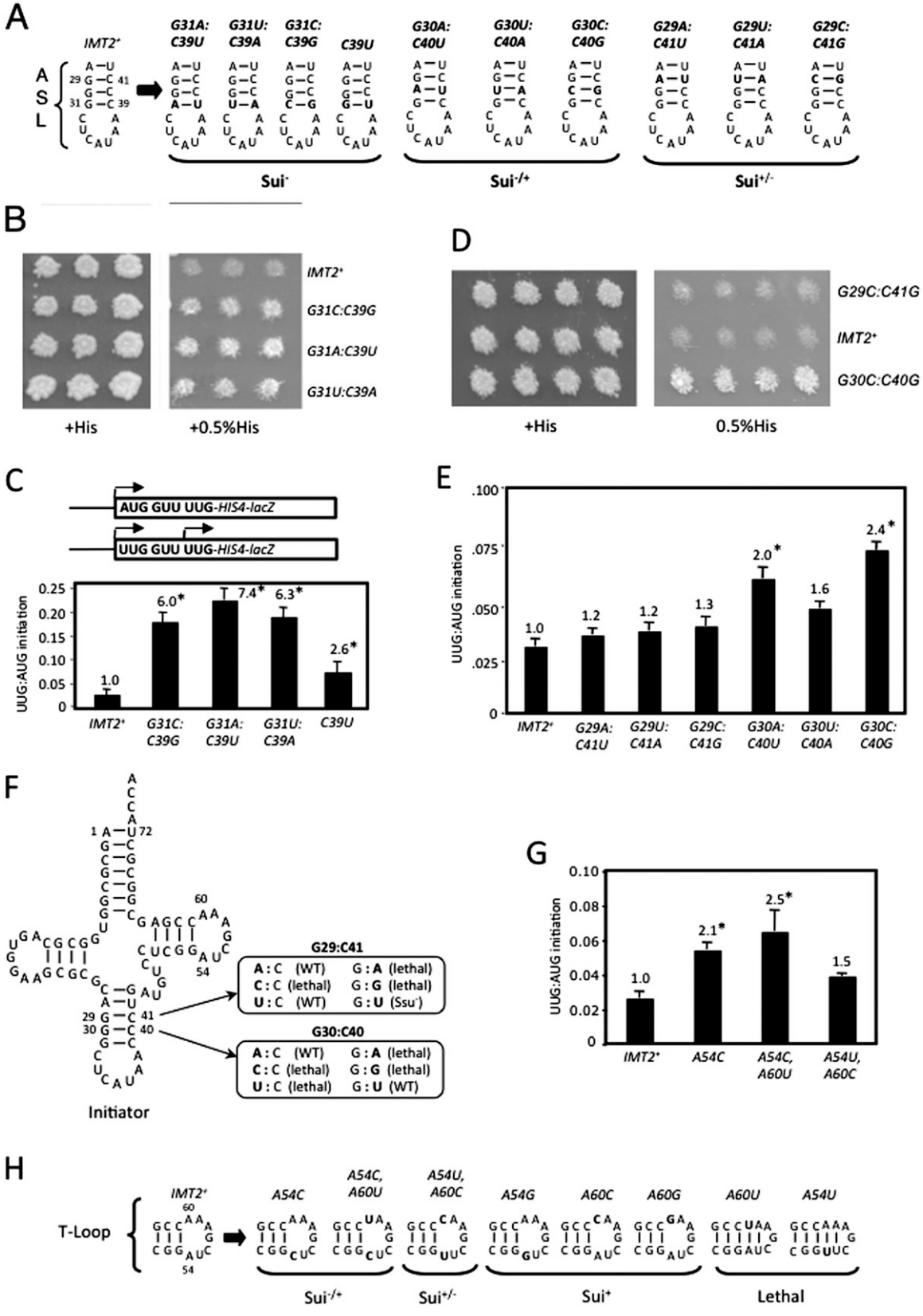
A
IMT2+
ASL
G31A: C39U
G31U: C39A
G31C: C39G
C39U
G30A: C40U
G30U: C40A
G30C: C40G
G29A: C41U
G29U: C41A
G29C: C41G
Sui-
Sui-/+
Sui+/-
B
IMT2+
G31C:C39G
G31A:C39U
G31U:C39A
+His
+0.5%His
D
G29C:C41G
IMT2+
G30C:C40G
+His
0.5%His
C
AUG GUU UUG-HIS4-lacZ
UUG GUU UUG-HIS4-lacZ
UUG:AUG initiation
1.0
6.0*
7.4*
6.3*
2.6*
IMT2+
G31C: C39G
G31A: C39U
G31U: C39A
C39U
E
UUG:AUG initiation
1.0
1.2
1.2
1.3
2.0*
1.6
2.4*
IMT2+
G29A: C41U
G29U: C41A
G29C: C41G
G30A: C40U
G30U: C40A
G30C: C40G
F
G29:C41
A : C (WT) G : A (lethal)
C : C (lethal) G : G (lethal)
U : C (WT) G : U (Ssu-)
G30:C40
A : C (WT) G : A (lethal)
C : C (lethal) G : G (lethal)
U : C (lethal) G : U (WT)
Initiator
G
UUG:AUG initiation
1.0
2.1*
2.5*
1.5
IMT2+
A54C
A54C, A60U
A54U, A60C
H
T-Loop
IMT2+
A54C
A54C, A60U
A54U, A60C
A54G
A60C
A60G
A60U
A54U
Sui-/+
Sui+/-
Sui+
Lethal

produce His^+ phenotypes (Fig. 2.3D and data not shown) and evoked <30% increases in the UUG:AUG ratio (Fig. 2.3E). W:C replacements of the 2nd G:C pair conferred somewhat greater increases in the UUG:AUG ratio (Fig. 2.3E), and a His^+ phenotype only for G30C:C40G (Fig. 2.3D). As noted above, C40U and C41U substitutions that introduce G:U wobble pairs at 29:41 and 30:40 do not confer Sui^- phenotypes (Fig. 2.3F). Thus, W:C substitutions at each of the ASL G:C pairs reduce initiation accuracy, with the strongest defects for the 31:39 substitutions, adjacent to the anticodon loop, and the weakest for the 29:41 substitutions furthest from the anticodon loop (Fig. 2.3A). One way to explain these findings is to propose that the ASL G:C pairs promote initiation accuracy by affecting the conformation of the anticodon loop, with the 31:39 pair closest to the loop having the greatest effect on accuracy.

Ssu^- disruptions of 31:39 destabilize the closed/P_{IN} conformation of the PIC

The fact that G31C and G31U evoke Ssu^- phenotypes suggests that these mutations destabilize the closed/P_{IN} state of the PIC normally triggered by start codon recognition. To test this interpretation, we examined the effects of these substitutions on the equilibrium and rate constants governing TC binding to the 40S subunit. We first determined that [^{35}S]-Met-$tRNA_i$ variants harboring these substitutions all efficiently form TC with eIF2 and GDPNP (Table 2.2). Subsequently, we measured the affinities of the TCs for the 40S subunit in the presence of saturating eIF1, eIF1A and a model mRNA containing an AUG or UUG start codon, using native gel electrophoresis to separate bound and unbound fractions of TC. Interestingly, G31C and G31U increased the affinity of TC for 40S complexes lacking mRNA while greatly reducing affinity in the presence

Table 2.2. Affinity of Met-tRNA$_i$ for eIF2-GDPNP

tRNA	K_d (nM)
WT	9 ± 2
G31C	19 ± 1
G31U	12 ± 3
G31C:C39G	11 ± 3
G31A:C39U	7 ± 1
G31U:C39A	30 ± 10
G70A	27 ± 5
C3U:G70A	11 ± 3
C3U	40 ± 15

Values are the averages of at least 3 independent experiments. Errors are average deviations.

Of mRNA(AUG) (Fig. 2.4A and Table 2.3). Strikingly, the affinity of these mutant TCs for the 43S·mRNA(UUG) complex is so low that no complex formation could be detected at the highest concentrations of 40S subunits employed (≥250nM) (data not shown and Table 2.3). These findings support the prediction that G31C and G31U destabilize the closed/P_{IN} state; and the fact that TC affinity is much lower for the UUG versus AUG complex is consistent with the Ssu^- phenotype of these mutations (Fig. 2.1H). Moreover, considering that the WT TC has a much lower affinity for 43S versus 43S·mRNA(AUG) complexes (Kapp et al. 2006) (Table 2.3), the fact that G31C/G31U essentially eliminate this differential in stability indicates that they abolish thermodynamic coupling between Met-$tRNA_i$ and the start codon.

We previously proposed that the endpoints of curves for TC binding at high concentrations of 40S subunits reflect the distribution of PICs in the open vs. closed states; the open state was proposed to be unstable during electrophoresis, and therefore could not be visualized, leading to endpoints of <1 (measured as fractions of TC bound to 40S complexes) in cases where open complex persists (Kapp et al. 2006; Kolitz et al. 2009). Consistent with this idea, G31C and G31U, which we propose bias the system towards the open/P_{OUT} state, decrease the endpoints of TC binding in both the absence and presence of mRNA(AUG) (Fig. 2.4A and Table 2.3).

To gain more insight into the effect of these mutations on formation and stability of the PIC, we measured the rate constants for TC forming and dissociating from PICs. The kinetics of TC binding was measured by mixing TC containing [^{35}S]-Met-$tRNA_i$ with varying concentrations of 40S subunits and saturating eIF1, eIF1A and mRNA(AUG) or mRNA(UUG). Time points were removed and reactions terminated

Figure 2.4. Disrupting ASL base pair G31:C39 and replacing it with other W:C base pairs have opposite effects on the stability of 43S·mRNA complexes. (A-B) Determination of K_d values for TC (with WT or the indicated variant of [^{35}S]-Met-tRNA$_i$) binding to 40S•eIF1•eIF1A complexes assembled with mRNA(AUG) (A) or mRNA(UUG) (B). **(C-D)** Determination of k_{on} values for TC binding to 40S•eIF1•eIF1A complexes from plots of observed rate constants (k_{obs}) versus 40S concentration with mRNA(AUG) (C) or mRNA(UUG) (D). **(E-F)** Analysis of TC dissociation from 43S·mRNA complexes for mRNA(AUG) (E) or mRNA(UUG) complexes (F). Representative curves from at least 2 independent experiments are shown. K_{off} values and end-points for dissociable complexes are given in Table 2.5

Figure 2.4.

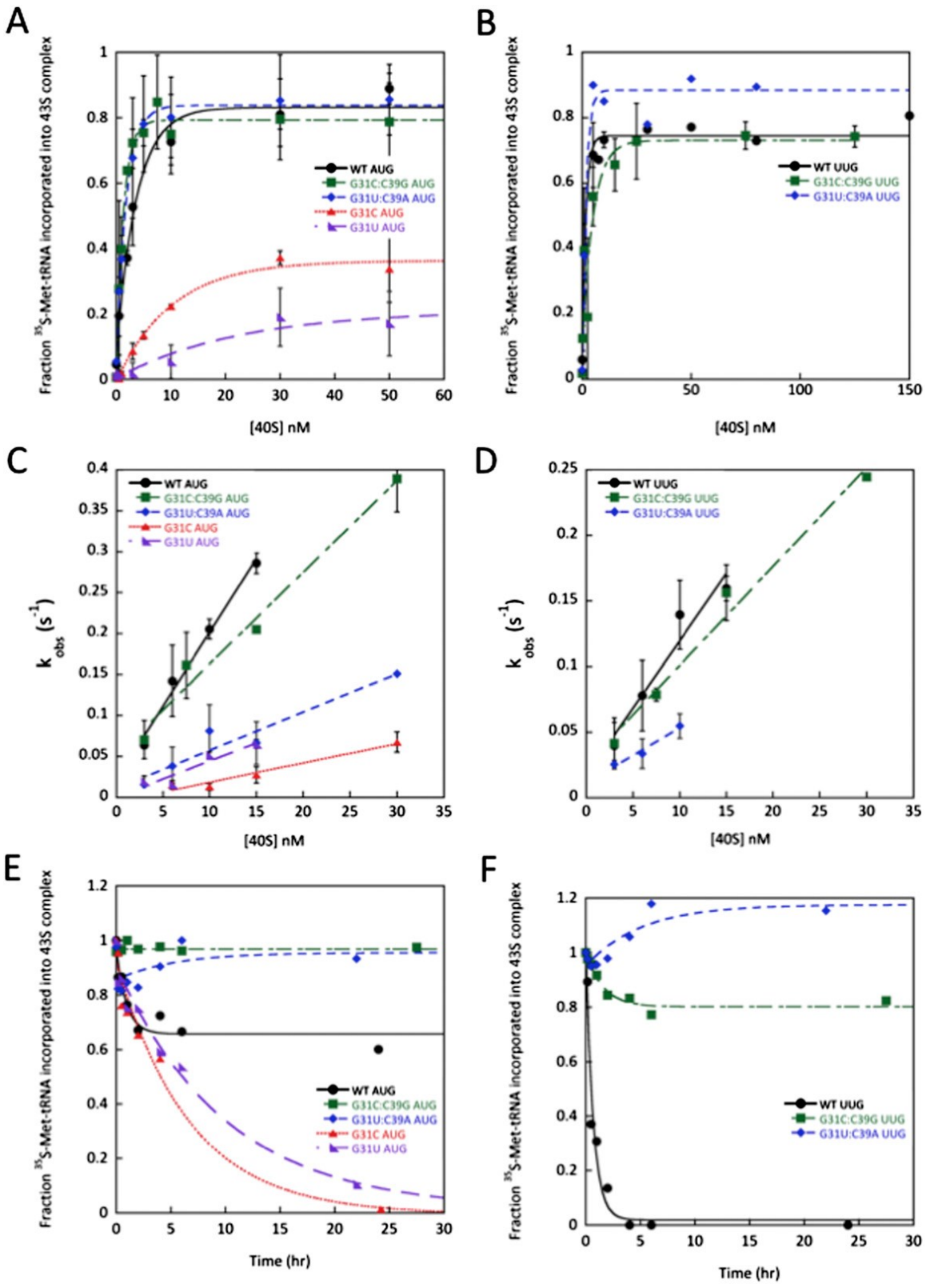
A
Fraction 35S-Met-tRNA incorporated into 43S complex
[40S] nM
WT AUG
G31C:C39G AUG
G31U:C39A AUG
G31C AUG
G31U AUG
B
Fraction 35S-Met-tRNA incorporated into 43S complex
[40S] nM
WT UUG
G31C:C39G UUG
G31U:C39A UUG
C
kobs (s-1)
[40S] nM
WT AUG
G31C:C39G AUG
G31U:C39A AUG
G31C AUG
G31U AUG
D
kobs (s-1)
[40S] nM
WT UUG
G31C:C39G UUG
G31U:C39A UUG
E
Fraction 35S-Met-tRNA incorporated into 43S complex
Time (hr)
WT AUG
G31C:C39G AUG
G31U:C39A AUG
G31C AUG
G31U AUG
F
Fraction 35S-Met-tRNA incorporated into 43S complex
Time (hr)
WT UUG
G31C:C39G UUG
G31U:C39A UUG

Table 2.3. Affinity of TC for 40S·eIF1·eIF1A·mRNA complexes

		K_d (nM)			Endpoint (fraction bound)		
Phenotype	$tRNA_i$	(A) No mRNA	(B) +mRNA (AUG)	© +mRNA (UUG)	(D) No mRNA	(E) +mRNA (AUG)	(F) +mRNA (UUG)
	WT	60 ± 5	≤1	≤1	0.47 ± 0.14	0.85 ± 0.09	0.80 ± 0.10
Ssu^-	G31C	29 ± 15	11 ± 2	>250	0.28 ± 0.10	0.29 ± 0.16	n/a
Ssu^-	G31U	18 ± 10	34 ± 4	>250	0.25 ± 0.06	0.23 ± 0.06	n/a
$Sui^- Gcd^+$	G31C:C39G	38 ± 23	≤1	≤1	0.35 ± 0.19	0.81 ± 0.14	0.77 ± 0.05
$Sui^- Gcd^+$	G31U:C39A	41	≤1	≤1	0.44	0.86 ± 0.07	0.93 ± 0.05
$Sui^- Gcd^-$	G70A	33 ± 7	≤1	≤1	0.58 ± 0.01	0.76 ± 0.06	0.68 ± 0.18
$Sui^{-/+}$	C3U:G70A	25 ± 11	≤1	≤1	0.74 ± 0.20	0.91 ± 0.06	0.80 ± 0.05

Values are the averages of at least two independent experiments with the exception of G31U:C39A in the absence of mRNA. Errors are average deviations. (n/a) Not applicable.

with excess unlabeled TC, and the amount of labeled TC in PICs was measured by native gel electrophoresis. The slope of the plot of the pseudo-first-order rate constants (k_{obs}) for PIC formation vs. 40S concentration yields the second-order rate constant (k_{on}) (Kolitz et al. 2009).

The G31C and G31U mutations decrease k_{on} for TC in the presence of mRNA(AUG) by 8- and 4-fold, respectively (Fig. 2.4C and Table 2.4). The corresponding values with mRNA(UUG) could not be determined because TC binding with these mutants is too weak to measure. One possible interpretation of these data is that the mutations slow conversion of the open/P_{OUT} state of the PIC to the closed/P_{IN} state, which is dramatically accelerated by start codon recognition in WT PICs and has a strong influence on the observed rate of PIC formation (Kolitz et al. 2009). Slowing of this step would be consistent with the mutants' Ssu^- phenotypes.

Next we measured the rate at which TC made with the mutant tRNAs dissociates from PICs. After assembling 43S·mRNA complexes as above, we quantified the amount of [^{35}S]-Met-$tRNA_i$ remaining in the slowly-migrating PIC band as a function of time after adding a chase of excess unlabeled TC made with WT Met-$tRNA_i$. With WT PICs formed with mRNA(AUG), TC dissociates from ~40% of the PICs with a rate constant of 0.4 hr^{-1}, whereas the remaining ~60% of the complexes are completely stable over this time period (Fig. 2.4E and Table 2.5). We presume that the former fraction of PICs contain Met-$tRNA_i$ bound in the P_{IN} state, whereas the latter arise by isomerization of Met-$tRNA_i$ from P_{IN} to a new state where it is fully locked-in to the P-site. This putative highly stable state might be closer to the classical P/P state than the P/I state observed

Table 2.4. Rate constants for TC association with 40S·eIF1·eIF1A·mRNA complexes

		k_{on} (X 10^6 M^{-1} s^{-1})	
$tRNA_i$	eIF1A	(A) +mRNA(AUG)	(B) +mRNA(UUG)
WT	WT	18.0 ± 0.2	11.6 ± 0.1
G31C	WT	2.3 ± 0.2	n/a
G31U	WT	4.4 ± 0.2	n/a
G31C:C39G	WT	9.1 ± 2.9	5.1 ± 1.8
G31U:C39A	WT	5.6 ± 0.4	3.7 ± 1.3
G70A	WT	0.7 ± 0.4	7.5 ± 0.9
C3U:G70A	WT	7.1 ± 2.6	11.6 ± 0.5
G70A	17-21	43.0 ± 1.2	3.3 ± 1.3
WT	17-21	4.7 ± 0.3	10.1 ± 0.7

Values are the averages of at least two independent experiments. Errors are average deviations.

Table 2.5. Rates of TC dissociation from 40S•eIF1•eIF1A•mRNA complexes

		k_{off} (hr^{-1})		Endpoint (fraction bound)	
Phenotype	$tRNA_i$	(A) +mRNA(AUG)	(B) +mRNA(UUG)	© +mRNA(AUG)	(D) +mRNA(UUG)
	WT	0.42 ± 0.08	1.23 ± 0.51	0.53± 0.07	0
Ssu^-	G31C	0.23 ± 0.11	n/a	0	n/a
Ssu^-	G31U	0.11 ± 0.04	n/a	0.11 ± 0.01	n/a
$Sui^- Gcd^+$	G31C:C39G	ND[1]	0.44 ± 0.13	ND	0.77 ± 0.01
$Sui^- Gcd^+$	G31U:C39A	ND	ND	ND	ND
$Sui^- Gcd^-$	G70A	ND	0.53 ± 0.28	ND	0.74 ± 0.10
$Sui^{-/+}$	C3U:G70A	ND	1.96 ± 0.47	ND	0.49 ± 0.04

[1]ND, no dissociation observed.

Values are the averages of at least two independent experiments. Errors are average deviations.

Recently in reconstituted mammalian PICs (Hashem et al. 2013; Lomakin and Steitz 2013), which can be regarded as the P_{IN} conformation. (As the AUG codon-dependent conversion to the initial closed/P_{IN} state is rapid (Kolitz et al. 2009), it is unlikely that the two states represent open/P_{OUT} and closed/P_{IN} because if the rate of reversion of the closed/P_{IN} state back to the open/P_{OUT} state was slow, all the complexes should be in the closed/P_{IN} state, whereas if the rate of reversion was fast all the complexes should dissociate on chasing with unlabeled TC.) Importantly, dissociation of WT TC from PICs assembled on mRNA(UUG) goes to completion and occurs with a rate constant of 1.2 hr^{-1} (Fig. 2.4F), suggesting that PICs do not achieve the highly stable state with a UUG codon in the P site.

Interestingly, both G31C and G31U increase the fraction of AUG complexes from which TC can dissociate, from ~40% with WT to 100% with the mutants (Fig. 2.4E), resembling the behavior of WT complexes at UUG (Fig. 2.4F). Thus, the Ssu^- mutations decrease the ability of the PIC to enter the highly stable state accessible to the WT complex.

Sui^- W:C substitutions of 31:39 stabilize the closed/P_{IN} state

As described above, the Ssu^- phenotypes of the G31C and G31U mutations in the ASL are suppressed by the compensatory C39G and C39A mutations that restore W:C pairing at this position; and these double mutants produce Sui^- phenotypes instead, suggesting that they shift the balance in favor of the closed/P_{IN} state. Consistent with this proposal, G31C:C39G and G31U:C39A dramatically reduce the K_ds for TC binding to the 40S complex with both mRNA(AUG) and mRNA(UUG) relative to the K_ds with the

G31C and G31U single substitutions, and they also restore the endpoints of TC binding (Fig. 2.4A, B and Table 2.3). These data suggest that the double mutations stabilize the closed/P_{IN} state.

Analysis of dissociation kinetics revealed that G31C:C39G and G31U:C39A produce complexes from which >80% of the TC does not dissociate with mRNA(AUG) or mRNA(UUG) (Fig. 2.4E-F), indicating that they not only favor the closed/P_{IN} state, but lead to more complexes entering the highly stable state. The magnitude of these changes appear to be bigger with mRNA(UUG) (compare curves for WT vs. G31C:C39G and G31U:C39A in Figs. 2.4E-F), consistent with the elevated UUG:AUG initiation ratios observed in vivo for these variants.

Analysis of association kinetics showed that the k_{on} value in the presence of mRNA(AUG) with the G31C:C39G mutant was increased 4-fold relative to that with G31C (Fig. 2.4C and Table 2.4), suggesting that restoring this base pair speeds up conversion of the open/P_{OUT} state to the closed/P_{IN} state on start codon recognition. The G31U:C39A mutation does not enhance the rate of TC loading relative to that seen with the Ssu^- G31U mutant however (Fig. 2.4C and Table 2.4), suggesting that the key effect of the Sui^- mutations is on stability of the closed/P_{IN} state, which is reflected in the dissociation rates. Stable complexes could not be formed on mRNA(UUG) with the G31C and G31U mutants, but restoring base pairing at position 31:39 restores stable complex formation, as noted above. The k_{on} values for mRNA(UUG) complexes with the G31C:C39G and G31U:C39A mutants were 2 to 3-fold lower than with WT (Fig. 2.4D and Table 2.4), but because k_{on} values could not be measured with the single mutants, we cannot determine the extent to which restoring the base pair increases k_{on}.

T-loop residue A54 contributes to stringent AUG selection.

The results described above indicate that Ssu$^-$ substitutions G31C and G31U destabilize TC binding to 43S·mRNA complexes in vitro (Table 2.3). We observed the same outcome previously on replacing G31:C39 with the U:U pair found in tRNA$_e^{Met}$ (Kapp et al. 2006); and importantly, we concluded above that G31U:C39U likewise confers an Ssu$^-$ phenotype in vivo (Fig. 2.2B-D). We also reported that substitutions A54U and A60C of the two signature T-loop residues of tRNA$_i$ reduced the deleterious effect of G31U:C39U on the affinity of TC for 43S·mRNA(AUG) complexes (Kapp et al. 2006). We reasoned that if the Ssu$^-$ phenotype of G31U:C39U results from less stable binding of Met-tRNA$_i$ to the closed/P$_{IN}$ state of the PIC, as proposed above for G31C and G31U, then the A54U,A60C substitutions should suppress the Ssu$^-$ phenotype of G31U:C39U.

Remarkably, combining A54U,A60C with G31U:C39U restores the His$^+$ phenotype (Fig. 2.2C, cf. rows 4 & 7 vs. row 1) and reinstates the elevated UUG:AUG ratio conferred by *SUI5* in *IMT2*$^+$ cells (Fig. 2.2D, cf. columns 3 & 6 vs. column 1). A54U,A60C also produces a modest Sui$^-$ phenotype in otherwise WT cells, increasing the UUG:AUG ratio (Fig. 2.2B). Consistent with this, A54U,A60C exacerbates the Sui$^-$ phenotype of *SUI5,* decreasing growth on +His but not –His medium (Fig. 2.2C, rows 1,6) and elevating the UUG:AUG ratio above that seen in *SUI5 IMT2*$^+$cells (Fig. 2.2D, columns 1 & 5). Note also that G31U:C39U reverses the Slg$^-$ phenotype of the A54U,A60C substitution in *SUI5* cells on +His medium (Fig. 2.2C, +His, rows 1,6,7), which likely reflects the ability of G31U:C39U to mitigate the elevated UUG initiation conferred by A54U,A60C in *SUI5* cells (Fig. 2.2D, columns 5-6). Thus, replacing both

highly conserved T-loop residues with the corresponding bases in $tRNA_e^{Met}$ decreases the accuracy of AUG selection (Sui^-) and suppresses the hyperaccurate (Ssu^-) phenotype of the ASL substitution G31U:C39U, and these substitutions mutually suppress their opposing effects on initiation accuracy. The fact that A54U,A60C suppresses the destabilizing effect on TC binding to 43S·mRNA PICs in vitro (Kapp et al. 2006) as well as the Ssu^- phenotype of G31U:C39U in cells (Fig. 2.2C-D) provides strong evidence that the stability of the closed/P_{IN} state of the PIC is a critical determinant of initiation accuracy in vivo.

We went on to explore which T-loop substitution confers the moderate Sui^- phenotype of A54U,A60C. Neither A60C nor A60G single substitutions affected the UUG:AUG ratio (data not shown, summarized in Fig. 2.3H). These findings, together with the fact that A54C alone confers a Sui^- phenotype (Fig. 2.3G), suggest that A54U is responsible for the Sui^- phenotype of A54U,A60C. However, we cannot eliminate the possibility that A60C contributes to the Sui^- phenotype of the A54U,A60C double mutant. Interestingly, both A54U and A60U are lethal (Table 2.1), which might derive from their ability to extend the T-stem as depicted in Fig. 2.3H. However, A54C alone, or in combination with A60U, increases the UUG:AUG ratio by a factor of 2.0-2.5 (Fig. 2.3G), whereas A54G does not significantly affect the UUG:AUG ratio (data not shown). We conclude that a purine residue is required at position 54 in the T-loop for WT discrimination against UUG start codons.

Acceptor stem residue G70 is crucial for stringent AUG selection

To identify additional determinants of initiation accuracy, we screened a library of mutant *IMT2* plasmids produced by random mutagenesis for a His^+ phenotype in the *his4-301* strain and identified the G70U substitution in the acceptor stem as a novel Sui^- mutation (Fig. 2.5C, -His, rows 1-2; Fig. 2.5D, columns 1 & 6). C3:G70 is a highly conserved feature of $tRNA_i$ in all kingdoms of life (Marck and Grosjean 2002), but its possible function in initiation was unknown. Interestingly, site-directed mutagenesis showed that G70A, G70C and C3G confer even stronger

His^+/Sui^- phenotypes (Figs. 2.5C) and larger (≥9-fold) increases in UUG:AUG initiation compared to G70U (Fig. 2.5D). However, C3A and C3U confer smaller increases in the UUG:AUG ratio (~2.5-fold; Fig. 2.5D) and little growth on –His medium (Fig. 2.5C). The strength of the His^+/Sui^- and elevated UUG:AUG initiation phenotypes of these substitutions (Fig. 2.5C, -His; Fig. 2.5D) correlate well with their effects on cell growth (Fig. 2.5C, +His). Thus, disrupting W:C pairing at 3:70 confers a Sui^- phenotype whose severity varies with the substitution (summarized in Fig. 2.5A).

C3U, which introduces a U:G wobble pair (Fig. 2.5A), produces one of the weakest Sui^- phenotypes among the single-base changes in the 3:70 base pair (Figs. 2.5C-D). Consistent with this, combining C3U with G70A to introduce a W:C replacement at the 3:70 base pair (Fig. 2.5A), effectively diminishes the Slg^-, His^+, and elevated UUG:AUG initiation phenotypes conferred by G70A (Fig. 2.5B-D). Similar findings were obtained when G70C and G70U were combined with the appropriate C3 substitutions to reinstate W:C pairing; although suppression of the strong Sui^- phenotypes of G70C and G70U was less pronounced, as the double substitutions retained weak His^+ phenotypes and significantly elevated UUG:AUG ratios (Fig. 2.5A-D). Nevertheless, it is

Figure 2.5. C3:G70 in the acceptor stem is crucial for accurate AUG selection and rapid TC binding to PICs in vivo. (A) Acceptor stem structures and phenotypes (in order of severity: $Sui^{3-} > Sui^{2-} > Sui^{-} > Sui^{-/+}$) for 3:70 substitutions. **(B)** Slg^{-} phenotypes on +His medium analyzed as in Fig. 1C. **(C)** His^{+}/Sui^{-} phenotypes analyzed as in Fig. 2B. (Results in (B-C) were obtained in parallel from the same plates and rearranged only for ease of interpretation.) **(D)** UUG:AUG initiation ratios were determined as in Fig. 1B. **(E)** β-galactosidase expressed from the *GCN4-lacZ* reporter on p180 measured as in Fig. 1B.

Figure 2.5.

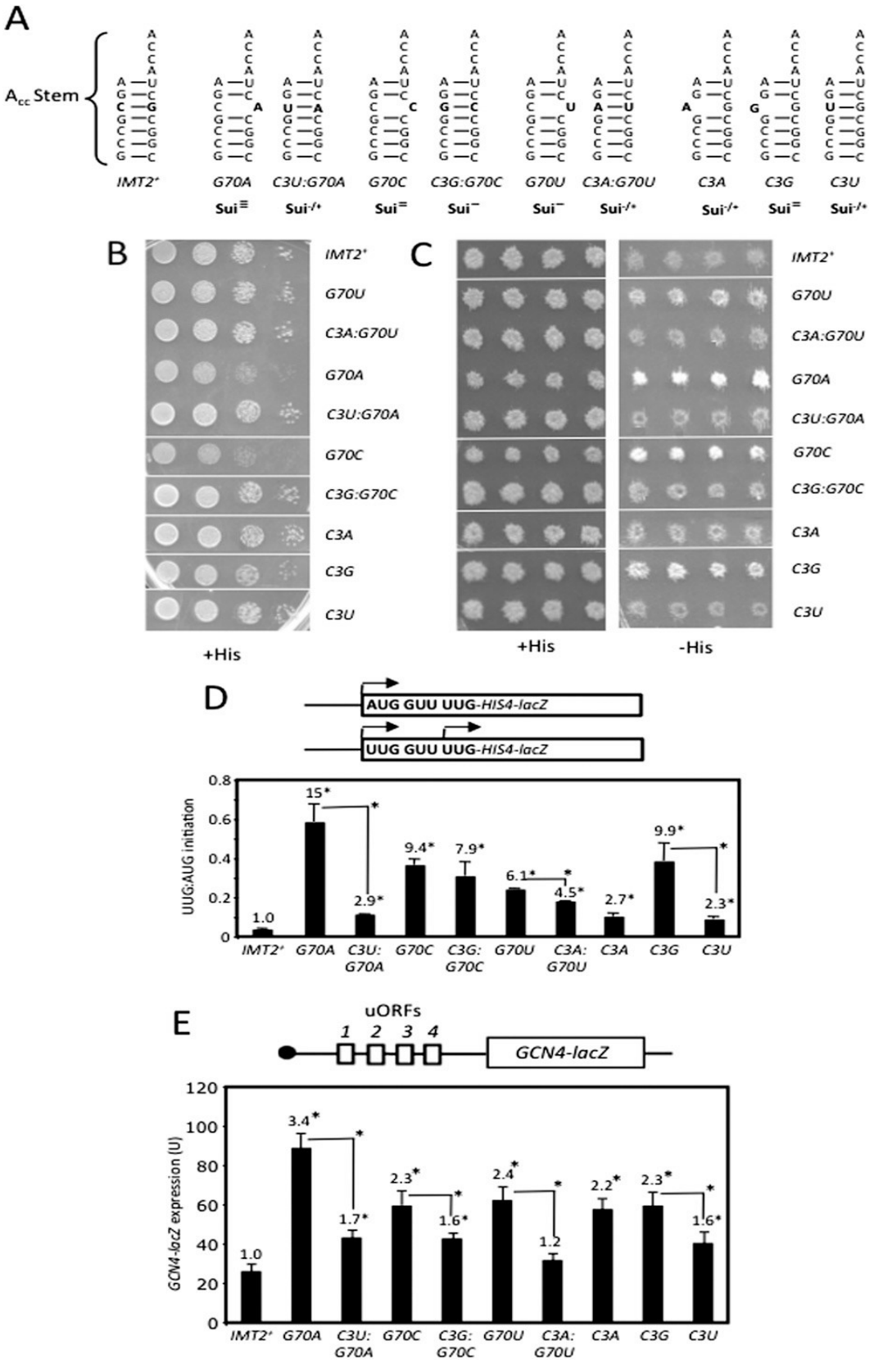
A
A_cc Stem
IMT2+
G70A
C3U:G70A
G70C
C3G:G70C
G70U
C3A:G70U
C3A
C3G
C3U
Sui≡
Sui-/+
Sui=
Sui−
Sui−
Sui-/+
Sui-/+
Sui=
Sui-/+
B
C
+His
+His
-His
D
AUG GUU UUG-HIS4-lacZ
UUG GUU UUG-HIS4-lacZ
UUG:AUG initiation
1.0
15*
2.9*
9.4*
7.9*
6.1*
4.5*
2.7*
9.9*
2.3*
E
uORFs
1 2 3 4
GCN4-lacZ
GCN4-lacZ expression (U)
1.0
3.4*
1.7*
2.3*
1.6*
2.4*
1.2
2.2*
2.3*
1.6*

noteworthy that combining these mutations mitigated rather than exacerbated their respective Sui$^-$/Slg$^-$ phenotypes. We conclude that base pairing *per se* plus the identity of the W:C pair at position 3:70 both contribute to discrimination against UUG start codons.

C3:G70 substitutions confer Gcd$^-$ phenotypes without decreasing TC abundance in vivo.

Interestingly, we found that the Sui$^-$ substitutions at C3:G70 confer constitutive derepression of a *GCN4-lacZ* reporter, the Gcd$^-$ phenotype, indicating a reduced rate of TC binding to 40S subunits in vivo. A decrease in the rate of TC binding to 40S subunits derepresses *GCN4-lacZ* expression because scanning 40S subunits that have already translated uORF1 can bypass the start codons of the inhibitory uORFs 2-4 before rebinding TC, and then reinitiate further downstream at the *GCN4* AUG codon instead (Hinnebusch 2005). Whereas G70A, G70C, G70U, C3A, and C3G, all disrupting C3:G70, confer 2 to 3-fold increases in *GCN4-lacZ* reporter expression in nonstarvation conditions, the C3U:G70 wobble substitution and C3U:G70A, C3G:G70C, and C3A:G70U double substitutions (producing W:C replacements) have smaller (< 1.7-fold) effects on *GCN4-lacZ* expression (Fig. 2.5E). In particular, C3U:G70A suppresses the marked derepression of *GCN4-lacZ* conferred by G70A (Fig. 2.5E, columns 2-3). None of the G70 or C3 single substitutions significantly affected expression of a *GCN4-lacZ* reporter lacking all four uORFs (data not shown), indicating that they alter translational control of *GCN4-lacZ* expression. The severity of the Gcd$^-$ phenotypes provoked by disrupting or altering C3:G70 is generally correlated with that of the Sui$^-$ phenotypes produced by these mutations (cf. Figs. 2.5D & 2.5E), suggesting that these defects are

mechanistically linked. Moreover, none of the strong Sui$^-$ substitutions involving W:C replacements of G31:C39 confers a Gcd$^-$ phenotype (data not shown), suggesting distinct mechanisms underlying the Sui$^-$ phenotypes of 31:39 versus 3:70 substitutions.

Importantly, none of the Gcd$^-$ G70 substitutions (G70A, G70C, and G70U) reduces $tRNA_i$ abundance (data not shown) or $tRNA_i$ aminoacylation in vivo (Fig. 2.6A and data not shown). Given the location of C3:G70 in the acceptor stem, which contacts eIF2 (Shin et al. 2011), G70 substitutions might reduce TC formation as the means of derepressing *GCN4* translation. In fact, our in vitro measurements of Met-$tRNA_i$ binding to eIF2 revealed ~4-fold increases in K_d for C3U and G70A that were mitigated in the C3U:G70A double mutant (Table 2.2). Accordingly, we measured native TC levels in cell extracts by immunoprecipitating FLAG-tagged eIF2β (FL- Sui3) expressed in the *IMT2* mutants of interest, probed immune complexes by Northern analysis for $tRNA_i$ levels, and normalized the $tRNA_i$ signal for amounts of immunoprecipitated FL-Sui3 (Fig. 2.6B-D). We verified that only a low background level of $tRNA_i$ was immunoprecipitated from the parental *IMT2*$^+$ strain containing untagged eIF2β (Fig. 2.6C-D, (-)tag); and that the eIF2γ-N135D substitution (Alone et al. 2008) reduces the amount of $tRNA_i$ coimmunoprecipitating with eIF2β-FL (data not shown). Using this assay, we observed no difference between WT and the G70U, G70A, and G70C mutants (Fig. 2.6B-D), suggesting that G70 substitutions do not significantly reduce TC abundance in vivo. Accordingly, their Gcd$^-$ phenotypes likely result instead from reducing the rate of TC binding to 40S subunits scanning downstream from uORF1, which induces reinitiation at *GCN4* (Hinnebusch 2005).

Figure 2.6. Evidence that the Sui$^-$ and Gcd$^-$ phenotypes of the G70A substitution have a common molecular basis. (A) Substitutions of C3:G70 do not affect aminoacylation *in vivo*. Analysis conducted as in Fig. 1E. **(B-D)** Substitutions of C3:G70 do not impair TC assembly *in vivo*. WCEs from strains harboring a *SUI3-FL* plasmid or empty vector were immunoprecipitated with FLAG antibodies and 5% of each immune complex was subjected to Western analysis with FLAG or Gcd11/eIF2γ antibodies (B). RNA extracted from the remainder was subjected to Northern analysis of $tRNA_i$ (C). The 2nd lane in (C) derives from the *IMT2*$^+$ strain with untagged *SUI3*; all others derive from *SUI3-FL* strains. Northern signals in (C) quantified by phosphorimaging were normalized for FL-Sui3/eIF2β Western signals in (B), quantified with the Odyssey Infrared imaging system, and the resulting ratios were normalized to those determined for the *IMT2*$^+$*SUI3-FL* strain. Mean ratios and S.E.M.s from 3 independent immunoprecipitations were plotted. **(E)** *his4-301* strains harboring chromosomal P_{GAL1}*-TIF11* and plasmid-borne *TIF11*$^+$ or *tif11-17-21* and the indicated *IMT2* allele analyzed as in Fig. 2B. **(F)** *GCN4-lacZ* expression was assayed in cells cultured in SD+His ("0") or with 1mg/L sulfometuron methyl (SM) for 3h or 6h. **(G)** UUG:AUG initiation ratios were determined as in Fig. 1B. **(H)** *GCN4-lacZ* expression was measured as in Fig. 1B.

Figure 2.6.

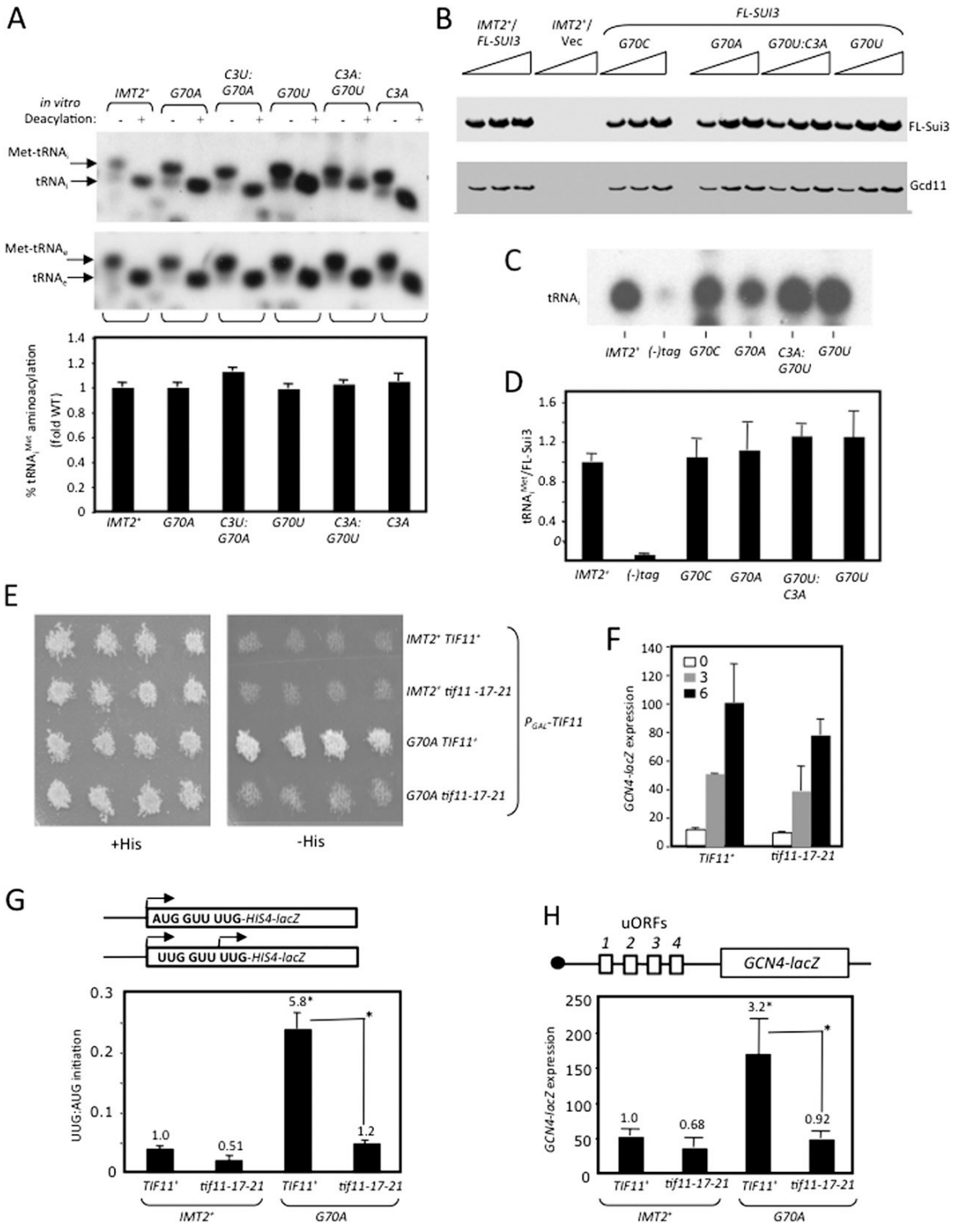
A
in vitro Deacylation:
IMT2+
G70A
C3U: G70A
G70U
C3A: G70U
C3A
Met-tRNAi
tRNAi
Met-tRNAe
tRNAe
% tRNAiMet aminoacylation (fold WT)
B
IMT2+/ FL-SUI3
IMT2+/ Vec
FL-SUI3
G70C
G70A
G70U:C3A
G70U
FL-Sui3
Gcd11
C
tRNAi
IMT2+
(-)tag
G70C
G70A
C3A: G70U
G70U
D
tRNAiMet/FL-Sui3
IMT2+
(-)tag
G70C
G70A
G70U: C3A
G70U
E
IMT2+ TIF11+
IMT2+ tif11 -17-21
G70A TIF11+
G70A tif11-17-21
PGAL-TIF11
+His
-His
F
0
3
6
GCN4-lacZ expression
TIF11+
tif11-17-21
G
AUG GUU UUG-HIS4-lacZ
UUG GUU UUG-HIS4-lacZ
UUG:AUG initiation
5.8*
1.0
0.51
1.2
TIF11+
tif11-17-21
IMT2+
G70A
H
uORFs
1 2 3 4
GCN4-lacZ
GCN4-lacZ expression
3.2*
1.0
0.68
0.92
TIF11+
tif11-17-21
IMT2+
G70A

eIF1A mutation *17-21* co-suppresses Sui$^-$ and Gcd$^-$ phenotypes of C3:G70 substitutions.

We showed previously that mutations in the SE elements of the eIF1A CTT confer Sui$^-$ and Gcd$^-$ phenotypes that are co-suppressed by the Ssu$^-$ mutation *17-21* in the SI element of the eIF1A NTT. This and other findings led us to conclude that SE mutations destabilize the open conformation of the 40S subunit and P_{OUT} mode of TC binding. Destabilization of the open/P_{OUT} state reduces the rate of TC binding and confers the Gcd$^-$ phenotype, as TC binds most rapidly to the open conformation, and also shifts the balance from the open/P_{OUT} to closed/P_{IN} state to permit more frequent initiation at UUG codons for the Sui$^-$ phenotype. The 17-21 substitution suppresses both defects by stabilizing the open/P_{OUT} state, restoring rapid TC loading and maintaining the scanning-conducive conformation at UUG codons (Saini et al. 2010).

Thus, it was of interest to determine whether the *17-21* mutation can also co-suppress the Sui$^-$ and Gcd$^-$ phenotypes of the G70A substitution. To this end, we constructed strains in which expression of WT eIF1A from a chromosomal P_{GAL1}-*TIF11* allele is repressed on glucose medium and either WT or 17-21 forms of eIF1A are expressed constitutively from plasmid-borne alleles under the native promoter. Remarkably, the His$^+$/Sui$^-$ phenotype (Fig. 2.6E) and elevated UUG:AUG initiation ratio (Fig. 2.6G), as well as the Gcd$^-$ phenotype (Fig. 2.6H), conferred by *G70A* were essentially eliminated in the *tif11-17-21* strain. This co-suppression of G70A phenotypes suggests that, like eIF1A SE elements, the C3:G70 base pair preferentially stabilizes the open/P_{OUT} conformation of the PIC.

We also demonstrated that *tif11-17-21* has little effect on induction of *GCN4-lacZ* expression in cells expressing WT $tRNA_i$ in response to starvation for isoleucine and valine, which lowers TC abundance via phosphorylation of eIF2α (Fig. 2.6F). The ability of *tif11-17-21* to block derepression of *GCN4-lacZ* in response to the G70A substitution (Fig. 2.6H), but not in response to amino acid starvation (Fig. 2.6F), supports our proposal that G70A reduces the rate of TC binding to the PIC rather than reducing TC abundance.

Evidence that substituting G70 destabilizes the open/P_{OUT} conformation of the PIC.

We sought to test our interpretation of the genetic data that G70A reduces the rate of TC binding to the PIC in a manner mitigated by the eIF1A 17-21 mutation. Measuring the rate constant for TC binding to PICs containing model mRNA(AUG), as described above, revealed a dramatic ~25-fold reduction in k_{on} for TC assembled with the G70A variant of Met-$tRNA_i$. This defect was strongly diminished in the C3U:G70A double mutant and, remarkably, was fully suppressed by the 17-21 variant of eIF1A (Fig. 2.7A and Table 2.4). The fact that the C3U substitution and eIF1A-17-21 both overcome the defect in TC binding in vitro and the Gcd^- phenotype in vivo conferred by G70A strongly suggests that a W:C pair at position 3:70 is required for rapid binding of TC to the open/P_{IN} conformation of the PIC (Saini et al. 2010).

Despite the ~20-fold decrease in k_{on}, the G70A substitution does not show a detectable increase in the K_d for TC in 43S·mRNA(AUG) complexes (Table 2.3), which implies that it also substantially reduces the k_{off} value for these PICs. Indeed, G70A eliminates detectable dissociation of TC from 43S·mRNA(AUG) complexes, leading to

Figure 2.7. Disrupting acceptor stem base pair 3C:G70 shifts the equilibrium from P_{OUT} to P_{IN}. (A-B) Determination of k_{on} values for TC association with 40S•eIF1•eIF1A complexes and mRNA(AUG) (A) or mRNA(UUG) (B). Each value is the average of at least two independent experiments. Errors are average deviations. **(C-D)** Analysis of TC dissociation from 43S·mRNA complexes for mRNA(AUG) (C) or mRNA(UUG) complexes (D). Representative curves from at least 2 independent experiments are shown. K_{off} values and end-points for dissociable complexes are given in Table 2.5 of the Supplemental Material. **(E)** PyMol rendering of the structure of yeast $tRNA_i$ from the X-ray diffraction (pdb: 1YFG), using color-coding to designate the acceptor stem (red), T-stem-loop (green), D-stem-loop (blue), and ASL (gold), and depicting by spheres bases or base-pairs implicated in start codon recognition. **(F)** Model summarizing the deduced roles of conserved $tRNA_i$ residues in start codon recognition. See Fig. 2.1 for description of the open/P_{OUT} and closed/P_{IN} states of the PIC and roles of eIF1 and the SE/SI elements of eIF1A in regulating conformational rearrangements and reactions accompanying AUG recognition. Results in this report indicate that base pair C3:G70 functions together with eIF1 and eIF1A SE elements to stabilize the P_{OUT} conformation of TC binding, whereas residues A54/A60 impede rearrangement to the P_{IN} state in manner overcome efficiently only with the perfect codon:anticodon duplex formed at AUG. G31:C39, and most likely the other two ASL G:C pairs, are required for thermodynamic coupling between AUG and $tRNA_i$ in the P_{IN} state. Not summarized here is the fact that replacing G31:C39 with other Watson-Crick pairs further stabilizes P_{IN} and thereby increases initiation at NUG near-cognates (See Figs. 2.8-2.10 for further details.)

Figure 2.7.

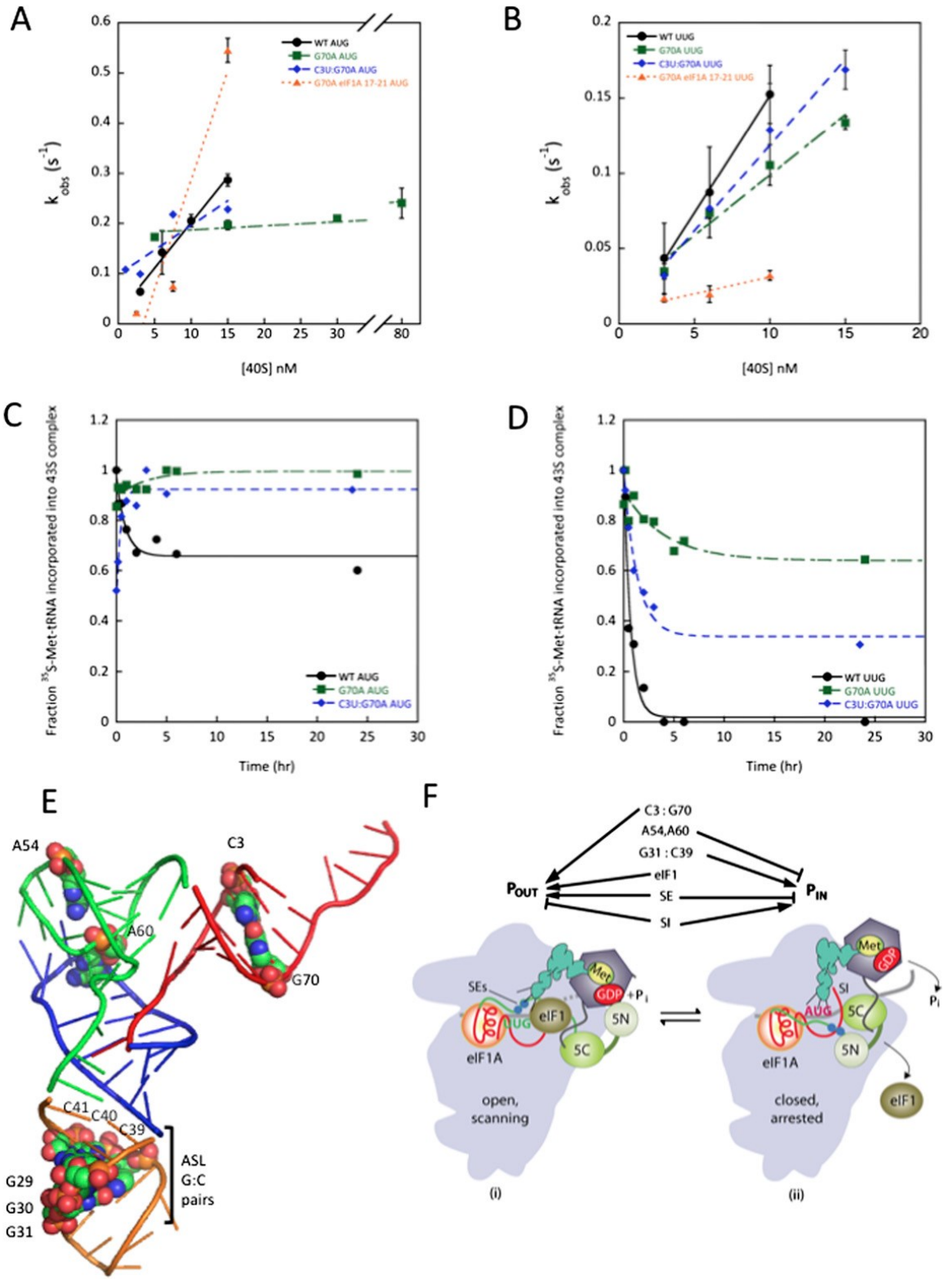
A
B
C
D
E
F
WT AUG
G70A AUG
C3U:G70A AUG
G70A eIF1A 17-21 AUG
WT UUG
G70A UUG
C3U:G70A UUG
G70A eIF1A 17-21 UUG
[40S] nM
Time (hr)
Fraction 35S-Met-tRNA incorporated into 43S complex
A54
C3
A60
G70
C41
C40
C39
G29
G30
G31
ASL
G:C
pairs
C3 : G70
A54,A60
G31 : C39
eIF1
SE
SI
POUT
PIN
SEs
Met
GDP
+Pi
eIF1
AUG
5N
5C
eIF1A
open,
scanning
closed,
arrested
(i)
(ii)

nearly 100% of the complexes being in the highly stable state (Fig. 2.7C). G70A also significantly increases the fraction of 43S·mRNA(UUG) complexes in the highly stable state, from almost none with WT to ~70% for the mutant (Fig. 2.7D). These findings support the idea that, by destabilizing TC binding to the open/P_{OUT} conformation, G70A shifts the equilibrium towards the closed/P_{IN} state, which increases the probability of UUG initiation. Supporting this interpretation, combining C3U with G70A in the double mutant, which diminishes the Sui$^-$ phenotype of G70A, also diminishes the increased formation of the highly stable state by 43S·mRNA(UUG) complexes conferred by G70A alone, from ~70% with G70A to ~35% with C3U:G70A (Fig. 2.7D).

It is intriguing that the G70A substitution has little effect on the k_{on} for 43S·mRNA(UUG) complexes, despite the fact that G70A reduces k_{on} for 43S·mRNA(AUG) complexes by ~20-fold (Fig. 2.7A,B; Table 2.4). If we adhere to our conclusion above that G70A decreases k_{on} for 43S·mRNA(AUG) complexes by reducing occupancy of the open/P_{OUT} state, we would expect a similar decrease for 43S·mRNA(UUG) complexes, as codons are not recognized in the open/P_{OUT} conformation. One explanation might be that the predicted reduction in k_{on} for 43S·mRNA(UUG) complexes conferred by slower TC loading to the open/ P_{OUT} state is offset by an increase of nearly equal magnitude in the rate of P_{OUT}-to-P_{IN} isomerization at UUG, but not AUG codons. To explain why G70A would selectively accelerate the P_{OUT}-to-P_{IN} transition at UUG, it could be proposed that G70A perturbs interaction of Met-$tRNA_i$ with eIF2 in a way that alters the orientation of TC in the P-site to favor base-pairing specifically with UUG, which entails a U:U mismatch at the first position of the codon:anticodon duplex, but not for the perfect codon:anticodon duplex at AUG. We

came to a similar conclusion recently regarding a Sui$^-$ mutation in eIF5 (*SUI5* encoding G31R) that stabilizes P_{IN} at UUG while destabilizing it at AUG (Martin-Marcos et al. 2014).

G31:C39 discriminates preferentially against near-cognates with 1st position mismatches.

Results above indicate that Sui$^-$ substitutions in the ASL and acceptor stem decrease initiation accuracy by distinct mechanisms. We asked whether they also differ in their effects on utilization of different near-cognates by comparing expression of firefly luciferase reporters harboring different start codons normalized for expression of a renilla luciferase reporter bearing an AUG codon (Takacs et al. 2011). Interestingly, the G31A:C39U ASL substitution elevates utilization of UUG, CUG, or GUG triplets, all 1st base mismatches, but not AUA or ACG near-cognates with 2nd or 3rd base mismatches; whereas this bias does not exist for the G70A substitution in the acceptor stem (data not shown). Thus, G31A:C39U differs from G70A by increasing utilization of near-cognates with 1st position mismatches.

ASL Sui$^-$ substitution G31A:C39U does not alter N6-threonylcarbamoyl modification of A37.

N6-threonylcarbamoyl modification of A37 (t^6A37) immediately adjacent to the anticodon triplet in tRNA is thought to stabilize the first base pair of the codon:anticodon duplex for the subset of tRNAs that decode ANN triplets (Agris 2008), which includes decoding of AUG by $tRNA_i$. Consistent with this, mutations that reduce t^6A37 formation

in yeast impair recognition of AUG codons (Lin et al. 2009; Daugeron et al. 2011; Srinivasan et al. 2011) and can increase the ratio of GUG to AUG initiation (El Yacoubi et al. 2011). To eliminate the possibility that G31:C39 substitutions confer Sui$^-$ phenotypes by impairing t^6A37 formation, we purified WT and G31A:C39U mutant $tRNA_i$, digested them with nuclease P1, and resolved the nucleoside products by HPLC. Quantification of the HPLC tracings revealed that both mutant and WT $tRNA_i$ contain ~1 mol of t^6A per mol of tRNA (data not shown).

DISCUSSION

In this study, we have probed the roles of highly conserved, signature residues of $tRNA_i$ in the ASL, T-loop and acceptor stem (Fig. 2.7E) in determining the stability of TC binding to the PIC in vitro and the accuracy of translation initiation in vivo. Our findings implicate the ASL base pair G31:C39, T-loop residues A54,A60 and acceptor stem base pair C3:G70 in stringent AUG selection in yeast cells, and indicate that these residues function by distinct biochemical mechanisms. All substitutions introducing purine:purine mismatches at any of the three G:C pairs in the ASL are lethal; as are most substitutions creating pyrimidine:pyrimidine mismatches at the 1st or 2nd G:C pair. By contrast, pyrimidine:pyrimidine mismatches are tolerated at the 3rd G:C pair, as are A:C or G:U wobble pairs at all three positions (Figs. 2.2F & 2.3F). We interpret these findings to indicate that disruption of the ASL helix is lethal, and that substitutions eliminating both W:C and wobble pairing have a greater effect on helix stability for the 1st or 2nd G:C pairs, owing to their internal locations, versus the 3rd G:C pair at the end of the helix. With the exception of the G:U replacement of the 3rd G:C pair, non-lethal substitutions

introducing wobble pairs at any of these positions either have no effect on initiation accuracy or, for C41U and G31A, confer moderate hyperaccuracy (Ssu$^-$) phenotypes. Much stronger Ssu$^-$ phenotypes were observed for the viable replacements of the 3rd G:C pair with the pyrimidine:pyrimidine mismatches C:C, U:C, or U:U. One way to explain these findings is to propose that any substitution that prevents both W:C and wobble pairing at any of these three positions impairs start codon recognition. For the lethal substitutions, AUG as well as near-cognate recognition would be substantially reduced, whereas non-lethal Ssu$^-$ substitutions would impair AUG recognition less dramatically while still conferring a marked reduction in near-cognate (UUG) initiation.

Our biochemical analysis of the Ssu$^-$ substitutions G31C and G31U, which introduce C:C or U:C mismatches at the 3rd G:C pair, supports this view by revealing order-of-magnitude increases in K_d for TC in PICs with mRNA(AUG) and an inability to form stable 43S·mRNA(UUG) complexes. By contrast, these substitutions do not reduce the affinity of TC for 43S PICs lacking mRNA, indicating that they disrupt thermodynamic coupling between Met-tRNA$_i$ and the start codon in the closed/P$_{IN}$ state. The fact that G31C and G31U evoke a more extensive reduction in the stability of the closed/P$_{IN}$ state at UUG versus AUG codons is consistent with the reduced UUG:AUG initiation ratio conferred by these Ssu$^-$ mutations in vivo (Figs. 2.7F & 2.8).

Further support for this interpretation comes from the fact that the U:U substitution of the 3rd G:C pair, found here to confer an Ssu$^-$ phenotype, was shown previously to increase the K_d for TC in mRNA(AUG) complexes, but not in 43S complexes lacking mRNA (Kapp et al. 2006)—the same finding made here for G31C and G31U Ssu$^-$ substitutions. This defect in TC binding was fully reversed by T-loop

Figure 2.8. Model accounting for the Ssu$^-$ phenotype of the G31C substitution that disrupts base pairing at G31:C39 in the ASL of tRNA$_i$. (A) The Ssu$^-$ phenotype of *G31C* is scored in cells harboring the *SUI5* Sui$^-$ mutation in eIF5 (substitution G31R, green asterisk in the 5N domain), which confers a Sui$^-$ phenotype by stabilizing the closed/P$_{IN}$ state at UUG codons (thick green arrow between (ii) and (iii)) (Maag et al. 2005; Martin-Marcos et al. 2013). The WT G31:C39 base pair in tRNA$_i$ stabilizes the P$_{IN}$ state on start codon recognition (black arrow above between (ii) and (iii)). **(B)** The G31C substitution (red asterisk in ASL), introducing a C31-C39 mismatch in the ASL, disrupts thermodynamic coupling between tRNA$_i$ and the start codon, destabilizing the P$_{IN}$ state (red dotted line above between (ii) and (iii)) and shifting the balance away from P$_{IN}$ at a UUG start codon. As this effect of G31 is greater at near-cognate UUG versus AUG start codons, it compensates for the ability of the *SUI5* mutation to stabilize P$_{IN}$, thereby suppressing the elevated UUG:AUG initiation ratio and Sui$^-$ phenotype conferred by *SUI5*. All symbols are as described in Fig. 2.1.

Figure 2.8.

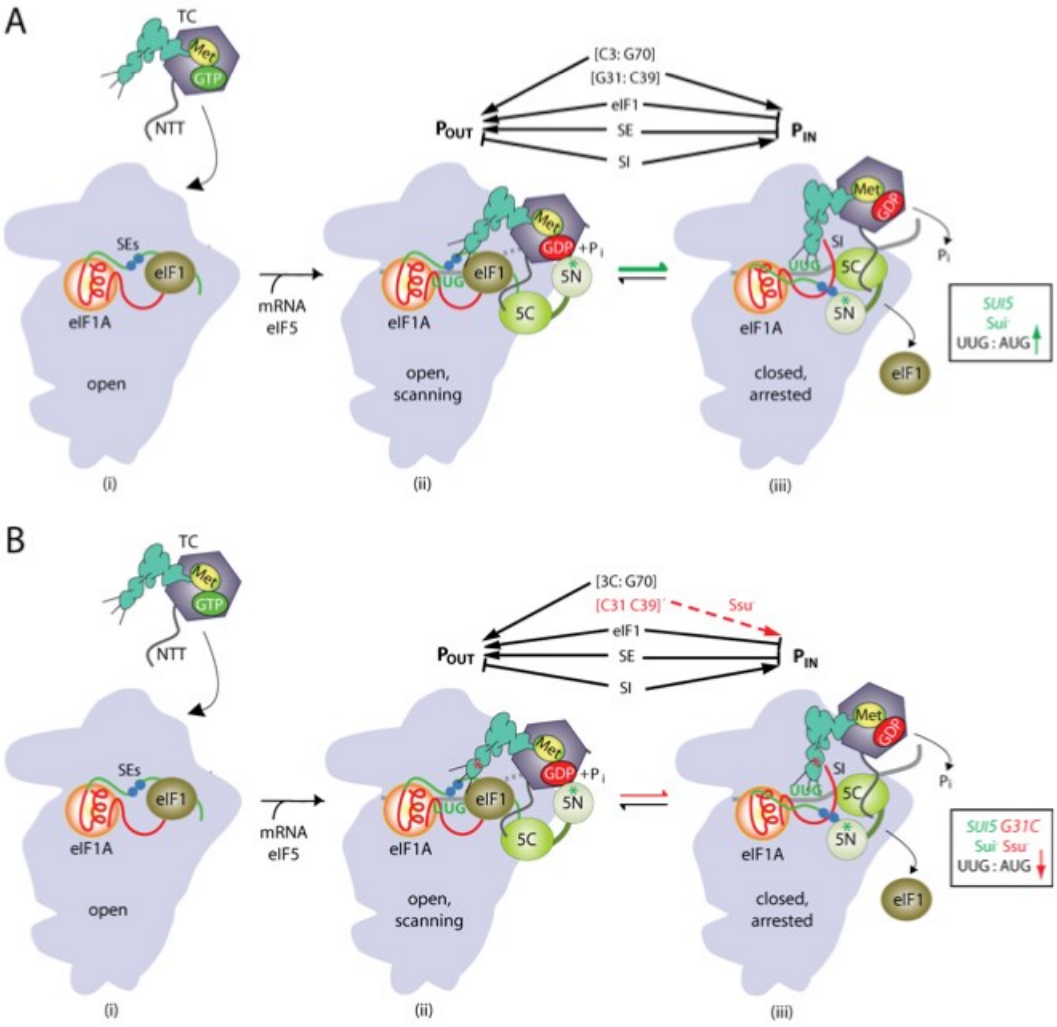
A
TC
Met
GTP
NTT
SEs
eIF1
eIF1A
open
(i)
mRNA
eIF5
[C3: G70]
[G31: C39]
eIF1
SE
SI
POUT
PIN
Met
GDP
+Pi
UUG
5N
5C
open,
scanning
(ii)
closed,
arrested
(iii)
Pi
SUI5
Sui-
UUG : AUG
B
[3C: G70]
[C31 C39]
Ssu-
SUI5 G31C
Sui- Ssu-

substitutions A54U,A60C (Kapp et al. 2006), and we found here that the Ssu$^-$ phenotype of the U31:U39 substitution is likewise reversed by A54U,A60C. The strong concordance between these biochemical and genetic data provides compelling evidence that the hyperaccuracy phenotypes of disrupting the 3rd G:C pair result from a diminished contribution of base pairing between the start codon and Met-tRNA$_i$ to the stability of the P_{IN} state, which is exacerbated by the less stable codon:anticodon duplex formed at UUG triplets (Figs. 2.7F & S2.8). It is possible that these mutations produce this effect by increasing the energetic barrier to a conformational change in the ASL that is required to attain the P_{IN} state.

How might T-loop substitutions compensate for the reduced ability to access the P_{IN} state at UUG codons conferred by the U31:U39 replacement? Perhaps altering the T-loop removes a structural impediment to the P_{IN} state that is normally overcome by the perfect AUG:anticodon duplex (Fig. 2.7F). Transition to P_{IN} might require deforming Met-tRNA$_i$ structure, and A54C/U substitutions would increase the flexibility of Met-tRNA$_i$ to reduce the energetic cost of this transition and increase its frequency at UUG codons. Interestingly, A54, A60 and m^{1}A58 in the T-loop and A20 in the D-loop participate in hydrogen bonds that rigidify the T-loop and its connection to the D-loop (Basavappa and Sigler 1991) (Fig. 2.7E). Thus, weakening T-loop/D-loop interaction by A54 substitutions might facilitate the proposed distortion of Met-tRNA$_i$ required to achieve P_{IN} in the absence of a perfect codon:anticodon match at near-cognates.

In crystal structures of bacterial 70S·mRNA·tRNA complexes, G1338 and A1339 of 16S rRNA are poised to make A-minor interactions with the minor grooves of the 1st and 2nd G:C pairs in the ASL (Korostelev et al. 2006; Selmer et al. 2006), and there is

evidence that these interactions stabilize Met-tRNA$_i$ binding to the 70S P site (Lancaster and Noller 2005) (Qin et al. 2007). Our finding that purine:purine and most pyrimidine:pyrimidine mismatches are not tolerated at the 1st and 2nd G:C pairs is consistent with this mechanism operating in yeast. This model can also explain our previous results indicating that nearly all substitutions of the corresponding yeast 18S rRNA residues (G1575 and A1576) are lethal and impair AUG recognition in cells co-expressing WT rRNA (Dong et al. 2008). The lethal or Ssu$^-$ phenotypes of substitutions disrupting W:C pairing at the 3rd G:C pair might also be attributed to an indirect disruption of A-minor interactions made by the adjacent G:C pairs. Our finding that W:C substitutions at 29:41 or 30:40 have little effect on cell growth is not inconsistent with the model because, with few exceptions, the stabilities of A-minor interactions vary little with different W:C pairs as receptors (Doherty et al. 2001; Battle and Doudna 2002). Harder to explain however is the absence of strong phenotypes associated with various substitutions that introduce wobble pairs at 29:41 or 30:40, which should strongly destabilize A-minor interactions (Battle and Doudna 2002). Therefore, more work is required to determine whether A-minor interactions of G1575 and A1576 with the ASL G:C pairs play a critical role in stabilizing the P$_{IN}$ conformation and account for the lethal or hyperaccuracy phenotypes of disrupting the ASL G:C base pairs.

In contrast to the Ssu$^-$ phenotypes produced by mutations that eliminate base pairing in the ASL, it is striking that replacing the 3rd G:C pair with any other W:C pair reduces accuracy and confers a marked Sui$^-$ phenotype. Our biochemical analysis of Sui$^-$ substitutions G31C:C39G and G31U:C39A showed that they increase the stability of TC binding with AUG and UUG codons in the P site to the point where dissociation of TC

from the PICs was undetectable. Because TC formed with WT Met-tRNA$_i$ dissociates more rapidly from UUG than from AUG complexes, the stabilization of PICs conferred by these substitutions appears to be relatively greater at UUG codons, consistent with their Sui$^-$ phenotypes. Interestingly, the G31A:C39U replacement specifically increased utilization of near-cognates with 1st position mismatches (CUG and GUG in addition to UUG) but not 2nd or 3rd position mismatches (AUA and ACG). Thus, while a base pair *per se* is required at position 31:39 for thermodynamic coupling between the start codon and anticodon of tRNA$_i$, a G:C pair is needed specifically to enforce a requirement for an A:U pair at the first position of the codon:anticodon helix.

One way to explain our finding that W:C replacements of G31:C39 stabilize P$_{IN}$ at AUG or UUG codons is to propose that, compared to other Watson-Crick base pairs, the WT G31:C39 base pair imposes an impediment to P$_{IN}$ that can be overcome efficiently only with the perfect codon:anticodon duplex formed at AUG codons. In this view, W:C replacements at 31:39 reduce this impediment, allowing "NUG" near-cognates to overcome the impediment more effectively. We envision that G31:C39, being the last base pair of the ASL, promotes a rigid conformation of the anticodon loop that clashes with a P-site element, and this clash is eliminated by a conformational change triggered by the 1st base pair of the codon:anticodon duplex. G31:C39 would be optimized to impart this inhibitory conformation of the anticodon loop in a way that could not be replaced by other W:C pairs at this position. The fact that W:C replacements at the 1st or 2nd G:C pairs evoke considerably weaker Sui$^-$ phenotypes could be explained by proposing that they act indirectly to diminish the critical function of G31:C39 in blocking the transition to P$_{IN}$ at NUG near-cognates (Fig. 2.9). Interestingly, the ASL in

Figure 2.9. Model accounting for the Sui$^-$ phenotype of the G31C:C39G double substitution that replaces G31:C39 with W-C base pair C31:G39 in the ASL of tRNA$_i$. (A) Scanning and AUG recognition in WT cells is depicted as in Fig. 2.1A. **(B)** Replacing G31:C39 with C31:G39 (green asterisk in ASL) stabilizes the P_{IN} state at NUG start codons (thick green arrows between (ii) and (iii)) to confer a Sui$^-$ phenotype specific for these near-cognate triplets. All symbols are as described in Fig. 2.1.

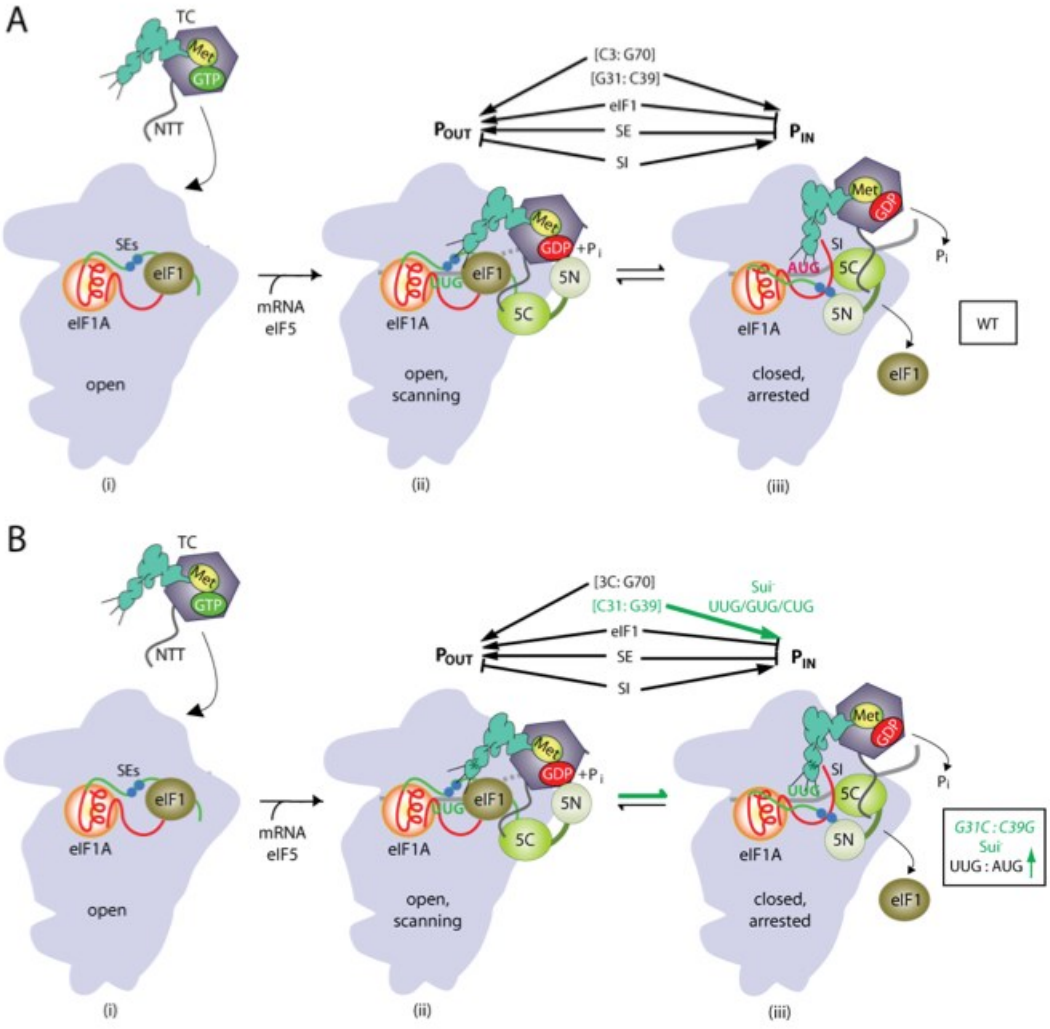

the crystal structure of *E. coli* $tRNA_i$ displays a non-canonical conformation wherein A37 interacts with G29:C41 instead of stacking on residue 36 of the anticodon loop, the ASL helix is extended by a C32:A38 base pair and its major groove is obscured (Barraud et al. 2008). If this non-canonical conformation occurs in yeast $tRNA_i$, it might be stabilized by G31:C39, and an A:U base pair at the first position of the codon:anticodon duplex could be required for isomerization to the conformation needed for a stable P_{IN} state.

There is evidence that the G1338A substitution of 16S rRNA, which appears to enhance its A-minor interaction with the ASL of $tRNA_i$, decreases initiation fidelity by compensating for mismatches in the start codon:anticodon helix (Qin et al. 2007). It is unlikely that this phenomenon is involved in the moderate Sui^- phenotypes of W:C replacements at G29:C41 and G30:C40 because these W:C replacements should, if anything, decrease the stability of A-minor interactions and increase accuracy by discriminating against mismatched codon:anticodon duplexes. Hence, we favor the alternative explanation that the W:C replacements at G29:C41 and G30:C40 decrease accuracy indirectly by impairing the critical function of G31:C39 in discriminating against near-cognates.

Although the C3:G70 base pair in the acceptor stem is a highly conserved feature of $tRNA_i$ (Marck and Grosjean 2002), no function had been ascribed to it. We found that mutations disrupting W:C pairing at C3:G70 decrease accuracy but, unlike Sui^- substitutions of G31:C39, also confer the Gcd^- phenotype signifying slower TC loading to the open conformation of the PIC. Importantly, the Sui^- and Gcd^- phenotypes of G70 substitutions were co-suppressed by the 17-21 substitution in the eIF1A NTT. The *17-21* mutation was shown previously to stabilize the open/P_{OUT} conformation of the PIC

(Fekete et al. 2007; Saini et al. 2010), and to co-suppress Gcd$^-$ and Sui$^-$ phenotypes conferred by mutations inactivating the SE elements in the eIF1A CTT (Saini et al. 2010) (Fig. 2.1) and by other mutations eliminating 40S-contact sites in eIF1 (Martin-Marcos et al. 2013). Hence, an attractive model is that C3:G70 in $tRNA_i$ acts together with eIF1 and the eIF1A Ses to promote TC binding in the P_{OUT} conformation. Disrupting C3:G70 would destabilize P_{OUT}, reducing the rate of TC loading (for the Gcd$^-$ phenotype), and allow more frequent rearrangement to the P_{IN} conformation at UUG codons (for the Sui$^-$ phenotype) (Figs. 2.7F & 2.10).

Strong support for this model comes from our in vitro findings that G70A greatly reduces the k_{on} for TC binding to 43S·mRNA(AUG) complexes in a manner mitigated by the C3U substitution (that restores W-C pairing) and fully suppressed by eIF1A-17-21. Because 17-21 stabilizes the open/P_{OUT} conformation (Cheung et al. 2007; Fekete et al. 2007; Saini et al. 2010), its ability to suppress the k_{on} defect of G70A supports the idea that G70A decreases the rate of TC binding specifically to the P_{OUT} conformation. Consistent with this, G70A stabilizes the P_{IN} state, as it reduces the rate of TC dissociation from PICs reconstituted with mRNA(AUG) or mRNA(UUG), and this defect for mRNA(UUG) complexes was diminished by C3U. This last finding supports the idea that by disrupting C3:G70, G70A elevates UUG initiation by stabilizing P_{IN} at UUG codons. Because G70A has a much smaller effect on the k_{on} of TC in PICs reconstituted with mRNA(UUG) versus mRNA(AUG), we inferred that it also increases the rate of P_{OUT}-to-P_{IN} isomerization specifically at UUG codons, which should contribute to its Sui$^-$ phenotype (Fig. 2.10).

Figure 2.10. Model accounting for the Sui$^-$ and Gcd$^-$ phenotypes of the G70A substitution in the acceptor stem and their suppression by eIF1A NTT mutation *17-21*. (A) Because the WT C3:G70 base pair specifically stabilizes the P_{OUT} mode of TC binding, the *G70A* substitution, introducing a C3:A70 Wobble pair (green asterisk) in the $tRNA_i$ acceptor stem, destabilizes the P_{OUT} state (green dotted arrows between (ii) and (iii)). As described in Fig. 2.1B for the eIF1A SE* substitution, this alteration decreases the rate of TC loading to the open complex to confer the Gcd$^-$ phenotype, but once TC binds and scanning commences, it allows rearrangement to the closed/P_{IN} state with an increased frequency at UUG codons to confer the Sui$^-$ phenotype. **(B)** Also as described in Fig. 2.1C for suppression of eIF1A-SE*, the 17-21 substitution of the SI element in the eIF1A NTT (red asterisk) counteracts the effect of the G70A substitution to restore the open/P_{OUT} conformation, rescuing rapid TC loading to diminish the Gcd$^-$ phenotype and reducing rearrangement to the closed/P_{IN} state at UUG codons to suppress the Sui$^-$ phenotype conferred by *G70A*. All symbols are as described in Fig. 2.1.

Figure 2.10.

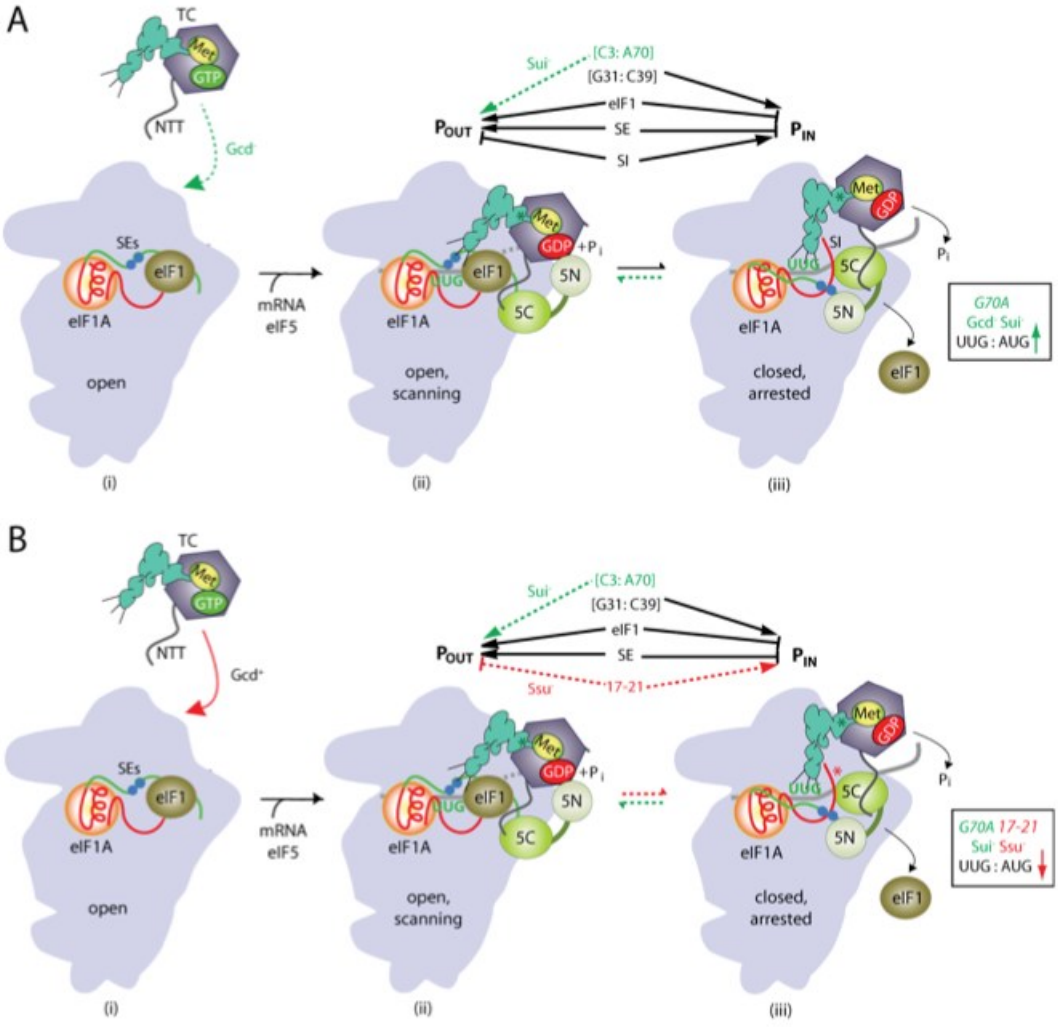
A
TC
Met
GTP
NTT
Gcd-
SEs
eIF1
eIF1A
open
(i)
mRNA
eIF5
Sui-
[C3: A70]
[G31: C39]
eIF1
SE
SI
POUT
PIN
Met
GDP
+Pi
UUG
5C
5N
open,
scanning
(ii)
closed,
arrested
(iii)
Pi
G70A
Gcd- Sui-
UUG : AUG
B
Gcd+
Ssu-
17-21
G70A 17-21
Sui- Ssu-
UUG : AUG

One way to explain the ability of G70A to disfavor the P_{OUT} mode of TC binding is to propose that eliminating the C3:G70 pair destabilizes the acceptor stem and renders the connection between Met-$tRNA_i$ and eIF2 more flexible, in a manner that is particularly detrimental for binding in the P_{OUT} state. The recent crystal structure of a *Tetrahymena* 40S·eIF1·eIF1A complex reveals that the SI element of the eIF1A NTT bridges a connection between the head and body of the 40S subunit (Weisser et al. 2013), which might indicate that the 17-21 substitution in the NTT shifts the equilibrium from P_{IN} to $P_{OUT,}$ and thereby restores rapid TC loading by the G70A variant, by weakening this connection within the 40S subunit. However, why this enhancement occurs at AUG but not UUG codons is not yet clear.

In summary, our results provide compelling evidence that the distinctive C3:G70 base pair in the acceptor stem is important for rapid TC binding in the P_{OUT} conformation of the PIC, and functions with eIF1 and the eIF1A SE elements to discriminate against UUG start codons by impeding the P_{OUT}-to-P_{IN} transition at near-cognate triplets. By contrast, G31:C39 in the ASL and A54 in the T-loop appear to function differently to block UUG initiation by imposing an impediment to P_{IN} that can be overcome only with a perfect AUG:anticodon duplex, with G31:C39 specifically enforcing the requirement for an A:U pair at the first position of the AUG:anticodon duplex. While G31:C39 discriminates against NUG near-cognates, a Watson-Crick base pair is required at this position in the ASL for P_{IN} stability and efficient start codon recognition, and disrupting base pairing at this position discriminates against near-cognates. Thus, different regions of $tRNA_i$ perform distinct functions in the PIC to promote AUG recognition in vivo. Considering that the signature residues of $tRNA_i$ are conserved in all kingdoms of life,

the functions ascribed here to these residues of yeast $tRNA_i$ likely apply to $tRNA_i$ in mammals and other eukaryotes.

MATERIALS AND METHODS

Plasmids and yeast strains. Plasmids and strains for in vivo analyses of initiator tRNA function were constructed as described (Dong et al. 2014)

Biochemical analyses of yeast cells. Northern analyses of $tRNA_i$ expression was conducted as described previously (Anderson et al. 1998). tRNA aminoacylation in vivo was analyzed using RNA isolated (Zaborske et al. 2009) and subjected to Northern analysis (Varshney et al. 1991) as previously described using oligonucleotide probes listed in the Supplemental Material. Assays of β-galactosidase activity in WCEs were performed as described previously (Moehle and Hinnebusch 1991), as were measurements of luminescence in WCEs (Dyer et al. 2000). Coimmunoprecipitation analysis of the TC was performed as described previously (Dev et al. 2010) using antibodies against FLAG (Sigma) and Gcd11 (provided by E. Hannig).

Biochemical analysis in the reconstituted yeast translation system.

M*easurements of Met-tRNA$_i$ K$_d$ values in eIF2·GDPNP·Met-tRNA$_i$ TCs.* A double filter-binding assay was utilized to measure the binding of Met-$tRNA_i$ variants to eIF2-GDPNP·Mg^{2+} (a non-hydrolyzable GTP analog) as described previously (Acker et al. 2007) with the following modifications. Recon buffer was the reaction buffer at final component concentrations of 30 mM HEPES-KOH [pH 7.4], 100 mM potassium acetate,

3 mM magnesium acetate and 2 mM dithiothreitol. The GDPNP·Mg^{2+} concentration was 500 μM. Reactions of 20 μL contained 15 μL of reaction buffer, 4 μL of the appropriate eIF2 dilution, and 1 μL of 20 nM [^{35}S]-Met-tRNA$_i$. After incubation at 26 °C the entire reaction was passed through stacked nitrocellulose–*top*–Nytran SPC (supercharged) membranes–*bottom* (both from Whatman) using a vacuum manifold (Hoefer FH225V) with 1-inch circular sample spaces. Membranes were immediately washed with 200 μL of assay buffer containing 2% glycerol. The fraction of [^{35}S]-Met-tRNA$_i$ bound to eIF2 was measured by scintillation counting of both filters and plotted against eIF2 concentration. The data were fit with a hyperbolic or quadratic binding equation, with the latter used for tight binding (Kapp and Lorsch 2004).

Measurements of TC K_d values in 40S·eIF1·eIF1A and 40S·eIF1·eIF1A·mRNA complexes. Gel shift assays were performed as described previously (Kolitz et al. 2009) with the following modifications. GDPNP·Mg^{2+} was used at 100 μM, as this lower concentration does not reduce complex formation (data not shown). TC was preformed for 15 min at 26 °C before mixing with 40S subunits at various concentrations and the remaining factors. 10X stocks of 40S subunits were prepared by serial dilution. Final component concentrations in the reactions were: 0.5 nM [^{35}S]-Met-tRNA$_i$, 100 μM GDPNP, 200 nM eIF2, 1 μM each of eIF1 and eIF1A, and mRNA (when present) at 1 μM. Complexes containing mRNA(AUG) were incubated at least 30 min at 26 °C, whereas complexes with mRNA(UUG) or lacking mRNA were incubated at least 90 min at 26 °C. Total reaction volumes were 12 μL and were mixed with 3 μL of native gel dye (Acker et al. 2007) before resolving 13 μL by gel electrophoresis at 25W for 40 min. Following

electrophoresis, gel wells were washed to remove excess free [^{35}S]-Met-tRNA$_i$. The fraction of [^{35}S]-Met-tRNA$_i$ bound to 40S·eIF1·eIF1A or 40S·eIF1·eIF1A·mRNA complexes was measured using a PhosphorImager (GE Healthcare), plotted against the 40S subunit concentration, and the data were fit with a hyperbolic or quadratic binding equation, with the latter employed for tight binding.

Kinetics of TC association and dissociation in 40S·eIF1·eIF1A·mRNA complexes

Measurements were carried out essentially as described previously (Kolitz et al. 2009). Reactions were performed in Recon buffer at final component concentrations of 250 nM eIF2, 1nM [^{35}S]-Met-tRNA$_i$, 1 μM eIF1, 1 μM eIF1A, and 10 μM mRNA. Dissociation rates (k_{off} values) were measured by monitoring the amount of labeled TC bound in 40S·eIF1·eIF1A·mRNA complexes over time using a native gel shift assay, as described above. 40S·eIF1·eIF1A·mRNA complexes were preassembled for 2h at 26°C in a reaction volume of 60 μL. Aliquots of 6 μL were removed at different times and mixed with 3 μL of a chase of unlabeled WT TC, containing 666 nM eIF2 and 300 nM Met-tRNA$_i$, representing a 300-fold excess over labeled TC. After addition of the chase to all time points, the reactions were mixed with native gel dye and loaded directly on a running native gel. A converging time course was employed so that all samples could be loaded simultaneously. The fraction of [^{35}S]-Met-tRNA$_i$ in 43S complexes was determined as described above and the data were fit with a single exponential equation.

Association rates were measured by mixing labeled TC with 40S·eIF1·eIF1A·mRNA complexes and quenching the binding reaction at various times by adding a 300-fold excess of unlabeled WT TC. Reactions were assembled as described

above using 6 µL of sample and 3 µL of chase, and completed reactions were mixed with 2 µL of native gel dye before resolving 10 µL by gel electrophoresis. As above, samples were loaded within minutes on a running native gel. The k_{obs} values were calculated by plotting the fraction of [^{35}S]-Met-tRNA bound to 40S·eIF1·eIF1A·mRNA complexes against time and fitting the data with a single exponential equation. The resulting k_{obs} values were plotted versus the 40S subunit concentrations used in different experiments and the data were fit to a straight line. The slopes of these lines correspond to the second-order rate constants (k_{ON}) for TC binding.

ACKNOWLEDGEMENTS

We are indebted to Sonia D'Silva and Eric Phizicky for analysis of t^6A37 in $tRNA_i$, Anders Bystrom and Katsura Asano for strains and plasmids, Ernest Hannig for Gcd11 antibodies, and Tom Dever for critical comments. This work was supported by the Intramural Research Program of NIH and by NIH grant GM62128 to J.R.L.

Chapter 3

Purification of yeast ribosomes using monolithic anion exchange chromatography

Antonio M Munoz[1], Jon R. Lorsch[1], Sarah E. Walker[1,2]

[1] National Institute of Child Health and Human Development, Bethesda, MD, USA

[2] Corresponding author

E-mail sarah.walker@nih.gov

ABSTRACT

Ribosomes are a critical reagent for in vitro studies of the mechanism and regulation of protein synthesis. Here, we present an optimized method for preparation of active yeast ribosomes. The use of a nitrogen mill for cell lysis coupled with chromatographic purification of the ribosomes results in 10-fold-increased yield and less variability compared to the traditional approach, which relies on sucrose cushion sedimentation. We demonstrate that these ribosomes are equivalent to those made using the traditional method in a host of in vitro assays, and that utilization of this new method will consistently produce high yields of active yeast ribosomes.

INTRODUCTION

Protein synthesis is a critical stage in gene expression and alterations in the process play key roles in a wide variety of diseases. As such, the purification of components of the translation apparatus is of great importance to many researchers. The general technique for obtaining ribosomes from yeast cell lysates via ultracentrifugation has not changed drastically since it was first developed in 1955, while the importance of active and intact yeast ribosomes for in vitro studies of translation has increased (Chao and Schachman 1955; Hinnebusch and Lorsch 2012). The ability to study the translation process in a fully reconstituted in vitro system has many advantages. Researchers can modulate concentrations of individual components while monitoring discrete steps in the translation pathway, and essential components may be modified or omitted to determine the molecular mechanisms of lethal mutations and essential components of the translation machinery. In vitro studies also allow for a more complete description of the kinetics and thermodynamics of this very complex system, by separating reactions into defined steps. In addition to kinetic and thermodynamic studies of translation, structural studies of the ribosome began with electron microscopy in the 1970s and the first crystals of bacterial ribosomes were produced in 1981 (Appelt et al. 1981). Since that time there has been significant progress starting with the first atomic resolution structures in 1991 (Bohlen et al. 1991) and more recently the cryo-EM and crystallographic studies of various eukaryotic ribosomal complexes (Passmore et al. 2007; Ben-Shem et al. 2011; Anger et al. 2013; Weisser et al. 2013; Lomakin and Steitz 2013; Taylor et al. 2009). Overall, the study of the eukaryotic ribosome continues to be a focus of much research and substantial

advantages are to be gained from improved purification of this critical cellular component.

Eukaryotic ribosomes are intrinsically challenging to purify compared to those from bacteria. Lysis of organelles in eukaryotic organisms releases cellular nucleases and proteases that require special care be taken to prevent degradation of the ribosomal RNA and protein components (Algire et al. 2002). This has often been addressed by the use of multiple protease inhibitors or the addition of heparin; however, most protocols still keep ribosomes in lysate for many hours. The common process for producing active eukaryotic ribosomes relies on ultracentrifugation of lysate through a series of sucrose cushions and gradients (Eyler and Green 2011; Fernandez et al. 2013; Acker et al. 2007). These protocols are cumbersome and the pelleting steps introduce high potential for variability and loss of product (Table 3.1). The small, glassy pellets are difficult to resuspend, can break into smaller particles that are difficult to see, and incomplete resuspension prior to running over gradients reduces total yield. Overall, the traditional protocol using sucrose cushion pelleting for ribosome purification is ripe for improvement.

Alternative protocols for ribosome purification have been employed in recent years. These include the use of various chromatographic methods (Inada et al. 2002; Leshin et al. 2010; Trauner et al. 2011) as well as PEG precipitation of ribosomes stabilized in an arrested state following cold shock (Ben-Shem et al. 2010). One such method that reduces the time ribosomes are exposed to degradatory enzymes employs a cysteine-charged resin to produce active ribosomes, but the resin is costly for large-scale purifications (Maguire et al. 2007; Leshin et al. 2010). The use of affinity tags is also common (Inada et al. 2002; Halbeisen et al. 2009) but the introduction of a tag limits the

Table 3.1. Ribosome yields from anion exchange column and sucrose cushion preparations

	40S pmols /L	**60S pmols /L**
Column Preparation (n=3)	1307 ± 61	1540 ± 139
Cushion and Nitrogen Mill (n=7)	224 ± 52	277 ± 61
Traditional Cushion Prep (n=17)	103 ± 14	134 ± 15

Mean ribosomal subunits per liter of culture are reported plus or minus the standard error of the mean.

number of strains from which researchers can purify ribosomes, and it is often preferable to test untagged components. Ribosomes are uniquely suited for anion exchange purification procedures given their ~67% rRNA content, providing large regions of negative charge density. For this reason, anion exchange chromatography has been recently employed for purification of ribosomes and various RNA transcripts (Koubek et al. 2013; Trauner et al. 2011).

Here we describe a protocol for the rapid purification of active yeast ribosomes using nitrogen mill lysis of cells and a monolithic anion exchange column for 80S separation from lysate. This strategy not only increases yields by 10-fold, but also results in higher consistency in yield and quality among preparations. We employed several in vitro assays to verify that ribosomal subunits purified by this method retain the same high activity in translation initiation as those obtained by conventional sucrose cushions. Together, these results demonstrate that anion exchange monolithic chromatography offers significant advantages for producing high yields of active yeast ribosomes in a fast and consistent manner.

RESULTS

Previous preparations of yeast ribosomes obtained by ultracentrifugation of lysates through sucrose cushions displayed a high degree of variability in yield of active ribosomes obtained (Table 3.1, (Acker et al. 2007)). We hypothesized that this variability stemmed from 1) differences in the efficiency of lysis of the yeast cells, 2) the long centrifugation steps during which ribosomes were exposed to crude lysate, and/or 3) differences in the resuspension of ribosomal pellets.

Use of Nitrogen Mill for lysis

Purification of yeast ribosomes has traditionally relied on glass beads, a blender, or a coffee grinder to lyse cells. Each of these methods has a high potential for variability leading to inconsistent efficiency of lysis when employed to extract proteins and ribosomes. To remedy this problem, we tested the efficiency of using a Nitrogen mill for lysing yeast cells for ribosome preparation. The Nitrogen mill operates similarly to a blender, in that it pulverizes yeast cells under liquid nitrogen, but offers a greater degree of control of precisely how long and at what speed cells are pulverized, allowing for less variability, and avoiding inevitable lysate explosions that occur during blender lysis when pockets of nitrogen gas build up under the cell lysate powder. Comparison of the average yield of subunits obtained using blender lysis (103 ± 14 pmols 40S/L and 134 ± 15 pmols 60S/L; n=17) to that obtained when lysis was performed with a nitrogen mill (224 ± 52 pmols 40S/L and 277 ± 61 pmols 60S/L; n=7) demonstrated a two-fold increase in ribosome recovery, indicating an increase in lysis efficiency with the nitrogen mill (Table 3.1).

Purification using monolithic QA column

In addition to differences in lysis efficiency, yields of active ribosomes could vary because of degradation during the long centrifugation in crude lysate as well as variability in the efficiency of resuspension of ribosome pellets after the two sucrose cushion steps (Algire et al. 2002). We therefore tested a chromatographic method for purification, which eliminates the sucrose cushion ultracentrifugation step as well as the

potential for variability during pellet resuspension. We chose to use a monolithic anion exchange column for several reasons. Because ribosomes are comprised of roughly 2/3 RNA, they bind anion exchange columns with high affinity. However, traditional resins generate substantial backpressure when large volumes of cell lysates are applied, so that slow flow rates must be used. A monolithic column varies from a traditional resin-packed column, in that it is made of a cross-linked polymer with a consistent, large pore size (Josic and Clifton 2007). This uniform large pore size reduces backpressure. As there are no interstitial voids, smaller cellular molecules pass quickly through the column. Because the column has a consistent pore diameter of ~1.5 μm larger species are able to bind the open structure of the monolith without reducing flow rate and introducing backpressure, thus allowing enhanced rapid and selective purification of large, megaDalton-sized molecules and complexes (Josic and Clifton 2007). The size of ribosomes (25-30 nm) is ideal for interacting with the large pores of a monolithic column. This allows higher flow rates to be used without accompanying increases in backpressure. A monolithic anion exchange column was recently used for purification of bacterial ribosomes, so we began with a similar strategy for purifying ribosomes from yeast cell lysates. To optimize binding conditions and determine the elution profile, we began by injecting salt-washed 80S ribosomes onto the column in binding buffer (20 mM HEPES•KOH [pH 7.4], 100 mM KOAc [pH 7.6], 2.5 mM $Mg(Oac)_2$, 2 mM DTT), and eluting with a linear salt gradient from 0 to 900 mM KCl (Figure 3.1A). The largest peak displayed an A_{260}:A_{280} ratio of 1.65 (data not shown), consistent with ribosome absorbance properties, and eluted at approximately 600 mM KCl (Fig. 3.1A; blue, red traces). We reasoned that because 80S ribosomes eluted at such a high salt concentration, we could increase the

Figure 3.1. Purification of ribosomes by sucrose cushion and monolithic column method. A. Elution profile of 80S on monolithic anion exchange column using a linear salt gradient. The X-axis corresponds to mL and the Y-axis is UV absorbance in mAU at 280nM (blue curve) and 260nM (red, mAu). Also shown is the concentration of buffer B (green, 0-100% Buffer containing 900 mM KCl). B. Binding the column in the absence of Dnase treatment results in two elution peaks. C. The effect of Dnase treatment on loading and elution of 80S on anion exchange column is increased yield. D. Sucrose gradient traces for cushion (D. top) and monolithic (E. bottom) methods showing separation of "junk" peak, 40S and 60S ribosomal subunits. F/G. Agarose gel of 40S and 60S ribosomal RNA quality comparison for the sucrose cushion (lanes 1 and 3) and anion exchange column (lanes 2 and 4) preparations (RNA standard far right). Bands representing specific rRNAs are labeled. G. Agarose gel as in panel F run for 30 additional minutes.

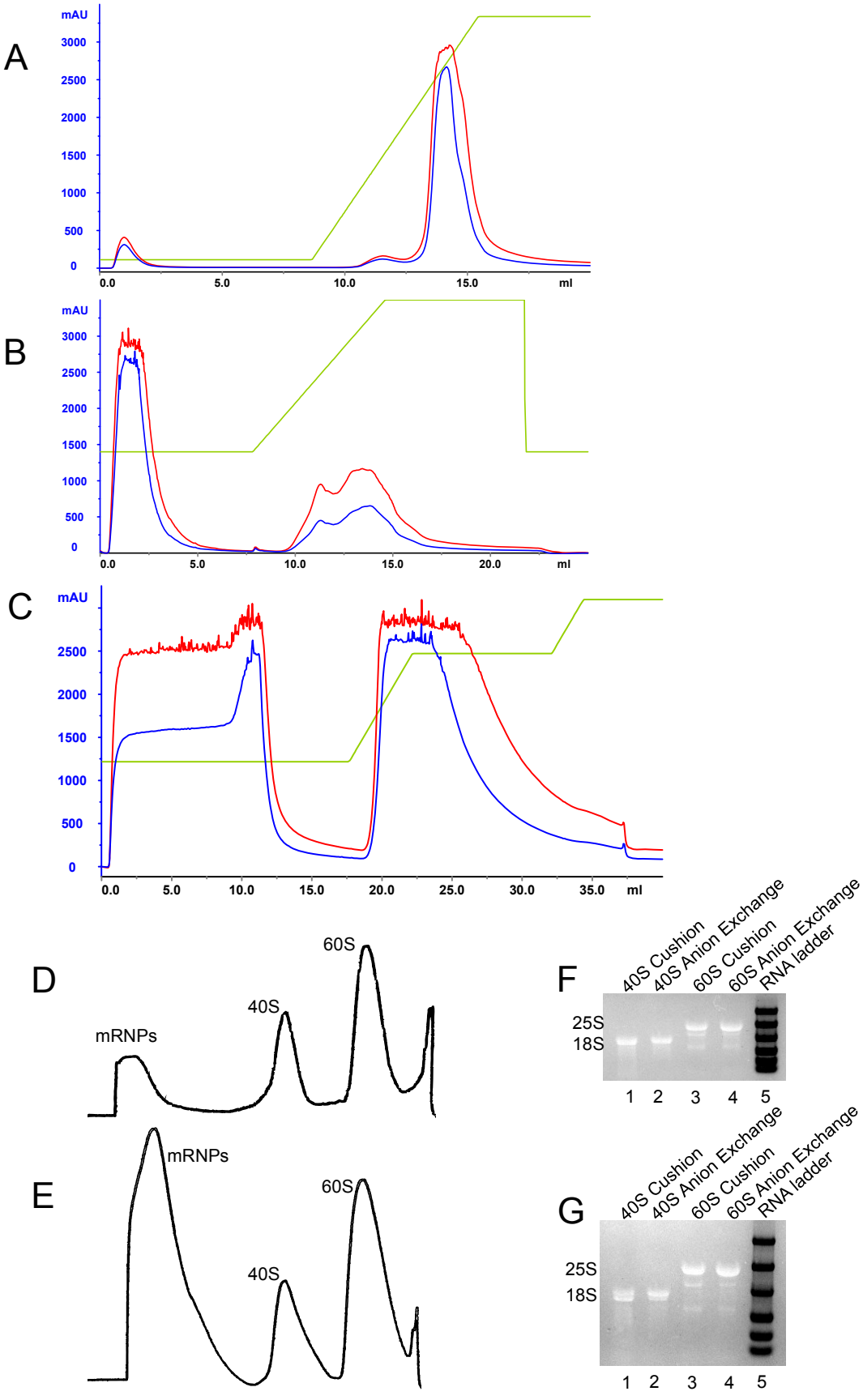
A
mAU
3000
2500
2000
1500
1000
500
0
0.0
5.0
10.0
15.0
ml
B
mAU
3000
2500
2000
1500
1000
500
0
0.0
5.0
10.0
15.0
20.0
ml
C
mAU
2500
2000
1500
1000
500
0
0.0
5.0
10.0
15.0
20.0
25.0
30.0
35.0
ml
D
60S
40S
mRNPs
E
mRNPs
60S
40S
F
40S Cushion
40S Anion Exchange
60S Cushion
60S Anion Exchange
RNA ladder
25S
18S
1 2 3 4 5
G
40S Cushion
40S Anion Exchange
60S Cushion
60S Anion Exchange
RNA ladder
25S
18S
1 2 3 4 5

binding capacity of the column by increasing the salt concentration in the binding buffer, which should prevent other negatively charged cellular components from binding weakly and occupying binding sites. We tested several concentrations of potassium chloride, and found that salt-washed ribosomes still bound the column effectively at 400 mM KCl (data not shown).,Yeast lysate was next applied to the column under these optimized binding conditions, but in contrast to the single peak observed with 80S ribosomes, we observed two elution peaks with cell lysate (Figure 3.1B). Previous work with bacterial ribosomes indicated that an additional peak eluting from anion exchange columns at a higher salt concentration from an anion exchange was DNA(Trauner et al. 2011), so we incorporated a Dnase treatment step. Running Dnase-treated lysates over the column with 400 mM KCl in the binding buffer resulted in a single elution peak (Figure 3.1C), indicating the peak eluting at the highest salt concentration in the first preparation corresponded to DNA or DNA-associated proteins bound to the column. Gel electrophoresis analysis of peak fractions alongside purified subunits indicated that ribosomal proteins and rRNA were the major components of the peak (data not shown). The elution peak was consistently found at ~600 mM KCl, so a 650 mM KCl step gradient was employed in subsequent preparations to prevent fractionation of ribosomal proteins.

Following purification of crude 80S ribosomes, subunits are dissociated by treatment with puromycin, followed by separation through a sucrose gradient. Ultracentrifugation through a sucrose gradient containing high salt serves to separate 40S and 60S subunits, and to strip the subunits of remaining RNAs and translation factors (Acker et al. 2007). To compare ribosomes from the original sucrose cushion preparation and those obtained with the anion exchange column protocol, we divided lysate from the

same culture and purified crude 80S ribosomes with each strategy. We treated the resultant crude ribosomes with puromycin, and compared the sucrose gradient traces following ultracentrifugation (Fig. 3.1D/E). Inactive ribosomes obtained previously by the sucrose cushion purification strategy have either displayed a high 40S:60S ratio due to degradation, or have not been effectively dissociated following treatment with puromycin, resulting in a high intensity apparent 80S peak and pelleted polysomes, but fewer separated subunits. Comparison of the sucrose cushion and monolithic anion exchange strategies indicates that both methods yielded gradient profiles similar to those observed previously for active ribosomes. It is worth noting that the anion exchange purification method displays a higher intensity peak for smaller cellular components (e.g. mRNPs), but these components are effectively separated from 40S subunits within the sucrose gradient.

The anion exchange column preparation yielded greater than five-fold more ribosomes (1307 ± 61 pmols 40S/L and 1540 ± 139 pmols 60S/L; n=3 for anion exchange column 40S and 60S respectively) than sucrose cushions (224 ± 52 pmols 40S/L and 277 ± 61 pmols 60S/L; n=7) (Table 3.1) when lysis of cells for both protocols was performed with a nitrogen mill. Together the combination of nitrogen mill and anion exchange column provides ~10 fold higher yield than obtained using previously published methods for blender lysis followed by sucrose cushions (103 ± 14 pmols 40S/L; 134 ± 15 pmols 60S/L culture, n=17).

Denaturing agarose gels were next used to analyze the quality of the ribosomal RNA (rRNA) from the ribosomal subunits collected after sucrose gradient centrifugation. The rRNA from the subunits made using either the sucrose cushion or chromatography

purification protocol displayed similar bands on a 1% denaturing agarose gel (Figure 3.1F). A second, lower molecular weight band in the 18S rRNA lanes from the 40S subunits, likely corresponding to nicked rRNA, is observed in both preparations when the gels are run for an extended time (Fig 3.1G). This lower rRNA band appears more intense in two independent experiments in the preparation generated using sucrose cushions than in that made using chromatography. It is possible that the shorter time spent in crude extracts decreases the amount of nicked rRNA in 40S subunits made using the anion exchange column. However, this nicked species has no effect on the activity of the ribosomes in several in vitro assays (discussed below).

Activity assays

To ensure the ribosomes purified by the anion exchange column are as active as the ribosomes purified using sucrose cushions, which have been extensively characterized, we tested ribosomes from each preparation scheme in a variety of in vitro assays monitoring individual steps of translation initiation.

We first measured the ability of the 40S subunits to form 43S preinitiation complexes, which consist of the eIF2•GTP•Met-tRNA$_i$ ternary complex (TC) and the 40S ribosomal subunit bound to initiation factors eIF1 and eIF1A (Acker et al. 2007). A non-hydrolyzable form of GTP, GDPNP, was used in these experiments to prevent P_i release. We used a native gel shift assay that monitors incorporation of ^{35}S-Met-tRNA$_i$ into the 43S preinitiation complex (PIC) to determine the dissociation constants (K_d) for TC binding in the presence or absence of a model mRNA containing an AUG codon (Acker et al. 2007). TC binds to 40S subunits from both preparations in the presence of eIF1,

eIF1A and model mRNA with a K_d below the limit of measurement (<1 nM) (Fig 3.2A; sucrose cushion, filled black circles; anion exchange, filled red squares), indicating very high affinity binding. Binding of TC in the absence of mRNA was substantially weaker, as expected for functional 40S subunits (K_ds of 13 ± 6 and 14 ± 2 nM for sucrose cushion and anion exchange subunits, n=3 respectively).

To test the ability of the ribosomal subunits to support all the steps in initiation, including 60S subunit joining to the PIC after start codon recognition, we performed a similar experiment but also included eIF5, eIF5B, and 60S subunits (Fig. 3.2B). Here, GTP was used in the TC instead of GDPNP in order to allow GTP hydrolysis by eIF2 and subsequent subunit joining. Again, no significant differences were observed between ribosomes prepared by anion exchange chromatography (even-numbered lanes) and ribosomes prepared by traditional sucrose cushion (odd-numbered lanes). Addition of GDPNP along with eIF5B traps a portion of the TC-bound complexes as 43S, but also stabilizes 80S•eIF5B complexes (lanes 1and 2; (Acker et al. 2006)). In the absence of eIF5B but presence of GDPNP (lanes 3 and 4) all complexes are then trapped in 43S. However, in the presence of eIF5B and the absence of GDPNP all PICs are joined with 60S to form 80S (lanes 5 and 6). This indicates that the subunits purified using anion exchange chromatography provide a similar level of function as that obtained from subunits purified in the traditional purification scheme in generating full 80S initiation complexes.

In addition to determining whether ribosomes bind various components and form initiation complexes, we tested their ability to undergo a conformational change from the

Figure 3.2. In vitro measurements of translation activity are consistent between the sucrose cushion (black circles) and anion exchange column (red squares) preparations. A. Formation of 43S PIC complexes is consistent between ribosome preparations. 43S PIC is measured by gel shift using radiolabeled Met-tRNA$_i$ to track TC affinity for the 40S subunit with increasing concentrations of 40S in the presence (closed points) or absence (open points) of an AUG containing model mRNA and saturating eIF1 and eIF1A. Quadratic and hyperbolic fits for the gel shown. There is no difference in affinity for ribosomes purified via traditional cushion versus chromatographic methods. B. 80S formation gel of sucrose cushion (odd numbered lanes) and anion exchange column (even lanes). 80S and 43S complexes are noted and were formed in the presence or absence of eIF5B and GDPNP (denoted with + or -). C. 1A dissociation performed on TECAN M1000 PRO using fluorescently labeled eIF1A in complexes with either sucrose cushion prepared or anion exchange column prepared 40S at AUG (closed) and UUG (open) containing model mRNAs. D. Benchtop GTPase assay displaying equivalent total level of GTP hydrolysis achieved between sucrose cushion (black) and anion exchange column (red) preparations. Rates for the first phase are 1.04 and 0.86 and for the second phase 0.056 and 0.11 for the sucrose cushion and anion exchange column preparations respectively. E. Recruitment of capped natural mRNA (*RPL41A*) to the 48S complex saturates at similar concentrations of eIF4A with ribosomes from both preparations. The fraction of radiolabeled mRNA (15 nM) bound to 43S PICs (15 nM) when incubated with 200 nM eIF3, 300 nM eIF4B and 50 nM eIF4E•eIF4G complex for 20 minutes was monitored at several indicated concentrations of eIF4A, demonstrating that ribosomes from both purification strategies behave equivalently in mRNA recruitment.

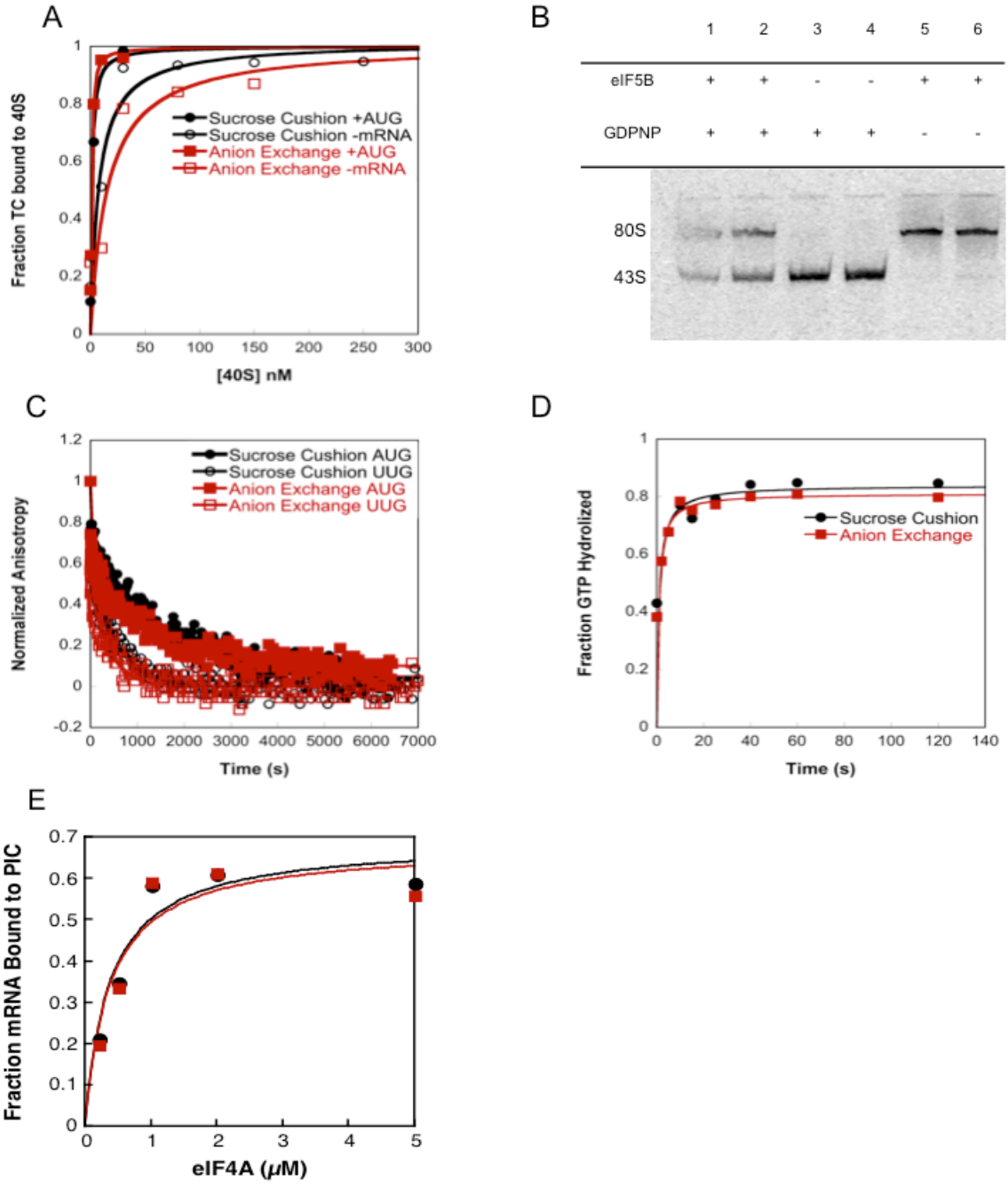
A
Fraction TC bound to 40S
[40S] nM
Sucrose Cushion +AUG
Sucrose Cushion -mRNA
Anion Exchange +AUG
Anion Exchange -mRNA
B
1 2 3 4 5 6
eIF5B + + - - + +
GDPNP + + + + - -
80S
43S
C
Normalized Anisotropy
Time (s)
Sucrose Cushion AUG
Sucrose Cushion UUG
Anion Exchange AUG
Anion Exchange UUG
D
Fraction GTP Hydrolized
Time (s)
Sucrose Cushion
Anion Exchange
E
Fraction mRNA Bound to PIC
eIF4A (μM)

open scanning competent state to the closed scanning arrested state upon start codon recognition (Hinnebusch and Lorsch 2012). Formation of the closed state is achieved after start codon recognition upon release of eIF1, movements of eIF1A, eIF5 and ribosomal elements, and the irreversible release of P_i from eIF2•GDP•P_i. We tested this activity in two ways: by monitoring the affinity of eIF1A for the PIC with mRNA with or without an AUG start codon, and by monitoring the GTPase activity of eIF2. Addition of a large amount of unlabeled eIF1A to PICs containing labeled eIF1A can be used to measure the rate of eIF1A dissociation, by following the decrease in fluorescence anisotropy of labeled eIF1A over time. Dissociation of eIF1A from the PIC occurs more slowly in the presence of an mRNA with an AUG start codon than with mRNA containing a near-cognate start codon, suggesting eIF1A binds more tightly to the closed, scanning-arrested complex. We measured eIF1A dissociation from ribosomes from both preparations (Fig. 3.2C). Ribosomes from both traditional sucrose cushion (black curves) and the anion exchange (red) preparations behave identically in this assay, giving slower rates of eIF1A dissociation with AUG (closed points) than with UUG (open points) containing mRNAs, suggesting the anion exchange column prep yields subunits that are fully capable of adopting a closed state of the PIC upon encountering a cognate start codon.

eIF2 is a GTPase and its activity is crucial for triggering downstream steps in translation initiation following start codon recognition by the PIC. Rapid GTP hydrolysis by eIF2 requires productive incorporation of the TC into a 43S PIC and the presence of the GTPase-Activating Protein eIF5. We measured the ability of 43S•mRNA complexes made with each preparation of 40S subunits to hydrolyze ^{32}P-γ-GTP incorporated into

TCs, following initiation of the reaction by addition of eIF5. Products of the reaction were separated by thin-layer chromatography, and the labeled inorganic phosphate produced quantified by phosphorimager analysis. Again, we did not observe a difference between the stocks of ribosomes prepared using sucrose cushions vs. those purified from the monolithic anion exchange column. Both samples achieve more than 80% GTP hydrolysis (Fig. 3.2D) with equivalent rate constants for the slow Pi release limited step (0.056 and 0.11 for sucrose cushion and anion exchange respectively). This indicates both pools of ribosomes are capable of rapidly adopting the closed conformation to promote irreversible GTP hydrolysis upon recognition of the start codon.

The final assay used to examine the activity of the ribosomes looked at the ability of 43S PICs to bind a natural, capped mRNA (*RPL41A*) and scan it to locate the start codon in the presence eIF3, eIF4A, eIF4B, eIF4E, and eIF4G. We found that PICs made with each preparation of 40S subunits gave similar endpoints of mRNA recruitment (0.8, sucrose cushion; 0.8, anion exchange; Fig. 3.2E) and the observed rate constants were consistent between the preparations (data not shown and (Walker et al. 2013; Zhou et al. 2014). Together, these results are consistent with a high quality of the ribosomes purified from both preparations.

In vitro studies provide critical knowledge of translation, such as information regarding concentration dependencies of individual steps that cannot be obtained in vivo. In order to ensure in vitro results of translation accurately report cellular function, it is essential to have high quality, fully active purified ribosomes. Historically, this process has involved large variability in output for reasons possibly stemming from exposure to cell lysates and variability in the techniques used to lyse cells and suspend ribosome

pellets. Here we report a protocol incorporating the use of a monolithic anion exchange column for increased yield of functional yeast ribosomes. The anion exchange column significantly reduces the time ribosomes are subjected to lysate and eliminates the pelleting steps used with traditional ultracentrifugation methods, and this results in a reduction in variability of the resulting ribosomal subunits collected (Table 3.1). When coupled to the use of a nitrogen mill for cell lysis we demonstrate greater than 10-fold increases in ribosome recovery per liter. We demonstrate here that this method produces functional ribosomes. We predict that this method will be applicable to a great number of researchers and could be easily adapted to other eukaryotic systems.

MATERIALS AND METHODS

Reagent Preparation

Eukaryotic initiation factors used in these studies, including eIFs 1, 1A, 2, and 5, as well as mRNA and ^{35}S-Met charged $tRNA_i$ were prepared as previously described (Acker et al. 2007; Walker and Fredrick 2008).

Growth and lysis of yeast cells

1.5L of YPD media in baffled Fernbach flasks were inoculated with strain YAS2488 and grown overnight to an OD_{600} of ~0.8-1 before being harvested by centrifugation at 4.5k rcf for 12 min. in a fixed angle rotor. Cells were resuspended in lysis buffer at 1/3 weight by volume and then dropped into liquid nitrogen to form “dots” which were then stored at -80°C (Acker 2007).

Lysis of frozen cells was performed using a nitrogen mill with the following parameters: Cycles=10, Precool=15min, Run=1min, Cool=2min, Rate=15. Lysates were stored as such at -80°C.

Anion Exchange Chromatography

Prior to loading on the column the lysate powder was resuspended in lysis buffer (20 mM HEPES•KOH [pH 7.4], 100 mM KOAc [pH 7.6], 2.5 mM $Mg(Oac)_2$, 2 mM DTT, 0.5 mM AEBSF, and 1 Roche complete EDTA-free protease inhibitor tablet per 50mL) at 15mL buffer/L of culture. Lysates were Dnase treated by 30 min incubation on ice with 1.25uL of Turbo Dnase (Ambion) per 10mL of resuspended lysate. It is worth noting that this Dnase is not active at higher salt concentrations. Therefore, cell lysate was only increased to 400 mM KCl after Dnase treatment prior to loading the column. Lysate was clarified by centrifugation for 30min at 13K rpm in SS34 tubes. After clarification, salt concentration was increased, by addition of 400mM KCl. Lysate was then filtered, first through glass fiber filters (Whatman) and second through 0.8 μm filters (Millipore). Filtered lysate was loaded onto the pre-equilibrated column at a flow rate of 10 mL/min. The column was washed with 25 column volumes (cv) of Buffer A (20 mM HEPES•KOH pH 7.4, 100 mM KOAc pH 7.6, 2.5 mM $Mg(Oac)_2$, 2 mM DTT, 400 mM KCl). Ribosomes were eluted using a step gradient at 50% buffer B (Buffer A + 900 mM KCl) for 5 cv, followed by 100% B for 5 cv and collected in 5 mL fractions. Figure 3.1C shows an example elution trace, with the riboosmes eluting at 50% B. Prior to storage, the column was regenerated by washing with 20 cv of 2 M NaCl. Ribosome fractions below 100 OD_{600} Units/mL were concentrated using 100K MWCO concentrators, and

fractions were pooled and diluted to 500 mM salt concentration and ~100 A260 Units/mL using no salt subunit separation buffer (50 mM HEPES•KOH [pH 7.4], 2 mM $MgCl_2$, 2 mM DTT,). Note, overconcentration of fractions can lead to ribosome precipitation, so only dilute fractions were concentrated. A 100 mM stock of puromycin was added to 1 mM final concentration and incubated for 15 minutes on ice followed by 10 minutes at 37°C. 1 mL of puromycin treated ribosomes was loaded onto prepared 5-20% sucrose gradients and spun at 27K rpm in an SW32 rotor (Beckman) for 8 hours 45 min. Gradients were pumped immediately following spin to avoid diffusion (Acker et al. 2007). Subunits were concentrated in 100K MWCO Amicon concentrators, and then buffer exchanged using no salt separation buffer until the concentration of KCl was less than 20uM, and stored at -80°C in small aliquots.

rRNA purity gels

Extracted ribosomal RNA was purified from 40S and 60S subunits using the Rneasy kit (Qiagen). 2 µg was separated on a 1% denaturing agarose gel in MOPS buffer (20 mM MOPS, 5 mM NaOAc, 1 mM EDTA, 1 mM EGTA) with 37% v/v formaldehyde, and visualized with Ethidium Bromide.

43S formation K_d measurements

Gel shift assays were performed as described previously (Kolitz et al. 2009). TC was formed by incubating GDPNP with eIF2 for 10 minutes, followed by a 5 minute incubation upon addition of tRNA.. Final reaction concentrations were 1X Recon buffer (300 mM Hepes-KOH pH 7.4, 1 M KOAc pH 7.6, 30 mM $Mg(Oac)_2$, 20 mM DTT), 300 µM GDPNP, 0.2 µM eIF2, 0.5 nM ^{35}S-Met-tRNA, 1 µM eIF1, 1 µM eIF1A, 1 µM

mRNA, and 40S concentrations as indicated. Complexes were formed by combining all components, and incubating those containing mRNA(AUG) for no less than 30 minutes, whereas complexes with mRNA(UUG) or lacking mRNA were incubated 90 minutes minimum to reach equilibrium. The fraction of radiolabeled tRNA bound to 40S was quantified in ImageQuant, plotted against 40S concentration, and fit with either hyperbolic or quadratic (in the case of apparent K_d within 3-fold that of tRNA concentration) equations.

80S Formation

Formation of 80S complexes was monitored as previously described (Acker et al. 2009).

1A dissociation kinetics

C-terminally fluorescein-labeled eIF1A was incubated with 40S, eIF1, eIF1A, mRNA and TC for 30 minutes at 26°C. Reactions were carried out in a Tecan microplate reader, with component concentrations as follows: 1X Recon buffer, 0.03 μM eIF1A-Fl, 1 μM eIF1, 0.12 μM 40S, 1 μM eIF5, 0.3 μM eIF2, 0.15 μM Met-tRNA$_i$, 0.25 mM GDPNP, and 10 μM mRNA. Final volume was 30 μL prior to injection of 15 μL in a flat black 396 well plate (Corning). Excitation and emission were 470 and 520 nm respectively. Z-position, gain, and g factor were all calculated using the preincubated sample and then set manually for the injection and kinetic monitoring. Anisotropy was monitored for the complex after addition of 3 μM excess unlabeled eIF1A via injector system. Plots were fit with a double exponential equation.

GTPase activity kinetics

GTP hydrolysis from 43S complexes was monitored as previously described (Nanda et al. 2013). 4X TC (3.2 μM eIF2, 3.2 μM Met-tRNA$_i$, 250 pM [ϒ-^{32}P]GTP) was formed for 15 min. at 26°C before mixing with 4X Ribosome complexes (1.2 μM 40S, 3.2 μM eIF1 and 3.2 μM eIF1A. 2 μM eIF5 and 20 μM mRNA(AUG) were added to the PIC and quenched with 100 mM EDTA at various times. Samples were run on polyethyleneimine-cellulose TLC plates in 0.4 M KOAc pH 3.4 buffer and the fraction of GTP hydrolyzed was quantitated using PhosphoImager analysis.

mRNA Recruitment

mRNA recruitment was measured as described (Walker et al. 2013).

Appendix A

Coordinated Movements of Eukaryotic Translation Initiation Factors eIF1, eIF1A and eIF5 Trigger Phosphate Release from eIF2 in response to Start Codon Recognition by the Ribosomal Preinitiation Complex

Jagpreet S. Nanda[‡], Adesh K. Saini[§1], Antonio M. Muñoz[‡], Alan G. Hinnebusch[§] and Jon R. Lorsch[‡]

[‡]Department of Biophysics and Biophysical Chemistry, Johns Hopkins University School of Medicine, Baltimore, MD 21205 and the [§]Laboratory of Gene Regulation and Development, Eunice K. Shriver NICHD, National Institute of Health, Bethesda, MD 20892.

[1]Present Address: Department of Biotechnology, Shoolini University, Solan, HP-173212, India.

Author Contribution:

Results presented in this appendix represent a published paper on the topic of the movement of initiation factors in response to the start codon in the Pre-Initiation Complex. Work performed as part of this publication by the author of this thesis includes but is not limited to the following results. The author performed Quikchange mutagenesis to produce 12 variant eIF5 expression vectors, and purified and fluorescently labeled five of these variant proteins. Initial analyses of mutant purity and activity were assessed by SDS-PAGE, fluorescence anisotropy for binding of eIF5 to eIF2, and eIF2-GTP hydrolysis triggered by the GTPase activating protein eIF5. The author screened for and found a FRET signal between one of these variants labeled in the eIF5 NTD and eIF1A CTD and performed initial stopped-flow kinetic analysis of this FRET change for this mutant. Some of this work is shown in Figures A.1 and A.2.

Abstract

Accurate recognition of the start codon in an mRNA by the eukaryotic translation pre-initiation complex (PIC) is essential for proper gene expression. The process is mediated by eukaryotic translation initiation factors (eIFs) in conjunction with the 40S ribosomal subunit and (initiator) $tRNA_i$. Here, we provide evidence that the C-terminal tail (CTT) of eIF1A, which we previously implicated in start codon recognition, moves closer to the N- terminal domain of eIF5 when the PIC encounters an AUG codon. Importantly, this movement is coupled to dissociation of eIF1 from the PIC, a critical event in start codon recognition, and is dependent on the scanning enhancer (SE) elements in the eIF1A CTT. The data further indicate that eIF1 dissociation must be accompanied by the movement of the eIF1A-CTT towards eIF5 in order to trigger release of phosphate from eIF2, which converts the latter to its GDP-bound state. Our results also suggest that release of eIF1 from the PIC and movement of the CTT of eIF1A are triggered by the same event, most likely accommodation of $tRNA_i$ in the P site of the 40S subunit driven by base-pairing between the start codon in the mRNA and the anticodon in $tRNA_i$. Finally, we show that the C-terminal domain of eIF5 is responsible for the factor's activity in antagonizing eIF1 binding to the PIC. Together, our data provide a more complete picture of the chain of molecular events that is triggered when the scanning PIC encounters an AUG start codon in the mRNA.

The initiation phase of translation in eukaryotes (Hinnebusch 2011; Aitken and Lorsch 2012; Jackson et al. 2010) begins with the assembly of a 43S pre-initiation complex (PIC). The PIC is formed when a ternary complex (TC) of eukaryotic initiation factor (eIF) 2, GTP and the methionyl initiator tRNA (Met-tRNA$_i$) binds to the 40S ribosomal subunit. Three initiation factors, eIFs 1, 1A and 3, associate with the 40S subunit and promote TC loading. The PIC then binds to the 5'-end of an mRNA with the assistance of the eIF4 factors, eIF3 and the poly (A)-binding protein, and subsequently scans the mRNA in search of an initiation codon. Once the initiation codon is encountered, base-pairing takes place between the anticodon of the initiator tRNA and the AUG in the mRNA, triggering a series of events that commit the complex to continuing the initiation process at that point on the message. These events include dissociation of eIF1 from the PIC and conversion of eIF2 to its GDP-bound form via gated phosphate (P_i) release, which requires the action of the GTPase activating protein (GAP) eIF5. Subsequent dissociation of eIF5 and eIF2•GDP from the 40S subunit clears the way for eIF5B•GTP-dependent joining of the 60S ribosomal subunit to form an 80S initiation complex. Subunit joining triggers GTP hydrolysis by eIF5B, releasing both it and eIF1A from the 80S complex and allowing the first round of peptide bond formation to begin.

Start codon recognition by the PIC is a critical event for accurate gene expression. Over the last decade, significant progress has been made in our understanding of the molecular mechanics underlying the accurate recognition of an AUG codon in an mRNA by the translational machinery. In the current model for this process (Hinnebusch and Lorsch 2012; Aitken and Lorsch 2012) the PIC binds to the message in an "open" conformation that is competent to scan in search of a start codon (Pestova et al. 1998). This open

conformation is induced in S. cerevisiae by eIF1 and eIF1A (Passmore et al. 2007), and is likely also stabilized by eIF3 as well. Genetic and biochemical data (Saini et al. 2010; Hinnebusch 2011) have suggested that the $tRNA_i$ in the scanning PIC is not fully accommodated in the P site of the 40S subunit and instead occupies a displaced state termed "P_{out}." Biochemical and structural studies have shown that eIF1 binds adjacent to the P site and, in fact, sterically hinders full accommodation of the initiator tRNA (Lomakin 2003; Rabl et al. 2011). The folded body of eIF1A binds in the A site of the 40S subunit, but its long, unstructured N- and C-terminal tails (NTT and CTT, respectively) reach into the P site (Yu et al. 2009). The position of the CTT is also thought to sterically occlude full access of the tRNA to the P site.

We previously showed that when the PIC encounters the start codon, eIF1 is ejected from the complex (Maag et al. 2005). We also showed that start codon recognition induces a strong direct or indirect interaction between eIF1A and eIF5 (Maag et al. 2006). A variety of data indicate that base-pairing between the anticodon of $tRNA_i$ and the start codon induces a transition from the open state to a closed one that is arrested on the mRNA (Kolitz et al. 2009). We have proposed that this codon:anticodon pairing drives the $tRNA_i$ fully into the P site (P_{in} state), which in turn ejects eIF1 and the CTT of eIF1A due to their steric clashes with the fully accommodated tRNA (Aitken and Lorsch 2012; Lorsch and Dever 2010). Release of eIF1 and interaction between eIF1A and eIF5 stabilize the closed conformation of the PIC. In addition, ejection of eIF1 was shown to set the rate of P_i release from eIF2, as eIF1 and P_i release occur with nearly the same rate constants and mutations in eIF1 that speed up or slow down its ejection have the same effect on P_i release (Algire et al. 2005; Nanda et al. 2009; Cheung et al. 2007).

Additional studies have further defined the roles played by eIF1A and eIF5 in start codon recognition, although the mechanistic basis for these roles has remained obscure (Fekete et al. 2005; Reibarkh et al. 2008). As noted above, a strong interaction between eIF1A and eIF5, dependent on the CTT of eIF1A, occurs upon start codon recognition. This interaction is sensitive to the codon in the P site and is strongly influenced by mutations in eIF5 and eIF1A that decrease (Sui^- phenotype) or increase (Ssu^- phenotype) the fidelity of start codon recognition in vivo (Maag et al. 2006; Fekete et al. 2007).

Recently, we identified elements in the CTT and NTT of eIF1A that play important roles in start codon recognition (Saini et al. 2010). Mutations in the two scanning enhancer (SE) elements in the CTT produce Sui^- phenotypes, and our data suggested that these residues function to antagonize the closed state of the PIC and/or stabilize the P_{out} state of the $tRNA_i$ relative to the P_{in} state. Two scanning inhibitor (SI) elements were also identified, one in the NTT and the other in a helix adjacent to the CTT. Mutations in these SI elements increase the fidelity of start codon recognition (Ssu^-), suggesting that the elements promote closed complex formation and/or transition to the P_{in} state of the $tRNA_i$. One way to explain these opposing functions of the SE and SI elements is that the former binds in the P site of the 40S subunit prior to start codon recognition, whereas the SI elements have affinity for a site(s) in the PIC that is incompatible with binding of the SE elements in the P site. In this model, mutation of the SE elements would facilitate removal of the CTT from the P site, stabilizing P_{in} relative to P_{out}, whereas mutation of the SI elements would have the opposite effect. Release of the eIF1A CTT from the P site upon start codon recognition presumably allows its direct or indirect interaction with eIF5

and this interaction might be the trigger for P_i release from eIF2.

There is also mounting evidence that eIF5 plays a direct role in start codon recognition in addition to its function as a GAP for eIF2. eIF5 consists of an N-terminal and a C-terminal domain (NTD and CTD), connected by a linker region (Fig. A.1A) (Wei et al. 2006; Conte et al. 2006). The NTD has an unstructured N-terminal tail, which contains the key arginine residue (R15) required for GAP function and which presumably interacts directly with the GTP- binding pocket in eIF2γ. This tail is followed by a region with a fold similar to that of eIF1 and the α/β globular domain of archaeal homologs of eIF2 β, which sits on top of a zinc-binding domain (ZBD) (Conte et al. 2006). The CTD of eIF5 is made up of a HEAT domain that has been shown to interact with eIF1, the unstructured NTT of eIF2β and the eIF3c-NTD, interactions that stabilize the yeast multifactor complex containing these eIFs (Reibarkh et al. 2008; Wei et al. 2006; Asano 2000; Yamamoto et al. 2005; Luna et al. 2012). Mutations in the eIF5 NTD have been obtained that produce either Sui^- or Ssu^- phenotypes (Huang et al. 1997; Singh et al. 2005; Asano et al. 2001), while mutations in the CTD that disrupt interaction with eIF1 and eIF2β produce Ssu^- phenotypes (Luna et al. 2012). One such Sui^- substitution in the eIF5 NTD (G31R) was shown to alter eIF5's interaction with eIF1A in a manner that stabilizes the closed complex at UUG but destabilizes it at AUG, strongly implicating the eIF5 GAP domain in the conformational rearrangement of the PIC on start codon recognition (Maag et al. 2006).

There is also evidence that eIF5 promotes AUG recognition by enhancing eIF1 dissociation from the PIC. We recently showed that high concentrations of eIF5

Figure A.1. FRET between fluorophores in the NTD of eIF5 and CTD of eIF1A in the PIC upon AUG recognition. (A) Ribbon representation of the human eIF5 NTD and yeast eIF5 CTD showing the single cysteine mutants generated in the Cys-lite background. Positions of native cysteines (C6, C289, C294) that are not involved in the Zinc-binding domain (ZBD) are shown in orange. Cytseines introduced at non-conserved surface residues are shown in blue. The cysteines involved in the ZBD (C99*, C102*, C121*, and C124*) are shown in orange. (B) Kinetics of GTP hydrolysis by eIF2, performed as described in Materials and Methods, in the presence of native eIF5 (closed circles), 'Cys-lite' eIF5 (closed squares), and Cys-lite eIF5 (S68C) (closed triangles). Points are averages from two independent experiments. (C) Steady-state fluorescence measurements demonstrating FRET in the PIC upon addition of mRNA (AUG) between the Cys- lite eIF5 (S68C) derivative labeled with fluorescein and eIF1A labeled C-terminally with TAMRA. The following complexes were assembled and their fluorescence measured as a function of emission wavelength (excitation wavelength = 490 nm): Cys-lite eIF5 (S68C)- Fl•eIF1A•eIF1•40S•TC (Donor alone; Green); eIF5(S68C)-Fl•eIF1A-TAMRA•eIF1•40S•TC (Donor + Acceptor; Blue); eIF5(S68C)-Fl•eIF1A-TAMRA•eIF1•40S•TC•mRNA(AUG) (Donor + Acceptor + AUG; Red); eIF5(S68C)-Fl•eIF1A•eIF1•40S•TC•mRNA(AUG) (Donor alone + AUG; black). The FRET change can be seen as both a decrease in fluorescein (donor) fluorescence at 520 nm and increase in TAMRA (acceptor) fluorescence at 580 nm upon addition of mRNA (AUG) to the Donor + Acceptor complex (red vs. blue curves). The emission seen at 580 nm in the Donor + Acceptor curve in the absence of mRNA (blue) is due to weak excitation of TAMRA by the incident light. No change in donor fluorescence is observed

in the absence of acceptor upon addition of mRNA (AUG) (green vs. black curves), demonstrating that the decrease in emission is due to FRET rather than a change in intrinsic fluorescence of the fluorescein moiety.

Figure A.1.

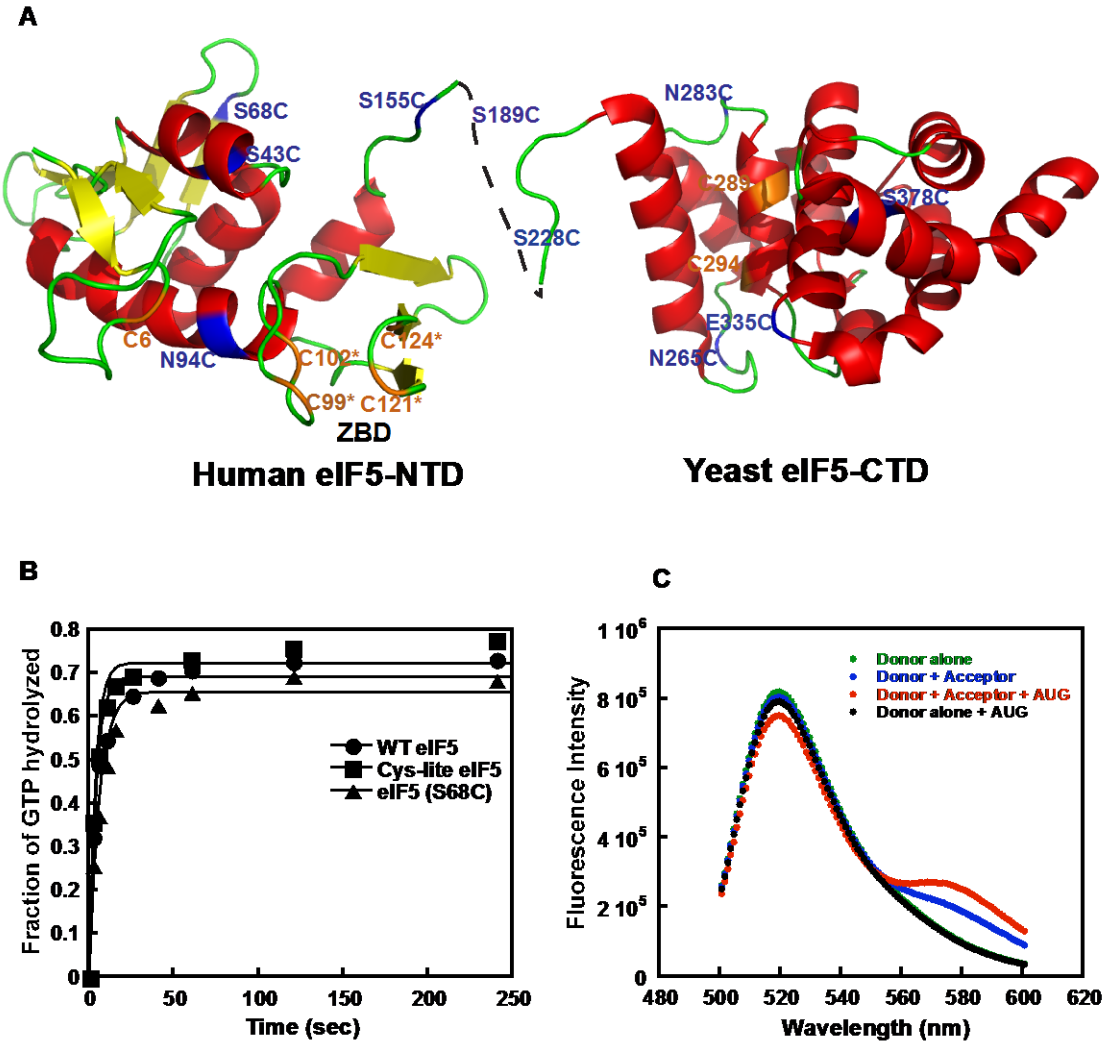

antagonize binding of eIF1 to the PIC in vitro (Nanda et al. 2009). Consistent with this observation, overexpressing eIF5 in yeast cells elevates utilization of near-cognate UUG start codons (Nanda et al. 2009), whereas overexpressing eIF1 has the opposite effect and suppresses UUG initiation (Saini et al. 2010; Valasek et al. 2004; Alone et al. 2008). Similarly, it was shown that overexpression of eIF5 in mammalian cells increases use of near-cognate codons and AUG codons in sub-optimal sequence contexts as start sites, and this effect is suppressed by co- overexpression of eIF1, consistent with the notion that high concentrations of eIF5 reduce the fidelity of start codon recognition in vivo by promoting release of eIF1 from the PIC (Loughran et al. 2012).

Based on the available data, we proposed a model in which start codon recognition induces movement of the CTT of eIF1A out of the P site, allowing it to interact with eIF5 (Maag et al. 2006; Fekete et al. 2007). This interaction could be the trigger for P_i release from eIF2, particularly if it was coupled to dissociation of the eIF5 GAP domain from the GTP-binding pocket in eIF2γ. As noted above, displacement of the eIF1A CTT from the P site should also facilitate accommodation of $tRNA_i$ in the P_{in} state of the closed complex required for AUG recognition (Saini et al. 2010; Yu et al. 2009). In addition, we proposed that upon eIF1's dissociation from the PIC one of the domains of eIF5 might move into eIF1's binding site (e.g., a site on the 40S subunit or in the unstructured NTT of eIF2 β), preventing rebinding of eIF1 and promoting transition to downstream steps in the initiation process (Nanda et al. 2009). This competition for the same binding site would explain the antagonism between eIF1 and eIF5. Recent results indicate that interaction of the eIF5 CTD with the eIF2β NTT is crucial for proper dissociation of eIF1 from the PIC and start codon recognition (Luna et al. 2012).

In this paper, we provide data that directly support and refine this model. Using fluorescence resonance energy transfer (FRET) between fluorophores on the C-terminus of eIF1A and on eIF5, we show that the CTT of eIF1A moves closer to the NTD of eIF5 in response to start codon recognition in a manner controlled by the rate of eIF1 dissociation from the PIC and dependent on the SE elements in the eIF1A CTT. Remarkably, mutations in the SE elements uncouple eIF1 release from P_i release, dramatically impairing both P_i release and movement of the eIF1A CTT while minimally affecting eIF1 release. These findings demonstrate that eIF1 dissociation is not sufficient for P_i release and that movement of the eIF1A CTT towards the eIF5 NTD is additionally required for this key step in start codon recognition. The available data suggest that eIF1 release determines the timing of these events in WT PICs by setting the rate of accommodation of $tRNA_i$ into the P site, which in turn triggers movement of the eIF1A CTT towards the eIF5 NTD. Finally, we show that the CTD of eIF5 is responsible for the factor's antagonism with eIF1 in binding to the PIC, reinforcing the notion that interaction of the eIF5 CTD with the eIF2β NTT is critical for eIF1 release and stable TC binding with $tRNA_i$ fully accommodated in the P site. Our data indicate that a multi-step series of movements of eIF1, eIF1A and eIF5 takes place in response to start codon recognition and that these events are coupled to one another in WT PICs, most likely beginning with the movement of the initiator tRNA into the P site.

Experimental Procedures

Buffers and reagents

The reaction ("recon") buffer was composed of 30 mM HEPES-KOH (pH 7.4), 100 mM

KOAc (pH 7.4), 3 mM $Mg(Oac)_2$, and 2 mM DTT. The enzyme storage buffer was composed of 20 mM HEPES-KOH (pH 7.4), 2 mM DTT, and 10% glycerol. Purification of all components was performed as described previously (Acker et al. 2007). The model mRNAs used were of the sequence $GGAA(UC)_7UNNN(CU)_{10}C$, where NNN was either AUG or AUC, (referred to as mRNA(AUG) and mRNA(AUC), respectively). The use of unstructured model mRNA obviates the need for mRNA recruitment and remodeling factors (e.g., eIF3 and eIF4F) as well as a 5'-cap and 3'-poly (A) tail.

Fluorescent labeling of WT and mutant versions of eIF1 and eIF1A WT eIF1, mutant G107K eIF1, WT eIF1A, and its mutants SE_1*SE_2* and SE_2*, where SE_1* designates (FGFESDE 121-127 AAAAAAA) and SE_2* designates (FEFGN 131-135 AAAAA) (Saini et al. 2010), were labeled at their C-termini with either Cys- Lys-e-fluorescein dipeptide, or Cys-Lys-e- TAMRA dipeptide using the Expressed Protein Ligation system as previously described (Maag and Lorsch 2003).

Fluorescent labeling of eIF5 cysteine mutants.

Single cysteine mutants of eIF5 in the Cys-lite background were generated using quick change PCR (Strategene). The eIF5 mutants were 114xpressed in BL21(DE3) Codon Plus cells (Stratgene) as described (Acker et al. 2007). The purified proteins were then fluorescently labeled with fluorescein-maleimide (Nanda and Lorsch 2014).

Measurement of TC binding kinetics

Measurement of the kinetics of TC binding to 40S subunits were carried out using the native gel assay as described (Nanda et al. 2009). Component concentrations were 0.5-1

nM [^{35}S]-Met-tRNA$_i$, 200 nM eIF2, 1 μM eIF1-G107K, 1 μM eIF1A, 200 nM 40S subunits and 1mM GDPNP•Mg^{2+}. The experiments were carried out in the absence of eIF5 and the presence of full-length eIF5, or the isolated eIF5 NTD or CTD. The concentration of eIF5 or its domains was saturating (2 μM) for effects on TC loading (data not shown). Data were fit with a first-order exponential equation to determine the observed pseudo-first order rate constants for TC binding. The reactions were pseudo-first order because the concentrations of 40S subunits and initiation factors were much higher than the concentration of labeled Met- tRNA$_i$.

Measurement of the dissociation from the PIC The kinetics of eIF1 dissociation from the PIC in response to recognition of a start codon was measured on an SX.180MV-R stopped-flow fluorometer (Applied Photophysics) as described previously (Nanda et al. 2009). Briefly 43S complex was made with 50 nM fluorescein-labeled WT eIF1 or eIF1-G107K (donor), 60 nM TAMRA–labeled WT or mutant eIF1A (acceptor), 100 nM 40S subunits, and 450 nM TC (made with GDPNP). This was mixed rapidly with an equal volume of 20 μM mRNA(AUG) and 6 □M unlabeled eIF1 as chase. When full-length eIF5 or its domains were included, they were used at a final concentration of 2 μM. Loss of FRET between the two factors was observed as an increase in fluorescein fluorescence. The data were fit with a double exponential equation, with the first phase corresponding to a conformational change and the second to eIF1 dissociation.

P$_i$ release kinetics

The kinetics of phosphate release from 43S complexes in response to start codon recognition was measured by monitoring GTP hydrolysis using a rapid quench device

(Kintek) as described previously (Nanda et al. 2009). TC was formed at 4X concentration: 3.2 μM eIF2, 3.2 μM Met-tRNA$_i$, and 250 pM □[^{32}P]GTP were incubated in 1X recon buffer for 15 min at 26℃. Ribosomal complex was also made at 4X concentration in 1X recon buffer using 800 nM 40S subunits, 3.2 μM eIF1, and 3.2 μM eIF1A. Equal volumes of TC and ribosomal complex were mixed with 2 μM of eIF5 and 20 μM mRNA (AUG) in a rapid quench. Reactions were quenched at different times with 100 mM EDTA. The samples were than run on PEI-Cellulose TLC plates using 0.3 M KPO_4 buffer, pH 4.0 as the mobile phase, followed by PhosphorImager analysis to quantify the fraction of GTP hydrolyzed over time. The data were fit with a double exponential rate equation. The first phase corresponds to GTP hydrolysis and the second phase corresponds to P_i release, which drives GTP hydrolysis forward (Algire et al. 2005).

Determination of steady state FRET efficiencies between eIF5-Fluorescein and eIF1A-TAMRA For each experiment two identical samples were prepared. One contained the 43S complex assembled with eIF5-Fl and unlabeled eIF1A. This was designated as a "donor alone" complex. The second complex was assembled with eIF5-Fl and eIF1A–TAMRA. This was designated as a "donor + acceptor" complex. In both cases the concentrations of reagents were 100 nM eIF5-Fl, 200 nM eIF1A (labeled or unlabeled), 100 nM 40S subunits, 1 μM eIF1, 200 nM TC and 10 μM mRNA (AUG). After mixing all the components, the fluorescein fluorescence was monitored as a function of time using λ_{ex} = 490 nm and λ_{em} = 520 nm on a Spex Fluorolog-3 fluorometer. When equilibrium had been achieved (as indicated by stabilization of fluorescence intensity), samples were excited at 490 nm and fluorescence emission was

measured as a function of wavelength from 505-600 nm. Repeated measurements of the same sample gave identical results. FRET efficiency was calculated as $1-I_{DA}/I_{D,}$ where I_{DA} is the fluorescence intensity at 520 nm of the donor + acceptor sample and I_D is the intensity at 520 nm of the donor alone sample (Shih et al. 2000).

Measurement of the kinetics of the change in eIF1A-eIF5 FRET in response to start codon recognition by the PIC Measurement of the change in eIF1A-eIF5 FRET in the PIC in response to start codon recognition was performed using an SX.180MV-R stopped- flow fluorometer (Applied Photophysics). Briefly, 43S PICs were assembled using 400 nM WT or mutant eIF1A-TAMRA, 200 nM eIF5-Fl, 200 nM 40S subunits, 400 nM TC (made with GDPNP), 800 nM eIF1 for 1hr at 26℃ in 1X recon buffer. This 2X complex was mixed with an equal volume of 20 μM mRNA (AUG or AUC). The increase in FRET between the dyes on the two labeled proteins with respect to time was measured as a decrease in fluorescein fluorescence. The data were fit with a double exponential equation.

General Kinetics

All kinetic experiments were repeated at least 3 times. The rate constants presented are averages, and the errors are mean deviations. Control experiments indicated that photo-bleaching was not significant on the time scale of any of the experiments.

Results

The CTT of eIF1A and N-terminal domain of eIF5 move closer to each other upon start codon recognition

We showed previously that a direct or indirect interaction of the eIF1A CTT with eIF5 is crucial for stabilizing the closed, scanning arrested conformation of the PIC (Maag et al. 2006). To further explore this interaction, we sought to observe fluorescence resonance energy transfer (FRET) between fluorescently labeled positions in eIF5 and the C-terminus of eIF1A. We reasoned that such a FRET signal could be used to monitor movements of eIF5 and eIF1A taking place within the PIC during the rearrangement from its open to closed conformations. To this end, we engineered a variety of eIF5 derivatives labeled site-specifically on single cysteine residues with fluorescein-maleimide and then tested for FRET in the PIC between these positions and eIF1A labeled C- terminally with TAMRA.

Yeast eIF5 has seven cysteines (Fig. A.1A; shown in orange), four of which are part of a stable zinc-binding domain (ZBD) in the N- terminal domain (eIF5-NTD) (Conte et al. 2006) (Figure A.1A; orange ZBD residues). The three non-ZBD cysteines, C6, C289, and C294, are located on the surface of the N- and C-terminal domains of the protein (Fig. A.1A), and are not conserved in eukaryotic eIF5s, including those found in various plant, animal and even other fungal species. We generated a "Cys-lite" derivative of eIF5 in which the three non-ZBD cysteines were changed to serines (Fig. A.1A). The ZBD cysteines were not changed, as they are important for maintaining the structure of eIF5 and are tightly coordinated to Zn^{2+} (Conte et al. 2006) and thus should be resistant to modification. Consistent with this last prediction, the Cys-lite protein is not modified by fluorescein- maleimide (data not shown). Cys-lite eIF5 was purified and its ability to stimulate GTP hydrolysis by eIF2 in PICs was tested using a reconstituted S. cerevisiae translation initiation system. The results show that 2 μM Cys-lite eIF5 stimulates GTP

hydrolysis to the same rate observed for the WT factor at the same concentration (Fig. A.1B). The ability of the Cys-lite eIF5 to promote closed complex formation in conjunction with eIF1A upon start codon recognition was also tested by measuring rates of eIF1A dissociation from the PIC in the reconstituted system (Maag et al. 2006) and the mutant protein was found to behave indistinguishably from native eIF5 (data not shown). Next we generated various single cysteine mutants of Cys-lite eIF5 by introducing cysteines at non-conserved, surface-exposed positions in the NTD, CTD, and linker region using site-directed mutagenesis (Table A.1). These mutants were then expressed in E. coli, purified and the cysteine residues labeled with fluorescein-maleimide (Nanda and Lorsch 2014). We also labeled the three naturally occurring cysteines at residues 6, 289, and 294 in variants containing each one as the only surface-exposed cysteine (Table A.1). We then screened all of our fluorescein-labeled Cys-lite eIF5 mutants for FRET with C-terminally TAMRA-labeled eIF1A in reconstituted PICs (also containing eIF1, TC and 40S subunits; TC contained GDPNP in place of GTP to prevent GTP hydrolysis and P_i release). The fluorescein dye was excited at 490 nm and emission monitored as a function of wavelength. Experiments were performed in the absence and presence of an unstructured model mRNA with a central AUG codon (mRNA (AUG)). Labels at two positions in the NTD of eIF5, S68C and N94C, showed FRET with the TAMRA on the C- terminus of eIF1A only after addition of the model mRNA, with the largest decrease in donor (fluorescein) emission at 520 nm. The FRET efficiency observed with the S68C (eIF5-S68C-Fl) mutant was ~10% (Fig. A.1C). A corresponding increase in acceptor (TAMRA) emission at 580 nm was also observed (compare red and blue curves in Fig. A.1C). No change in emission intensity upon

Table A.1: Fluorescently-labeled cys-lite eIF5 variants

eIF5 Variant	Domain
C6*	NTD
S43C	NTD
S68C	NTD
N94C	NTD
S155C	NTD
S189C	Linker
S228C	Linker
N265C	CTD
N283C	CTD
C289*	CTD
C294*	CTD
E335C	CTD
E378C	CTD

Φιγυρε Α.. Native Cysteines in eIF5

addition of mRNA (AUG) was observed with PICs made with eIF5-S68C-Fl and unlabeled eIF1A (Fig. A.1C, black curve, "donor alone + AUG") indicating that the decreased fluorescein emission observed with complexes containing eIF5-S68C-Fl and TAMRA-labeled eIF1A is due to FRET rather than a change in intrinsic fluorescence of the fluorescein dye. Similar results were observed with the N94C mutant, although the extent of the FRET change was smaller (~7 %) and thus we chose to pursue the S68C mutant instead. No FRET was observed with dyes in the linker region or the CTD, suggesting these domains are farther from the C- terminus of eIF1A in the PIC after start codon recognition than is the NTD of eIF5. The decrease in fluorescein fluorescence (increase in FRET) after mRNA binding suggests that AUG recognition leads to movements within the PIC that bring the C-terminus of eIF1A and the NTD of eIF5 closer together. The fluorescence anisotropy of eIF5-S68C-Fl bound to the PIC is 0.157 and that for eIF1A-TAMRA is 0.260. These values are considerably below the theoretical maximum of 0.4, indicating that the dyes in the PIC still have significant conformational flexibility and that changes in FRET are not due to changes in (fixed) orientations between the fluorophores (Lakowicz 1999). Thus the increase in FRET reflects a decrease in distance between the two dyes.

To probe the events reported on by this change in FRET, we monitored the kinetics of the decrease in fluorescein fluorescence upon addition of mRNA (Fig. A.2A). PICs containing eIF1A- TAMRA, eIF5-S68C-Fl, eIF1, TC and 40S subunits were rapidly mixed with mRNA (AUG) in a stopped-flow fluorimeter, and the decrease in fluorescein fluorescence monitored over time (λ_{ex} = 490 nm, λ_{em} = 520 nm). The resulting curve

Figure A.2. Increase in FRET between the eIF1A CTT and eIF5 NTD is dependent upon AUG codon recognition and is coupled to release of eIF1 from the PIC (A) Kinetics of eIF1A-eIF5 FRET change upon binding of mRNAs to the PIC. Increase in FRET (decrease in fluorescein fluorescence) between Cys-lite eIF5 (S68C)-Fl and eIF1A-TAMRA in the PIC after addition of mRNA(AUG) (red). No FRET change was observed when buffer alone was mixed with labeled PICs (black; -mRNA) or when the same model mRNA with an AUC codon in place of the AUG codon was used (green), indicating the FRET decrease is triggered by recognition of an AUG start codon. Curves were fit with a double exponential rate equation. Curves are the averages of three independent experiments. (B) Comparison of the kinetics of the eIF1-eIF1A FRET (red), eIF1A-eIF5 FRET change (orange), and P_i release (green) upon start codon recognition by PICs assembled with WT or mutant versions of eIF1. Values are averages from at least three independent experiments and error bars represent average deviations ($p < 0.05$ for differences in rates between WT and mutants).

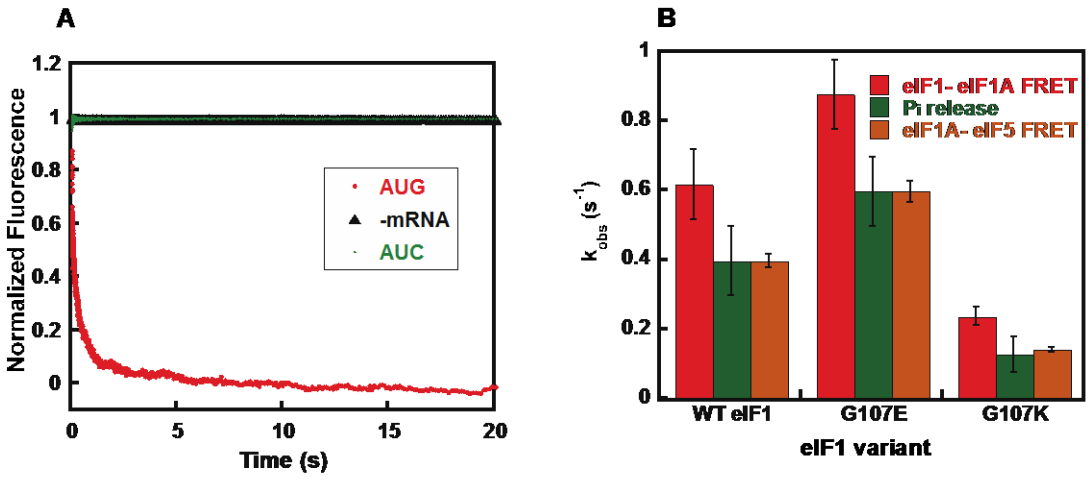

(Fig. A.2A) was biphasic; the first phase had a rate constant (k_1) of 24 s^{-1} and a normalized amplitude of 0.5, and the second phase had a rate constant (k_2) of 0.4 s^{-1} and an amplitude of 0.5. k_2 is strikingly close to the rate constants for release of eIF1 and P_i upon start codon recognition (0.6 and 0.4 s^{-1}, respectively). This observation suggests that these events are controlled by the same rate- limiting step in WT PICs. As for the eIF1 and P_i release steps (Maag et al. 2005; Algire et al. 2005) the rate of the increase in FRET efficiency between fluorophores on the C-terminus of eIF1A and the NTD of eIF5 depends on the identity of the start codon in the mRNA. Replacing the AUG codon with an AUC codon led to a complete loss of the increase in FRET, to the same extent as leaving out mRNA altogether and mixing the PICs with buffer alone (compare green AUC and black –mRNA curves in Fig. A.2A). Thus the change in FRET signal occurs in response to recognition of a start codon in the mRNA.

The increase in FRET between the eIF1A-CTT and eIF5-NTD is coupled to release of eIF1 from the PIC

The fact that the newly identified eIF1A- eIF5 FRET signal is dependent on an AUG start codon (Fig. A.2A) suggested that it might also be governed by eIF1 dissociation from the PIC. To address this possibility, we tested the effects of two mutations in eIF1 that were shown previously to speed up (G107E) or slow down (G107K) release of the factor from the PIC upon start codon recognition. In previous work these mutations were shown to have corresponding effects on the rate constant for P_i release (Nanda et al. 2009) and these findings were confirmed here for both mutants (Fig. A.2B, eIF1 release and P_i release; in both cases eIF5 was included in the PICs). The stopped-flow experiments

monitoring FRET between eIF1A and eIF5 were repeated with PICs made with eIF1-G107E or eIF1-G107K. Remarkably, as with the rate constants for eIF1 release and P_i release, we found that G107E consistently increased the rate constant for the slow phase of eIF1A-eIF5 FRET by 1.5-fold ($p < 0.05$). Likewise, the G107K mutant decreased the rate constant for the slow phase by 4-fold, the same extent as it decreased the rate constants for eIF1 and P_i release. These data support the possibility that the rate of eIF1 release directly or indirectly governs the rate of the movement of eIF1A and/or eIF5 that produces the FRET change.

Mutations in the SE elements in the CTT of eIF1A uncouple release of eIF1 and P_i from the PIC in response to start codon recognition

Having obtained evidence that the eIF1A CTT gets closer to the eIF5 NTD in the PIC on AUG recognition, we wished to determine the role of the SE elements in the CTT of eIF1A in this movement. The SE elements (SE_1 and SE_2) are comprised of two loosely conserved tandem repeats of 9-10 residues located in the beginning of the unstructured CTT, each containing a pair of invariant Phe residues as critical constituents. We showed previously that the SE elements have partially overlapping functions that stabilize the open conformation of the PIC and promote scanning through near-cognate start codons, and also support rapid TC loading in the P_{out} state. Replacing 7 of the 9 residues of SE_1 with alanines (SE_1*) and 5 of the 10 residues of SE_2 with alanines (SE_2*) is sufficient to inactivate each element, but combining these substitutions in a single mutant (SE_1*,SE_2*) is required to eliminate their overlapping contributions to TC recruitment and accurate start codon selection (Saini et al. 2010). As SE_2 is more potent than SE_1, we

chose to examine the SE_2* single mutant and SE_1*,SE_2* double mutant in the experiments described below.

Versions of these two mutant factors were labeled with TAMRA on their C-termini for use in FRET experiments. PICs were assembled with eIF5-S68C-Fl and either eIF1A-SE_2*-TAMRA or eIF1A-SE_1*,SE_2*-TAMRA and then mixed rapidly in the stopped-flow device with mRNA(AUG). The rate constants of the first phase of the decrease in fluorescein fluorescence were unchanged by the mutations relative to the values observed with WT PICs (28 and 20 s^{-1} with the SE_2* and SE_1*,SE_2* mutants, respectively vs 24 s^{-1} with WT eIF1A), although the amplitudes were decreased relative to the slow phases (Fig. A.3A; Table A.2). Remarkably, however, the rate constant for the slow phase was decreased 20-40-fold by the SE mutations relative to the value with the WT factor (Fig. A.3A; Table A.2). These findings indicate that the SE elements are required for rapid movement of eIF1A with respect to eIF5 upon start codon recognition.

We then asked whether the SE mutations evoke corresponding reductions in the rates of eIF1 and P_i release from reconstituted PICs. eIF1 release was monitored as a decrease in the efficiency of FRET between fluorescein-labeled eIF1 and the TAMRA-labeled eIF1A mutants. 2 μM eIF5 was included for consistency with the eIF1A-eIF5 and GTPase/P_i release assays. Using this assay with the WT factors, we previously showed that start codon recognition triggers a biphasic decrease in FRET (increase in fluorescein fluorescence) between the two fluorophores on the C-termini of the respective factors (33). The first phase is thought to correspond to a conformational change within the PIC that moves the two fluorophores apart and the second phase was shown to correspond to

Figure A.3. Effect of mutations in the SE elements in the eIF1A CTT on the kinetics of the eIF1A-eIF5 FRET change, eIF1 release, and P_i release in response to AUG recognition. (a) The kinetics of the increase in eIF1A-eIF5 FRET on AUG recognition was measured as a decrease in fluorescein (donor) fluorescence after rapid mixing with mRNA (AUG) in a stopped- flow fluorometer. Pre-initiation complexes were assembled with eIF5 (S68C)-Fl and either C- terminally TAMRA-labeled WT eIF1A (black); eIF1A-SE_1*,SE_2* (red); or eIF1A-SE_2* (blue). Curves were fit with double exponential rate equations. The data shown are the averages of three experiments. (b) The kinetics of the decrease in eIF1-eIF1A FRET in the PIC upon start codon recognition was monitored as an increase in fluorescein (donor) fluorescence between eIF1-Fl and eIF1A-TAMRA after rapid mixing of PICs and mRNA (AUG) in a stopped-flow fluorometer. Curves were fit with double exponential rate equations. The first phase corresponds to a conformational change in the PIC upon start codon recognition and second phase to eIF1 release. PICs were assembled with C-terminally labeled WT eIF1A (black); eIF1A-SE_1*,SE_2*(red); or eIF1A-SE_2*(blue). 2 μM eIF5 was included for consistency with eIF1A-eIF5 FRET and GTPase experiments. The data shown are averages from three experiments. (c) The kinetics of GTP hydrolysis and P_i release from 43S PICs was measured after addition of eIF5 and mRNA (AUG). Time points from reactions were stopped with 100 mM EDTA, and □-^{32}P-GTP and □-^{32}P-P_i were then separated using PEI-cellulose TLC and quantified by phosphorimager analysis. The fraction of GTP hydrolyzed versus time was plotted and the data fit with a double exponential rate equation. The fast phase corresponds to GTP hydrolysis and the slower phase to P_i release. PICs were assembled with WT eIF1A (black circles); eIF1A-SE_1*,SE_2* (red

squares); or eIF1A-SE2* (blue triangles).

Figure A.3.

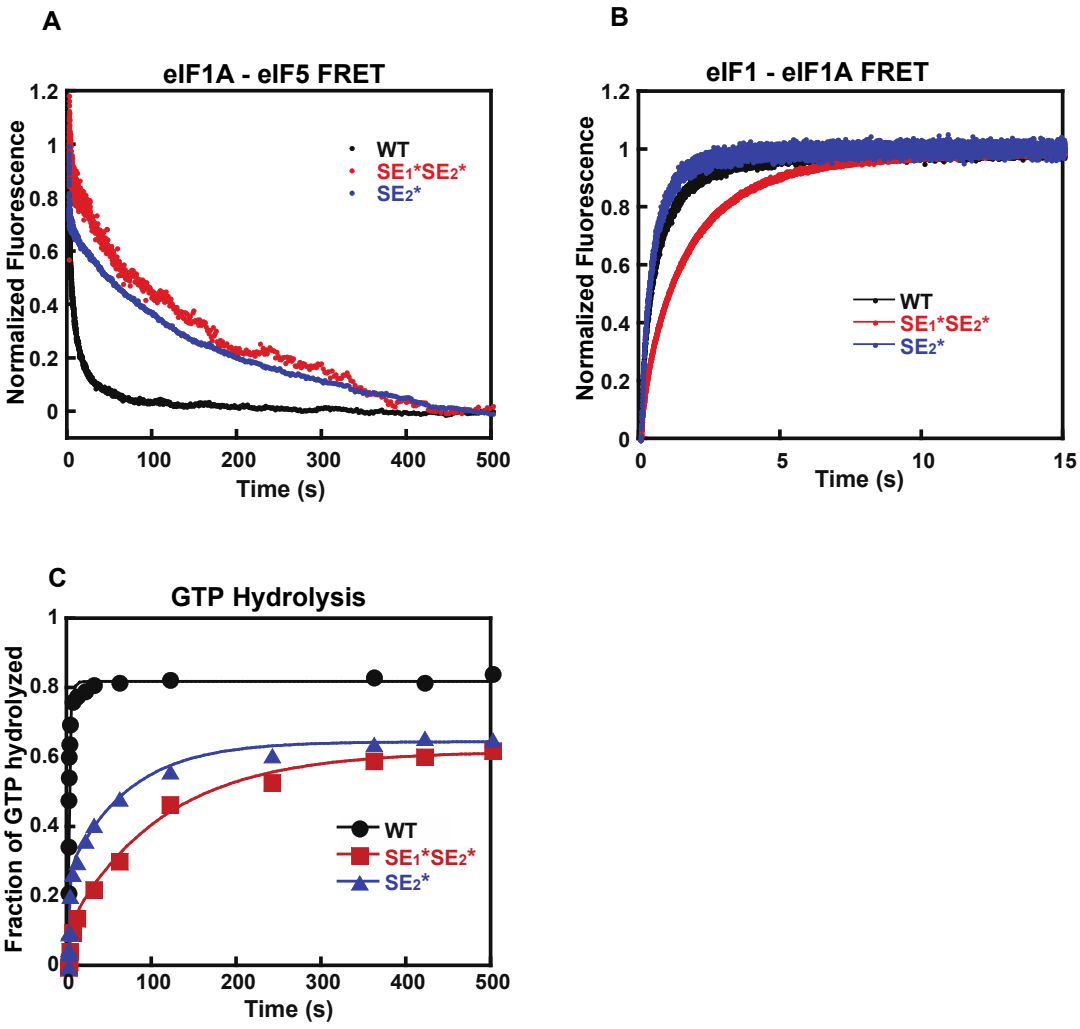

Table A.2: Kinetic parameters for the FRET change between eIF1A variants and eIF5 in PICs upon AUG recognition

eIF1A variant	k_{obs} (s^{-1})	Amplitude (a)
WT	k_1= 24 ± 4.0 k_2= 0.4 ± 0.1	a_1= 0.5 ± 0.1 a_2= 0.5± 0.1
SE_2*	k_1= 28 ± 6.0 k_2= 0.02 ± 0.1	a_1= 0.3 ± 0.05 a_2= 0.7 ± 0.1
SE_1*,SE_2*	k_1= 20 ± 8.0 k_2= 0.01 ± 0.005	a_1= 0.15 ± 0.05 a_2= 0.80 ± 0.05

release of eIF1 from the complex. (For simplicity we refer below to these two events as the fast and slow phases of eIF1 release.) With WT eIF1A in the PIC, addition of a saturating concentration of mRNA (AUG) results in a biphasic increase in fluorescein fluorescence with rate constants of 4 and 0.6 s^{-1} for the first (k_1) and second (k_2) phases, respectively, and roughly equal amplitudes (Fig. A.3B, black curve; Figs. 4A,B & Table A.3, eIF1 release) consistent with previous studies (Maag et al. 2005; Algire et al. 2005; Cheung et al. 2007). Despite its strong effect on the slow phase of eIF1A-eIF5 FRET, the SE_2* mutation did not change the rate constants or amplitudes of either phase of eIF1 release (Fig. A.3B, blue curve; Figs. A.4A,B; Table A.3), and the SE_1*,SE_2* mutation produced relatively small reductions in the rate constants of the fast and slow phases of eIF1 release of 4- and 2-fold, respectively (Fig. A.3B, red curve; Figs. A.4A,B; Table A.3). These results indicate that eIF1 release can proceed normally in the absence of proper movement of eIF1A and eIF5 relative to one another.

Finally, we measured the effect of these same mutations in eIF1A on P_i release from the PIC in response to start codon recognition. In these experiments, PICs containing [γ-^{32}P]-GTP are mixed in a rapid quench device with saturating mRNA(AUG) and eIF5, and the reactions are quenched after various times with EDTA. The amount of P_i generated over time is monitored using polyethylenimine (PEI) thin-layer chromatography followed by PhosphorImaging analysis. Similar to eIF1 release, the rate of P_i formation is biphasic, with the first phase corresponding to eIF5-dependent GTP hydrolysis within the PIC and the second to P_i release, which drives GTP hydrolysis to completion (Algire et al. 2005; Nanda et al. 2009). PICs assembled with WT eIF1A

Figure A.4. Comparison of rate constants for eIF1-eIF1A FRET change, GTP hydrolysis and eIF1A-eIF5 FRET change upon start codon recognition by the PIC. (A) Rate constants (k_1) for the first phase of the decrease in eIF1-eIF1A FRET (red), GTP hydrolysis (green) and increase in eIF1A-eIF5 FRET (orange) upon start codon recognition by the PIC. For eIF1-eIF1A FRET this phase corresponds to a first-order event, likely a conformational change. For the GTP hydrolysis reaction this phase corresponds to a step or steps that limit the rate of cleavage of GTP to produce GDP and P_i. (B) Rate constants (k_2) for the second phase of the decrease in eIF1- eIF1A FRET (red), GTP hydrolysis (green) and increase in eIF1A-eIF5 FRET (orange) upon start codon recognition by the PIC. For eIF1-eIF1A FRET this phase corresponds to eIF1 release from the PIC, and for GTP hydrolysis this phase corresponds to P_i release from eIF2, which drives the reaction to completion. PICs were assembled with WT eIF1A, eIF1A-SE1*SE2* or eIF1A-SE2*. Data shown are averages of at least three experiments and error bars represent average deviations.

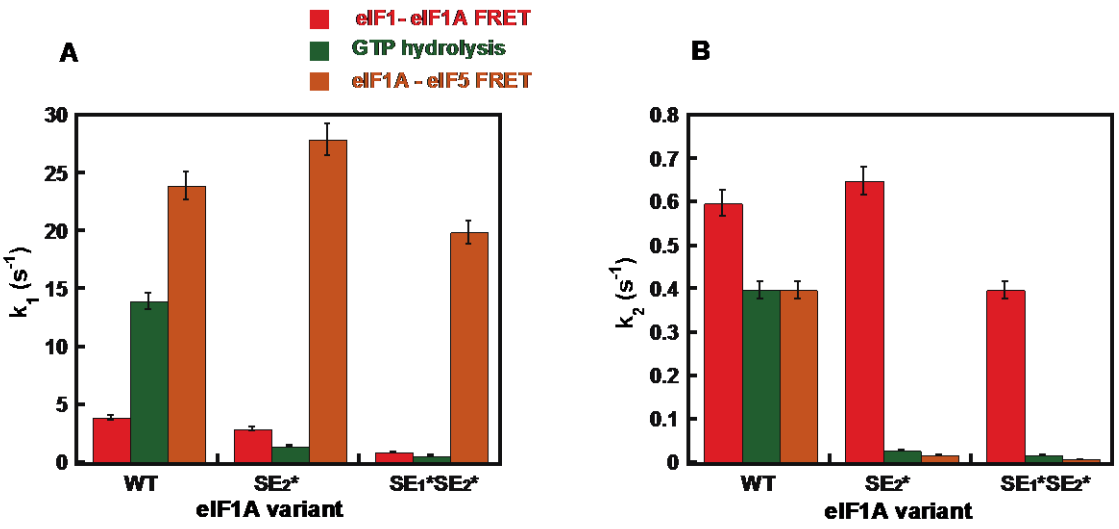

Table 3: Kinetic parameters for the eIF1-eIF1A FRET change and GTP hydrolysis in 43S PICs

eIF1A variant	eIF1 release k_{obs} (s^{-1})	GTP hydrolysis k_{obs} (s^{-1})
WT	k_1= 4 ± 1 a_1= 0.6 ± 0.05 k_2= 0.6 ± 0.1 a_2= 0.4 ± 0.05	k_1= 14 ± 4 a_1= 0.7 ± 0.1 k_2= 0.4 ± 0.1 a_2= 0.3 ± 0.1
SE_2*	k_1= 3 ± 1 a_1= 0.6 ± 0.1 k_2= 0.7 ± 0.1 a_2= 0.4 ± 0.1	k_1= 1.4 ± 0.6 a_1= 0.4 ± 0.1 k_2= 0.03 ± 0.01 a_2= 0.6 ± 0.1
SE_1*,SE_2*	k_1= 1 ± 0.5 a_1= 0.5 ± 0.1 k_2= 0.4 ± 0.1 a_2= 0.5 ± 0.1	k_1= 0.7 ± 0.2 a_1= 0.2 ± 0.1 k_2= 0.02 ± 0.005 a_2= 0.8 ± 0.1

hydrolyzed GTP with rate constants of 14 and 0.4 s^{-1} for the first (k_1) and second (k_2) phases, respectively (Fig. A.3C, black curve; Figs. A.4A,B & Table A.3, GTP hydrolysis). These values are consistent with previous results and with the fact that eIF1 release limits the rate of P_i release (Algire et al. 2005; Nanda et al. 2009; Cheung et al. 2007). Remarkably, the SE_2* substitution decreased the rates of both GTP hydrolysis (k_1) and P_i release (k_2) 10-fold (Fig. A.3C, blue curve; Figs. A.4A,B; Table A.3) even though it had no effect on the rate of eIF1 release (Fig. A.4B). Likewise, the SE_1*,SE_2* substitution decreased the rate constants for GTP hydrolysis and P_i release by 20-fold (Fig. A.3C, red curve; Figs. A.4A,B; Table A.3), whereas it had only a 2-fold effect on the rate constant for eIF1 release (Fig. A.4B).

The fact that the rate constants for the fast phases of the eIF1-eIF1A FRET change, GTP hydrolysis/P_i release and eIF1A-eIF5 FRET change cover a range from 4 to 23 s^{-1} in the WT system (Fig. .4A) suggests that they do not correspond to the same molecular event. This interpretation is further supported by the differing effects of the SE element mutations in the eIF1A CTT on these rate constants. For the eIF1-eIF1A FRET change, the SE_2* mutation has no effect on k_1, whereas the SE_1*,SE_2* mutation reduces k_1 by 4-fold. In contrast, k_1 for GTP hydrolysis/P_i release, which is thought to represent the rate- limiting step for GTP hydrolysis itself (Algire et al. 2005), is reduced ≥10-fold by both the SE_2* and SE_1*,SE_2* mutations. Finally, k_1 for the eIF1A-eIF5 FRET change is unaffected by either mutation. These data indicate that different molecular events correspond to each of the fast phases in the three assays.

On the other hand, the slow phases of the eIF1-eIF1A FRET change (eIF1 release), GTP

hydrolysis (P_i release), and eIF1A-eIF5 FRET change occur with similar rate constants in the WT system (Fig. A.4B), suggesting that they could correspond to the same molecular event. However, the fact that the SE mutations produce a much larger reduction in the rate of P_i release than in the rate of eIF1 release (Fig. A.4B) indicates that ejection of eIF1 from the PIC does not directly trigger P_i release, but requires the intermediary function of the eIF1A CTT. This proposal is consistent with our previous results demonstrating a functional interaction between the eIF1A CTT and eIF5 that is thought to stabilize the closed conformation of the PIC on start codon recognition (Maag et al. 2006). Moreover, our finding that the SE mutations dramatically reduce the rate of the slow phase of the eIF1A-eIF5 FRET change, mirroring their effects on P_i release, is consistent with the possibility that the event corresponding to the slow phase in the eIF1A-eIF5 FRET assay is a prerequisite for P_i release. Supporting this proposal, the eIF1A-eIF5 FRET change occurs with the non-hydrolyzable GTP analog GDPNP in the PIC, indicating that P_i release is not required for the FRET change to occur.

Taken together, our results suggest that eIF1 release is required for, and normally sets the rate of P_i release in WT PICs. eIF1 release is not sufficient for P_i release, however, which additionally requires the movement of the eIF1A CTT towards the eIF5 NTD manifested in the slow phase of the eIF1A-eIF5 FRET change. This movement of the two factors relative to each other is coupled to eIF1 release and is critically dependent on the SE elements in the eIF1A CTT. It is also noteworthy that both the SE2* and SE1*,SE2* mutants decrease the rate and amplitude of the fast kinetic phase of GTP hydrolysis in addition to their effects on the second phase. These data suggest that the CTT of eIF1A is involved in promoting full GTPase activation of eIF2, along with the GAP eIF5, in

addition to its proposed role in triggering P_i release.

The CTD of eIF5 promotes displacement of eIF1 from the PIC

We showed previously that eIF5 antagonizes binding of eIF1 to the PIC and that overexpressing it in yeast promotes recognition of near-cognate UUG start codons, whereas overexpressing eIF1 has the opposite effect, suggesting that the ability of eIF5 to displace eIF1 from the PIC is part of its function in start codon recognition (Nanda et al. 2009; Martin-Marcos et al. 2011). In this model, one of the domains of eIF5 would move into part of the binding site for eIF1 upon start codon recognition, promoting the latter factor's irreversible release from the PIC (Nanda et al. 2009; Conte et al. 2006). Consistent with an important role for competition between eIF5 and eIF1 in start codon recognition, recent work showed that overexpression of eIF5 in mammalian cells also reduces the fidelity of start codon recognition, in a manner that can be suppressed by overexpression of eIF1 (Loughran et al. 2012). To further explore the molecular basis of the interaction between these two factors and establish which domain of eIF5 is responsible for antagonizing eIF1 binding to the PIC, we expressed and purified the isolated NTD and CTD of eIF5 as separate proteins. Using C- terminally-fluorescein-labeled versions of these protein domains, we first measured their affinity for eIF2 and TC by monitoring fluorescence anisotropy (Fig. A.5A,B). Full-length eIF5 and the CTD bound to eIF2 with identical affinity (K_d = 40 nM) (Fig. A.5A). The NTD did not bind detectably at any concentration of eIF2 tested. Similar results were observed with the TC: Full- length eIF5 and the CTD bound with nearly the same affinity (K_d values of 40 and 90 nM, respectively), whereas no binding of the NTD could be detected (Fig. A.5B).

Figure A.5. The C-terminal domain of eIF5 antagonizes binding of eIF1 to the PIC. Full-length WT eIF5 (red curves, circle) and its isolated CTD (black curves, square), and NTD (blue curves, triangle) and were expressed and purified as described in Materials and Methods. In all cases, data are the averages of at least 2 independent experiments. (A) Binding of C-terminally fluorescein-labeled eIF5 derivatives (50 nM) to eIF2 was assessed by monitoring fluorescence anisotropy (λ_{ex} = 497 nm; λ_{em} = 520 nm) as a function of the concentration of eIF2. K_d values were determined by fitting the resulting data with a hyperbolic binding equation. The measured K_d values were 40 ± 3 nM for full-length eIF5 and 45 ± 5 nM for the eIF5 CTD; the eIF5 NTD did not detectably bind to eIF2 and thus no K_d was determined. (B) The binding of the eIF5 derivatives to ternary complex (eIF2• Met-tRNA$_i$•GDPNP) was measured using fluorescence anisotropy as in (A). The measured K_d values were 45 ± 5 nM for full-length eIF5 and 90 ± 5 nM for the eIF5 CTD. No binding was detected to the eIF5 NTD. (C) The binding of eIF5 derivatives to the 40S ribosomal subunit was determined by monitoring the change in fluorescence anisotropy of C-terminally fluorescein-labeled full-length eIF5 or the NTD or CTD (50 nM) as a function of concentration of 40S subunits. The measured K_d values were 300 ± 50 nM for full- length eIF5; 250 ± 30 nM for the NTD; 1500 ± 500 nM for the CTD. (D). Kinetics of GTP hydrolysis by eIF2 within the PIC stimulated by full-length eIF5 or the NTD or CTD (2 μM). Curves were fit with double-exponential rate equations to determine rate constants: full-length eIF5 (Red Circles); eIF5 CTD (Black square); eIF5 NTD (Blue triangles) (E) The effect of eIF5 and its domains on release of eIF1 G107K-Fl from the PIC in response to start codon recognition. The decrease in FRET between G107K-Fl and eIF1A-TAMRA within the PIC after rapid mixing with

mRNA (AUG) without or with 2 μM full-length eIF5 or the NTD or CTD was measured as an increase in fluorescein (donor) fluorescence: –eIF5 (green); +eIF5 (red); eIF5 CTD (black); eIF5 NTD (blue). Curves were fit with double-exponential rate equations to determine rate constants. (F) The effects of eIF5 NTD and CTD on the kinetics of TC recruitment to the PIC. TC containing ^{35}S-Met-tRNA$_i$ and GDPNP was mixed with 40S subunits, eIF1-G107K and eIF1A in the absence or presence of eIF5 or the NTD or CTD (2 μM). Time points were loaded directly on a running native gel and the fraction of TC bound over time analyzed by phosphorimaging: –eIF5 (green diamonds); +eIF5 (red circles); eIF5 CTD (black squares); eIF5 NTD (blue triangles). Curves were fit with single-exponential equations to determine observed pseudo-first order rate constants.

Figure A.5.

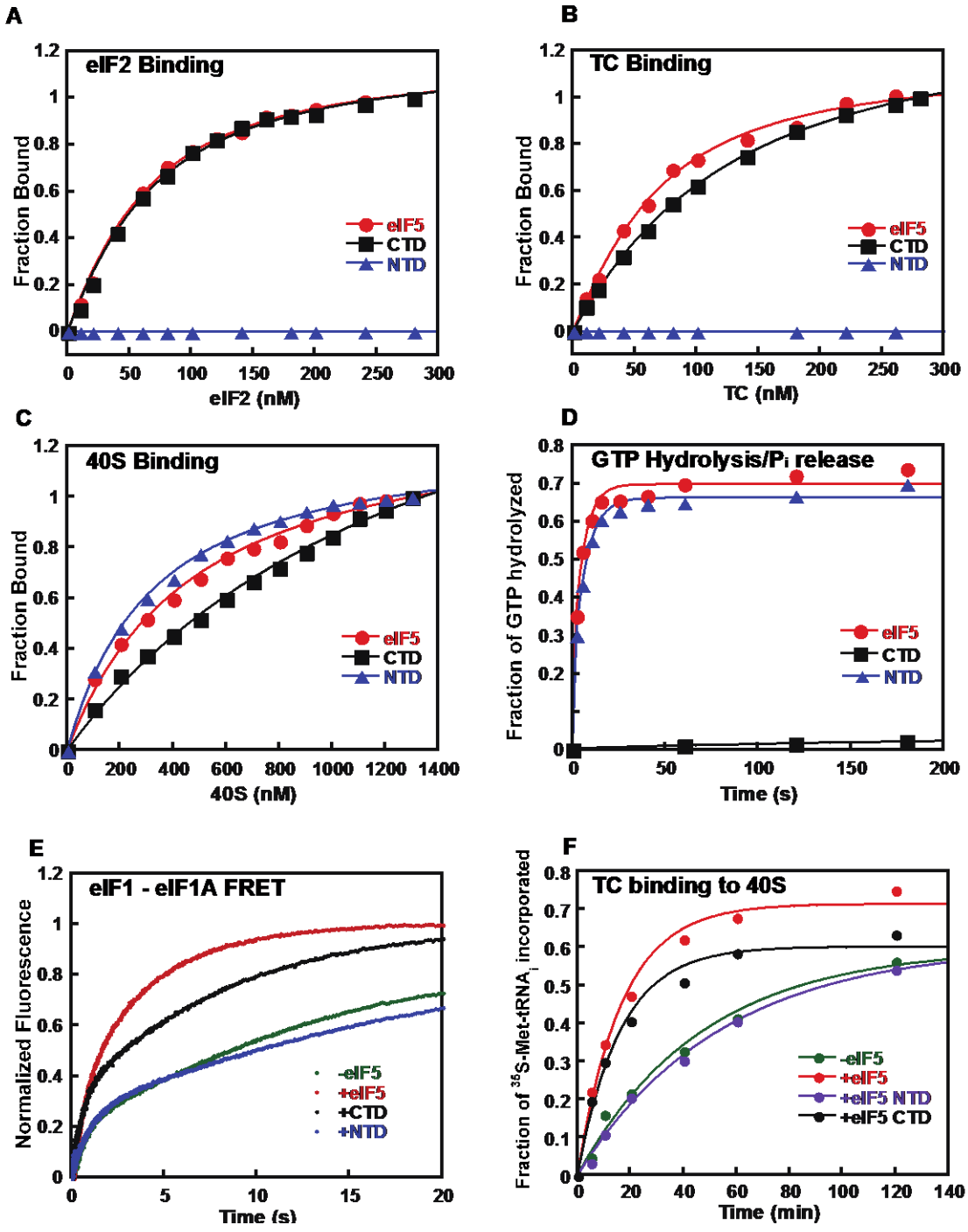
A
eIF2 Binding
Fraction Bound
eIF2 (nM)
eIF5
CTD
NTD
B
TC Binding
Fraction Bound
TC (nM)
eIF5
CTD
NTD
C
40S Binding
Fraction Bound
40S (nM)
eIF5
CTD
NTD
D
GTP Hydrolysis/Pi release
Fraction of GTP hydrolyzed
Time (s)
eIF5
CTD
NTD
E
eIF1 - eIF1A FRET
Normalized Fluorescence
Time (s)
-eIF5
+eIF5
+CTD
+NTD
F
TC binding to 40S
Fraction of 35S-Met-tRNAi incorporated
Time (min)
-eIF5
+eIF5
+eIF5 NTD
+eIF5 CTD

We next tested whether eIF5 and its domains bind to the 40S subunit itself (Fig. A.5C). Using the same C-terminally-labeled derivatives of full-length eIF5 and its domains, we monitored fluorescence anisotropy as a function of 40S subunit concentration. In this case, the full-length factor and the NTD bound with similar affinities (K_ds of 400 and 300 nM, respectively). The CTD also bound, but with a 3-fold higher K_d. Thus both domains of eIF5 are capable of binding directly to the 40S ribosomal subunit.

The NTD of eIF5 contains the R15 residue essential for the factor's GAP function. This domain was previously reported to be sufficient to promote GTP hydrolysis by eIF2 (Conte et al. 2006; Das et al. 2000; Alone and Dever 2006). Consistent with these results, we found that the NTD was capable of promoting full GTPase activity within the PIC, whereas the CTD did not stimulate GTP hydrolysis detectably (Fig. A.5D). These data indicate that although the NTD does not interact detectably with eIF2 or the TC free in solution, it must be able to do so in the context of the PIC, consistent with previous work showing an interaction between the NTD of eIF5 and the isolated γ-subunit of eIF2 (Alone and Dever 2006).

To determine which domain of eIF5 is responsible for promoting release of eIF1 from the PIC, we assembled 43S complexes using eIF1- G107K labeled on its C-terminus with fluorescein, eIF1A labeled on its C-terminus with TAMRA, TC and 40S subunits. Start codon recognition was initiated by rapid mixing in a stopped-flow device of mRNA(AUG) alone or mRNA(AUG) together with either full-length eIF5 or the isolated NTD or CTD (2 μM). Loss of FRET between the fluorescein and TAMRA labels was monitored (increase in fluorescein fluorescence) to follow the kinetics of eIF1 release from the complex. The G107K mutant of eIF1 was used because its release from the

complex is impaired, allowing the effect of eIF5 to be seen more readily in response to an AUG start codon; release of WT eIF1 is so facile on a cognate AUG codon that addition of eIF5 has only a small effect (Nanda et al. 2009). In the absence of eIF5, eIF1-G107K was released with a rate constant of 0.08 s^{-1} (Fig. A.5E and Table A.4), which is 5-fold lower than that observed for WT eIF1 in the absence of eIF5 (Maag et al. 2005). Addition of 2 μM eIF5-NTD had no effect on the rate constant for eIF1-G107K release, whereas addition of the same concentration of full-length eIF5 or the CTD increased the observed rate constant ≥2-fold to 0.25 and 0.17 s^{-1}, respectively. These data indicate that the CTD of eIF5 is responsible for promoting release of eIF1 from the PIC.

We previously presented data indicating that in the reconstituted yeast translation initiation system, binding of TC to the 40S subunit (in the presence of eIF1, eIF1A and model mRNA) occurs in two steps, an initial encounter that is not codon-dependent and cannot be detected in our native gel-based assay, followed by a start codon- dependent conformational change that locks the complex into a stable state that is detected in the native gel assay (Kolitz et al. 2009; Nanda et al. 2009). We showed that release of eIF1 is required for the transition to this stable state and that high concentrations of eIF5 accelerate the apparent rate of TC binding by enhancing eIF1 release from the PIC and thus conversion to the stable, closed state that is detected in the gel-based assay (Nanda et al. 2009). As a further test of the functions of the domains of eIF5 in promoting eIF1 release, we also measured their effects on the kinetics of TC binding to 40S subunits in the presence of eIF1-G107K and eIF1A, but absence of mRNA, using the native gel assay. At the concentration of 40S subunits used (200 nM) in the absence of eIF5 the

Table A.4: Rate constants for eIF1 dissociation from and TC recruitment to PICs

eIF5 Variant	eIF1-G107K dissociation k_{obs} (s^{-1})	TC recruitment to PIC k_{obs} (min^{-1})
-eIF5	0.05 ± 0.01	0.02 ± 0.01
+eIF5	0.25 ± 0.05	0.06 ± 0.01
+CTD	0.17 ± 0.03	0.05 ± 0.005
+NTD	0.05 ± 0.01	0.02 ± 0.01

observed pseudo-first order rate constant (k_{obs}) for detectable TC binding was 0.02 min^{-1}. Addition of 2 μM full-length eIF5 increased k_{obs} 3-fold to 0.06 min^{-1}. As in the eIF1 release experiments above, 2 μM of the eIF5-NTD had no effect on the rate of TC binding but the same concentration of the CTD increased the rate nearly as much as the full-length factor did (k_{obs} = 0.05 min^{-1}). Thus these experiments strongly support the conclusion that the CTD of eIF5 is responsible for the factor's ability to promote eIF1 release from the PIC with attendant enhancement of TC binding.

Discussion

Previous work has elucidated a number of key events taking place within the PIC when it encounters a start codon. These events trigger downstream steps and commit the complex to continuing initiation at the selected position on the mRNA. The data presented herein have significantly refined and strengthened the model for the events surrounding start codon recognition by providing evidence for new initiation codon- dependent movements of eIF1A and eIF5 within the PIC and elucidating the connections between P_i release from eIF2 and conformational changes in the initiation factors.

Coupling of start codon-dependent movements of eIF1, eIF1A and eIF5 to P_i release by eIF2

We have found a FRET signal between fluorophores on the C-terminus of eIF1A and the folded N-terminal domain of eIF5 that occurs upon start codon recognition, indicating that the CTT of eIF1A and the NTD of eIF5 move closer to each other after the AUG is encountered. Importantly, the rate of this rearrangement is strongly dependent on the SE

elements in the eIF1A CTT. These results are consistent with our previous data showing a strong interaction, either direct or indirect, between the CTT of eIF1A and eIF5 that takes place upon start codon recognition (Maag et al. 2006), and with more recent hydroxyl radical foot- printing results indicating that the CTT of eIF1A must move out of the P site of the 40S subunit when the initiator tRNA is fully engaged (Yu et al. 2009).

In addition, we have shown that mutations in the SE elements in the eIF1A CTT decouple the release of eIF1 from the release of P_i in response to start codon recognition. The SE_2* and SE_1*SE_2* mutations have ≤2-fold effects on the rate of eIF1 release, but evoke 13-20-fold reductions in the rate of P_i release. These data indicate that, although eIF1 dissociation is necessary for P_i release, it is not sufficient, and that the SE elements are additionally required for rapid P_i release from eIF2 on AUG recognition. The fact that the SE mutations also reduce the rate of GTP hydrolysis itself indicates that the CTT of eIF1A has a previously unrecognized function, working along with eIF5 to promote the GTPase activity of eIF2 in the PIC.

Taken together, our data suggest that release of eIF1 and movement of the CTT of eIF1A out of the P site towards the NTD of eIF5 are triggered separately by the same event. We consider the most likely candidate for this event to be accommodation of $tRNA_i$ fully into the P site because it is expected to produce steric clashes with both factors (Rabl et al. 2011; Yu et al. 2009) and because $tRNA_i$ binds more tightly to the PIC in the absence of eIF1 (Passmore et al. 2007). In this model, mutations in eIF1 that speed or slow release of the factor exert their influence on P_i release by, respectively, facilitating or impeding accommodation of the tRNA. This altered rate of tRNA accommodation would then

directly affect the rate of movement of the CTT of eIF1A out of the P site, which in turn would affect the rate of P_i release. Indeed, this is exactly what we observed with the G107E and G107K mutants of eIF1 (Fig. A.2B). The fact that the rate of the slow kinetic phase of the eIF1A-eIF5 FRET is always the same (within error) as the rate of P_i release (Fig. A.4B; k_2 values in Tables A.2 and A.3) supports the proposal that movement of the CTT is a key step for triggering P_i release required in addition to dissociation of eIF1.

The fast kinetic phase in the loss of eIF1- eIF1A FRET reflects a conformational change upon AUG recognition that increases the distance between eIF1 and the eIF1A CTT (Maag et al. 2005). As described above, our data indicate that this rearrangement and the fast kinetic phases of GTP hydrolysis and the eIF1A-eIF5 FRET change do not reflect the same molecular event. This conclusion argues against the possibility that the fast phases of either of the changes in FRET correspond to movement of the CTT of eIF1A because one of the fluorophores in each case is on the C-terminus of eIF1A and movement of the CTT that affected FRET with one partner (e.g., eIF5) would most likely affect FRET with the other partner (e.g., eIF1) as well. Instead, we suggest that the fast phases of the eIF1-eIF1A and eIF1A-eIF5 FRET changes correspond to movement of eIF1 and eIF5, respectively (see below). Overall, these data support the model that start codon recognition and attendant accommodation of the initiator tRNA into the P site of the 40S subunit cause movement of eIF1 away from its initial binding site in the PIC and subsequent movement of the CTT of eIF1A towards the NTD of eIF5, which in turn triggers P_i release from eIF2.

One seeming paradox is the fact that mutations in the SE elements increase utilization of

near-cognate UUG codons relative to AUG codons as start sites in vivo, yet they slow movement of the eIF1A CTT and P_i release from eIF2, steps that are thought to be important for commitment of the PIC to proceeding with initiation upon start codon recognition. A possible explanation to resolve this seeming paradox is that substituting the critical phenylalanine residues in the SE elements with alanines leads to elimination of the CTT from the P site and also impairs the interaction with the eIF5 NTD that is required to trigger dissociation of P_i from eIF2. Because the CTT with SE mutations is not in the P site, accommodation of the initiator tRNA is less hindered and can take place more readily in response to near-cognate codons. This enhanced transit of the $tRNA_i$ from the P_{out} to P_{in} state would correspondingly increase the rate of complex closure and arrest scanning PICs on near-cognate codons long enough to proceed with the remaining steps of initiation with increased frequency relative to WT complexes at the same sites (in this model the SE mutations cannot enhance transit to P_{in} to a level faster than that which already occurs on AUG codons in WT complexes). This proposal is consistent with our previous data suggesting that the SE mutations stabilize the closed/P_{in} state of the PIC relative to the open one at near-cognate codons (Saini et al. 2010).

This model can also explain why the SE element mutations do not slow release of eIF1 to the same degree they slow movement of the eIF1A CTT and P_i release: because the CTT of eIF1A with the SE mutations is not in the P site, its hindered movement does not impede accommodation of the initiator tRNA into the P site, or subsequent displacement of eIF1, upon start codon recognition. In addition, the proposal can explain why the SE mutations slow TC binding to the PIC (Saini et al. 2010) because proper positioning of

the eIF1A CTT within the complex could be required to directly stabilize binding of TC to the 40S subunit as well as to promote the open state of the complex to which TC initially binds.

The domains of eIF5 play multiple roles in start codonrecognition

Previous studies indicated that eIF5 plays multiple roles in start codon recognition in addition to its function as a GAP for eIF2. To better understand the various activities of eIF5, we tested the ability of the isolated NTD and CTD of the factor to interact with other components of the system and to promote release of eIF1 from the PIC. The isolated eIF5 CTD bound to eIF2 and TC with the same affinity as the full-length factor, whereas the eIF5 NTD did not bind detectably to either. In contrast, previous studies showed that the eIF5 NTD binds directly to the isolated eIF2γ subunit in solution (Alone and Dever 2006). Together, these data suggest that the binding site for the eIF5 NTD on eIF2γ is occluded in free eIF2 and TC in solution and raise the possibility that a conformational change occurs in the scanning PIC to open this binding site and allow the eIF5 NTD to interact with eIF2γ. One appealing possibility is that this switch involves displacement of eIF2β from eIF2 γ by the eIF5 NTD, as the NTD of eIF5 and eIF2 β share a common fold and both have a zinc- binding domain (ZBD). Consistent with this idea, the crystal structure of an archaeal counterpart of eIF2 (aIF2) (Yatime et al. 2007), reveals that the ZBD interacts with the γ subunit and places residues corresponding to those altered by Sui$^-$ substitutions in yeast eIF2β in proximity to the GTP binding pocket of aIF2 γ , including a Sui$^-$ mutation thought to elevate eIF2's latent GTPase activity. This and other findings support the notion that the WT eIF2β ZBD blocks the GTPase

activity of eIF2γ in a manner relieved by eIF5 in the PIC (Hinnebusch 2011; Huang et al. 1997; Yatime et al. 2007; Hashimoto et al. 2002). We suggest that the eIF2β ZBD is displaced from eIF2γ by the homologous ZBD domain of eIF5 in the scanning PIC, allowing the unstructured NTT of eIF5 (containing the key GTPase activating residue R15) to stimulate GTP hydrolysis by eIF2γ, and that the eIF5 NTT must be withdrawn from the GTP-binding pocket of eIF2γ to enable P_i release on AUG recognition (see below).

In addition to binding to eIF2, our data indicate that both domains of eIF5 can interact with the 40S subunit, with the NTD and full- length factor binding 3-4-fold more tightly than the CTD (Fig. A.5C). The mechanistic significance of these interactions is unclear, but they suggest the possibility that eIF5 could mediate communication between the ribosome and eIF2.

Importantly, we found that the eIF5 CTD is the domain responsible for promoting release of eIF1 from the PIC, as it functions nearly as well as the WT factor to promote release of eIF1-G107K from the PIC, whereas the isolated NTD has no detectable effect. Consistent with this, the eIF5 CTD promotes stable TC binding to PICs reconstituted with eIF1-G107K as effectively as does full-length eIF5, whereas the eIF5 NTD, again, has no detectable effect despite its ability to activate GTP hydrolysis.

A complex series of molecular rearrangements underlies the response to start codon recognition by the PIC

Based on all of the available data, we suggest the following model for the events surrounding start codon recognition by the PIC (Fig. A.6), which synthesizes and builds

Figure A.6. Model for the events taking place within the PIC upon start codon recognition. Stage 1: TC•eIF5 complex binds to the 40S subunit. eIF1 occupies a site on the platform of the 40S adjacent to the P site, and the body of eIF1A binds in the A site, with its NTT (purple) and CTT (light blue) binding in the P site. Stage 2: The scanning PIC is in an open conformation with the $tRNA_i$ in the P_{out} state. eIF1 binding is stabilized by a strong interaction with the NTT of eIF2ß. Stage 3: Entry of the start codon into the P site allows formation of the codon:anticodon helix between the mRNA and $tRNA_i$, which drives the tRNA into the P_{in} state. This displaces eIF1 to a second, weaker binding site on the 40S subunit, breaking its interaction with the eIF2ß NTT, which in turn binds strongly to the eIF5 CTD. Movements of the tRNA and/or eIF5 CTD result in changes in the orientation of the eIF5 NTD. Stage 4: eIF1 dissociates from the complex, which, along with accommodation of $tRNA_i$ into the P site, causes the CTT of eIF1A to move and interact with the eIF5 NTD. This interaction triggers P_i release from eIF2, possibly by moving the unstructured NTT of eIF5 (not shown for clarity). The resulting complex is in a closed, scanning arrested state.

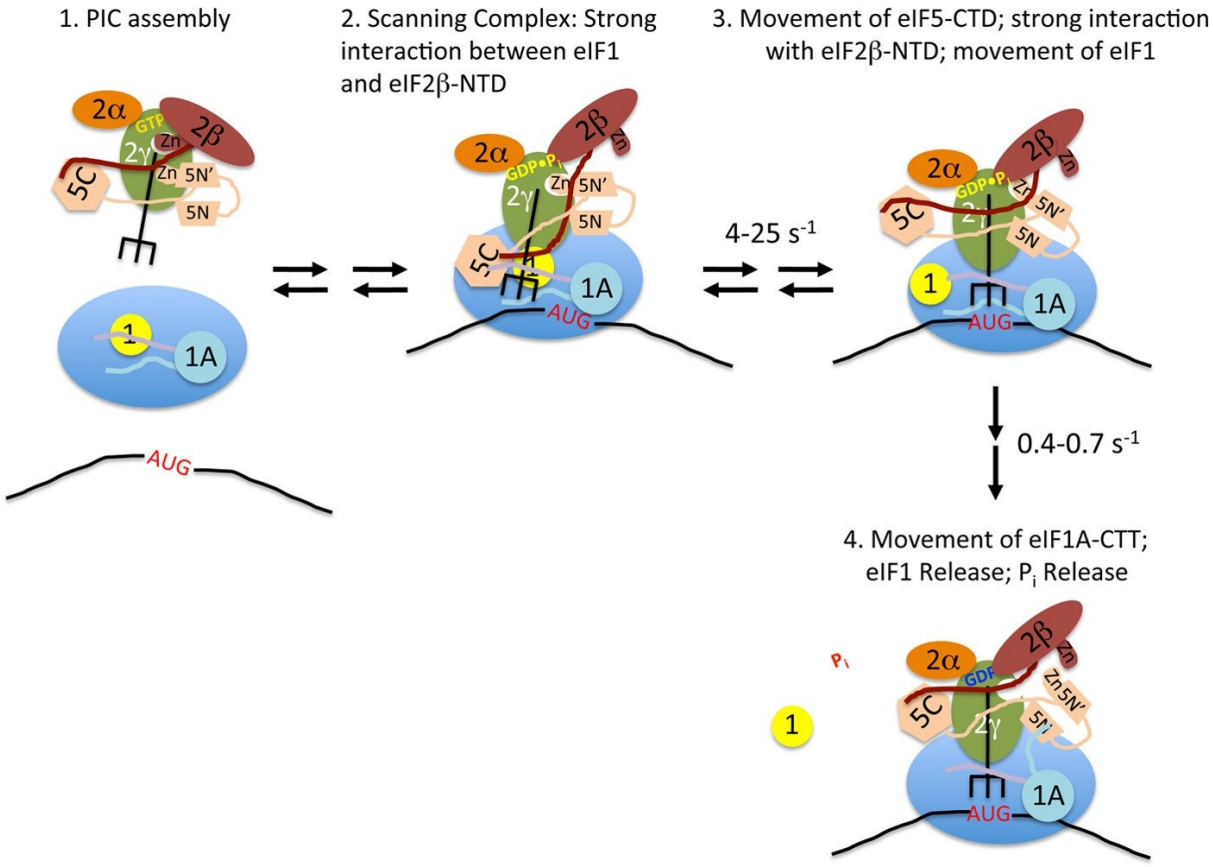
1. PIC assembly
2. Scanning Complex: Strong interaction between eIF1 and eIF2β-NTD
3. Movement of eIF5-CTD; strong interaction with eIF2β-NTD; movement of eIF1
4-25 s-1
0.4-0.7 s-1
4. Movement of eIF1A-CTT; eIF1 Release; Pi Release
2α
2β
2γ
GTP
GDP•Pi
GDP
Zn
5N'
5N
5C
1
1A
AUG
Pi

off of several previously proposed models (Saini et al. 2010; Nanda et al. 2009; Fringer et al. 2007; Luna et al. 2012). Prior to encountering a start codon, the PIC is in an open conformation, with $tRNA_i$ in the P_{out} state, not fully engaged with the P site of the 40S subunit (Fig. A.6, stage 2). eIF1 and the CTT of eIF1A partially occupy the P site, inhibiting full accommodation of the $tRNA_i$ (Saini et al. 2010; Lomakin 2003; Rabl et al. 2011; Yu et al. 2009). Binding of eIF1 to the open conformation of the PIC is stabilized by its interaction with the NTT of eIF2 β (Singh 2004) and possibly also its weak interaction with the CTD of eIF5, accounting for the previous finding that eIF1 substitutions that weaken these contacts reduce eIF1·PIC association and elevate UUG initiation (a Sui^- phenotype) (Reibarkh et al. 2008). Having demonstrated here 40S binding by the eIF5 CTD, we propose that this domain occupies a site adjacent to eIF1's binding site on the 40S platform, where it may interact weakly with both the eIF2β NTT and eIF1 (Luna et al. 2012; Singh 2004). We speculate that at this stage the ZBD of eIF2β has been displaced by the ZBD of eIF5, allowing the unstructured NTT of eIF5 (containing R15) to stimulate GTP hydrolysis by eIF2γ; however, the eIF5 NTT's position on eIF2γ prevents P_i release from the scanning complex. Entry of an AUG codon into the P site (Fig. A.6, stage 3) drives formation of the codon:anticodon helix, which pulls the initiator tRNA more fully into the P site (P_{in} state), ejecting the CTT of eIF1A and displacing eIF1 to a second, lower affinity binding site on the 40S platform. Movement of the tRNA and eIF1 allows strengthened interaction between the eIF5 CTD and the eIF2β NTT, resulting in displacement of eIF1 from eIF2β by the eIF5 CTD. Loss of this interaction between eIF1 and eIF2β in turn enhances the rate of eIF1 release from the PIC. High concentrations of full-length eIF5 or its CTD can exogenously compete

with eIF1 for binding to the NTT of eIF2β, thus weakening eIF1's binding to the PIC and promoting its release at near- cognate codons. This start codon-dependent switch in strong binding partners for the eIF2β NTT between eIF1 and the eIF5 CTD, which explains the observed effects of high concentrations of eIF5 and its CTD, is the main difference between our model and the one previously proposed by Luna et al., in which the NTT of eIF2β did not interact with eIF1 (Luna et al. 2012).

Consistent with the notion that the previously demonstrated interaction between eIF1 and the NTT of eIF2β has a role in stabilizing binding of eIF1 to the PIC, mutations in eIF1 that disrupt the interface between the two factors produce Sui$^-$ phenotypes (Reibarkh et al. 2008). In contrast, mutations that destabilize the interaction between the eIF5-CTD and eIF2β-NTT result in an Ssu$^-$ phenotype and decrease eIF5's ability to promote eIF1 release and closed complex formation upon AUG recognition (Luna et al. 2012; Laurino et al. 1998), consistent with the proposal that this interaction occurs after the start codon is encountered and competes with the interaction between the eIF2β NTT and eIF1 to promote eIF1 release from the PIC.

At this stage (Fig. A.6, stage 4), having been ejected from the P site, the eIF1A CTT now engages with the eIF5 NTD, dependent on the critical Phe residues of the SE elements, and this new interaction helps to displace the eIF5 NTT from the G domain of eIF2γ, triggering P_i release. These last features of the model are based on our discovery of eIF1A-eIF5 FRET upon start codon recognition and the fact that the slow kinetic phase of this FRET change and the rate of P_i release are the same and are reduced coordinately by the SE mutations in the CTT of eIF1A.

In this model, the fast phase of the change in eIF1-eIF1A FRET corresponds to initial movement of eIF1 away from the P site in response to accommodation of the initiator tRNA (stage 2 to stage 3). This rapid movement would be followed by slower dissociation of the factor from the PIC (stage 3 to stage 4). The fast phase of the increase in eIF1A-eIF5 FRET, which is >5- fold faster than the first phase of the decrease in eIF1-eIF1A FRET, could correspond to a conformational change in eIF5 induced by movements of the initiator tRNA and/or interaction between the NTT of eIF2β and the CTD of eIF5 (stage 2 to stage 3). Movement of the eIF1A CTT out of the P site would then correspond to the second, slower phase of the change in eIF1A-eIF5 FRET. This latter event may also involve breaking of the interaction between eIF1 and eIF1A (Maag and Lorsch 2003) upon dissociation of eIF1 from the PIC.

Although this is just one possible model that is consistent with currently available data, it should serve as a useful framework to plan and interpret future experiments aimed at developing a complete understanding of the molecular mechanics of start codon recognition during eukaryotic translation initiation.

Acknowledgements: We thank the members of our laboratories for their comments and suggestions.

Footnotes

*This work was supported, in whole or in part by National Institute of Health Grant GM 62128 (to J.R.L.) and by the NIH Intramural Research Program (to A.G.H)

References

Acker MG, Kolitz SE, Mitchell SF, Nanda JS, Lorsch JR. 2007. *Methods in Enzymology*. Elsevier.

Acker MG, Shin B-S, Dever TE, Lorsch JR. 2006. Interaction between eukaryotic initiation factors 1A and 5B is required for efficient ribosomal subunit joining. *J Biol Chem* **281**: 8469–8475.

Acker MG, Shin B-S, Nanda JS, Saini AK, Dever TE, Lorsch JR. 2009. Kinetic analysis of late steps of eukaryotic translation initiation. *Journal of Molecular Biology* **385**: 491–506.

Aitken CE, Lorsch JR. 2012. A mechanistic overview of translation initiation in eukaryotes. *Nature Structural & Molecular Biology* **19**: 568–576.

Algire MA, Maag D, Lorsch JR. 2005. Pi release from eIF2, not GTP hydrolysis, is the step controlled by start-site selection during eukaryotic translation initiation. *Molecular Cell* **20**: 251–262.

Algire MA, Maag D, Savio P, Acker MG, Z TS, Sachs AB, Asano K, Nielsen KH, Olsen DS, Phan L, et al. 2002. Development and characterization of a reconstituted yeast translation initiation system. *RNA* **8**: 382–397.

Alone PV, Cao C, Dever TE. 2008. Translation Initiation Factor 2 Mutant Alters Start Codon Selection Independent of Met-tRNA Binding. *Mol Cell Biol* **28**: 6877–6888.

Alone PV, Dever TE. 2006. Direct Binding of Translation Initiation Factor eIF2 -G Domain to Its GTPase-activating and GDP-GTP Exchange Factors eIF5 and eIF2B. *Journal of Biological Chemistry* **281**: 12636–12644.

Anger AM, Armache J-P, Berninghausen O, Habeck M, Subklewe M, Wilson DN, Beckmann R. 2013. Structures of the human and Drosophila 80S ribosome. *Nature* **497**: 80–85.

Appelt K, Dijk J, Reinhardt R, Sanhuesa S, White SW, Wilson KS, Yonath A. 1981. The Crystallizationof Ribosomal Proteins from th. 1–4.

Asano K. 2000. A multifactor complex of eukaryotic initiation factors, eIF1, eIF2, eIF3, eIF5, and initiator tRNAMet is an important translation initiation intermediate in vivo. *Genes Dev* **14**: 2534–2546.

Asano K, Shalev A, Phan L, Nielsen KH, Clayton J, Valasek L, Donahue TF, Hinnebusch AG. 2001. Multiple roles for the C-terminal domain of eIF5 in translation initiation complex assembly and GTPase activation. 1–12.

Basavappa R, Sigler PB. 1991. The 3 A crystal structure of yeast initiator tRNA:

functional implications in initiator/elongator discrimination. *EMBO J* **10**: 3105–3111.

Ben-Shem A, Garreau de Loubresse N, Melnikov S, Jenner L, Yusupova G, Yusupov M. 2011. The Structure of the Eukaryotic Ribosome at 3.0 A Resolution. *Science* **334**: 1524–1529.

Ben-Shem A, Jenner L, Yusupova G, Yusupov M. 2010. Crystal Structure of the Eukaryotic Ribosome. *Science* **330**: 1203–1209.

Bohlen von K, Makowski I, Hansen HAS, Bartels H, Berkovitch-Yellin Z, Zaytzev-Bashan A, Meyer A, Paulke C, Franceschi F, Yonath A. 1991. Characterization and Preliminary Attempts for Derivatization of Crystals of Large Ribosom$ Subunits fromHaloarcula marismortui Diffracting to 3 A Resolution. 1–5.

Chao F-C, Schachman HK. 1955. The Isolation and Characterization of a Macromolecular Ribonucleoprotein from Yeast. 1–11.

Cheung Y-N, Maag D, Mitchell SF, Fekete CA, Algire MA, Takacs JE, Shirokikh N, Pestova T, Lorsch JR, Hinnebusch AG. 2007. Dissociation of eIF1 from the 40S ribosomal subunit is a key step in start codon selection in vivo. *Genes Dev* **21**: 1217–1230.

Cochella L, Green R. 2005. An active role for tRNA in decoding beyond codon:anticodon pairing. *Science* **308**: 1178–1180.

Conte MR, Kelly G, Babon J, Sanfelice D, Youell J, Smerdon SJ, Proud CG. 2006. Structure of the Eukaryotic Initiation Factor (eIF) 5 Reveals a Fold Common to Several Translation Factors †,‡. *Biochemistry* **45**: 4550–4558.

Das S, Ghosh R, Maitra U. 2000. Eukaryotic Translation Initiation Factor 5 Functions as a GTPase-activating Protein. *Journal of Biological Chemistry* **276**: 6720–6726.

Dong J, Munoz A, Kolitz SE, Saini AK, Chiu W-L, Rahman H, Lorsch JR, Hinnebusch AG. 2014. Conserved residues in yeast initiator tRNA calibrate initiation accuracy by regulating preinitiation complex stability at the start codon. *Genes Dev* **28**: 502–520.

Drabkin HJ, Helk B, rajbhandary UL. 1993. The role of nucleotides conserved in eukaryotic initiator methionine tRNAs in initiation of protein synthesis. *J Biol Chem* **268**: 25221–25228.

Dreher TW, Uhlenbeck OC, Browning KS. 1999. Quantitative Assessment of EF-1 {middle dot}GTP Binding to Aminoacyl-tRNAs, Aminoacyl-viral RNA, and tRNA Shows Close Correspondence to the RNA Binding Properties of EF-Tu. *Journal of Biological Chemistry* **274**: 666–672.

Eyler DE, Green R. 2011. Distinct response of yeast ribosomes to a miscoding event during translation. *RNA* **17**: 925–932.

Fahlman RP, Dale T, Uhlenbeck OC. 2004. Uniform Binding of Aminoacylated Transfer RNAs to the Ribosomal A and P Sites. *Molecular Cell* 1–7.

Farruggio D, Chaudhuri J, Maitra U, rajbhandary UL. 1996. The A1 U72 Base Pair Conserved in Eukaryotic Initiator tRNAs Is Important Specifically for Binding to the Eukaryotic Translation Initiation Factor eIF2. 1–9.

Fekete CA, Applefield DJ, Blakely SA, Shirokikh N, Pestova T, Lorsch JR, Hinnebusch AG. 2005. The eIF1A C-terminal domain promotes initiation complex assembly, scanning and AUG selection in vivo. *EMBO J* **24**: 3588–3601.

Fekete CA, Mitchell SF, Cherkasova VA, Applefield D, Algire MA, Maag D, Saini AK, Lorsch JR, Hinnebusch AG. 2007. N- and C-terminal residues of eIF1A have opposing effects on the fidelity of start codon selection. *EMBO J* **26**: 1602–1614.

Fernandez IS, Bai XC, Hussain T, Kelley AC, Lorsch JR, Ramakrishnan V, Scheres SHW. 2013. Molecular Architecture of a Eukaryotic Translational Initiation Complex. *Science* **342**: 1240585–1240585.

Fringer JM, Acker MG, Fekete CA, Lorsch JR, Dever TE. 2007. Coupled release of eukaryotic translation initiation factors 5B and 1A from 80S ribosomes following subunit joining. *Mol Cell Biol* **27**: 2384–2397.

Halbeisen RE, Scherrer T, Gerber AP. 2009. Affinity purification of ribosomes to access the translatome. *METHODS* 1–5.

Hashimoto NN, Carnevalli LS, Castilho BA. 2002. Translation initiation at non-AUG codons mediated by weakened association of eukaryotic initiation factor (eIF) 2 subunits. 1–10.

Hinnebusch AG. 2011. Molecular Mechanism of Scanning and Start Codon Selection in Eukaryotes. *Microbiology and Molecular Biology Reviews* **75**: 434–467.

Hinnebusch AG, Lorsch JR. 2012. The Mechanism of Eukaryotic Translation Initiation: New Insights and Challenges. *Cold Spring Harbor Perspectives in Biology* **4**: a011544–a011544.

Huang HK, Yoon H, Hannig EM, Donahue TF. 1997. GTP hydrolysis controls stringent selection of the AUG start codon during translation initiation in Saccharomyces cerevisiae. *Genes Dev* **11**: 2396–2413.

Inada T, Winstall E, Z TS, Yates JR III, Schieltz D, Sachs AB. 2002. One-step affinity purification of the yeast ribosome and its associated proteins and mRNAs. 1–11.

Jackson RJ, Hellen CUT, Pestova TV. 2010. The mechanism of eukaryotictranslation initiation and principlesof its regulation. 1–15.

Josic D, Clifton JG. 2007. Use of monolithic supports in proteomics technology. *Journal*

of Chromatography A **1144**: 2–13.

Kapp LD, Kolitz S, Lorsch JR. 2006. Yeast initiator tRNA identity elements cooperate to influence multiple steps of translation initiation. *RNA* **12**: 751–764.

Kapp LD, Lorsch JR. 2004. GTP-dependent Recognition of the Methionine Moiety on Initiator tRNA by Translation Factor eIF2. *Journal of Molecular Biology* **335**: 923–936.

Kolitz SE, Takacs JE, Lorsch JR. 2009. Kinetic and thermodynamic analysis of the role of start codon/anticodon base pairing during eukaryotic translation initiation. *RNA* **15**: 138–152.

Koubek J, Lin KF, Chen YR, Cheng RP, Huang JJT. 2013. Strong anion-exchange fast performance liquid chromatography as a versatile tool for preparation and purification of RNA produced by in vitro transcription. *RNA* **19**: 1449–1459.

Laurino JP, Thompson GM, Pacheco E, Castilho BA. 1998. Subunit of Eukaryotic Translation Initiation Factor 2Binds mRNA through the Lysine Repeats and a RegionComprising the C. 1–9.

Leshin JA, Rakauskaite R, Dinman JD, Meskauskas A. 2010. Enhanced purity, activity and structural integrity of yeast ribosomes purified using a general chromatographic method. 1–7.

Lomakin IB. 2003. Position of eukaryotic initiation factor eIF1 on the 40S ribosomal subunit determined by directed hydroxyl radical probing. *Genes Dev* **17**: 2786–2797.

Lomakin IB, Steitz TA. 2013. The initiation of mammalian protein synthesis and mRNA scanning mechanism. *Nature* **500**: 307–311.

Lorsch JR, Dever TE. 2010. Molecular view of 43 S complex formation and start site selection in eukaryotic translation initiation. *J Biol Chem* **285**: 21203–21207.

Loughran G, Sachs MS, Atkins JF, Ivanov IP. 2012. Stringency of start codon selection modulates autoregulation of translation initiation factor eIF5. *Nucleic Acids Research* **40**: 2898–2906.

Luna RE, Arthanari H, Hiraishi H, Nanda J, Martin-Marcos P, Markus MA, Akabayov B, Milbradt AG, Luna LE, Seo H-C, et al. 2012. The C-Terminal Domain of Eukaryotic Initiation Factor 5 Promotes Start Codon Recognition by Its Dynamic Interplay with eIF1 and eIF2β. *Cell Reports* **1**: 689–702.

Maag D, Algire MA, Lorsch JR. 2006. Communication between eukaryotic translation initiation factors 5 and 1A within the ribosomal pre-initiation complex plays a role in start site selection. *Journal of Molecular Biology* **356**: 724–737.

Maag D, Fekete CA, Gryczynski Z, Lorsch JR. 2005. A conformational change in the

eukaryotic translation preinitiation complex and release of eIF1 signal recognition of the start codon. *Molecular Cell* **17**: 265–275.

Maag D, Lorsch JR. 2003. Communication between eukaryotic translation initiation factors 1 and 1A on the yeast small ribosomal subunit. *Journal of Molecular Biology* **330**: 917–924.

Maguire BA, Wondrack LM, Contillo LG, Xu Z. 2007. A novel chromatography system to isolate active ribosomes from pathogenic bacteria. *RNA* **14**: 188–195.

Marck C, Grosjean H. 2002. tRNomics: analysis of tRNA genes from 50 genomes of Eukarya, Archaea, and Bacteria reveals anticodon-sparing strategies and domain-specific features. 1–45.

Martin-Marcos P, Cheung YN, Hinnebusch AG. 2011. Functional Elements in Initiation Factors 1, 1A, and 2 Discriminate against Poor AUG Context and Non-AUG Start Codons. *Mol Cell Biol* **31**: 4814–4831.

Nanda JS, Cheung Y-N, Takacs JE, Martin-Marcos P, Saini AK, Hinnebusch AG, Lorsch JR. 2009. eIF1 controls multiple steps in start codon recognition during eukaryotic translation initiation. *Journal of Molecular Biology* **394**: 268–285.

Nanda JS, Lorsch JR. 2014. *Labeling of a Protein with Fluorophores Using Maleimide Derivitization*. 1st ed. Elsevier Inc.

Nanda JS, Saini AK, Munoz AM, Hinnebusch AG, Lorsch JR. 2013. Coordinated Movements of Eukaryotic Translation Initiation Factors eIF1, eIF1A and eIF5 Trigger Phosphate Release from eIF2 in response to Start Codon Recognition by the Ribosomal Pre-initiation Complex. *Journal of Biological Chemistry*.

Olejniczak M, Dale T, Fahlman RP, Uhlenbeck OC. 2005. Idiosyncratic tuning of tRNAs to achieve uniform ribosome binding. *Nature Structural & Molecular Biology* **12**: 788–793.

Pan D, Kirillov S, Zhang C-M, Hou Y-M, Cooperman BS. 2006. Rapid ribosomal translocation depends on the conserved 18-55 base pair in P-site transfer RNA. *Nature Structural & Molecular Biology* **13**: 354–359.

Pan D, Zhang CM, Kirillov S, Hou YM, Cooperman BS. 2008. Perturbation of the tRNA Tertiary Core Differentially Affects Specific Steps of the Elongation Cycle. *Journal of Biological Chemistry* **283**: 18431–18440.

Passmore LA, Schmeing TM, Maag D, Applefield DJ, Acker MG, Algire MA, Lorsch JR, Ramakrishnan V. 2007. The eukaryotic translation initiation factors eIF1 and eIF1A induce an open conformation of the 40S ribosome. *Molecular Cell* **26**: 41–50.

Pawel-Rammingen von U, Aström S, Byström AS. 1992. Mutational analysis of conserved positions potentially important for initiator tRNA function in

Saccharomyces cerevisiae. *Mol Cell Biol* **12**: 1432–1442.

Pestova T, Borukhov SI, Hellen CUT. 1998. Eukaryotic ribosomes requireinitiation factors 1 and 1Ato locate initiation codons. 1–6.

Rabl J, Leibundgut M, Ataide SF, Haag A, Ban N. 2011. Crystal Structure of the Eukaryotic 40S Ribosomal Subunit in Complex with Initiation Factor 1. *Science* **331**: 730–736.

Reibarkh M, Yamamoto Y, Singh CR, del Rio F, Fahmy A, Lee B, Luna RE, Ii M, Wagner G, Asano K. 2008. Eukaryotic Initiation Factor (eIF) 1 Carries Two Distinct eIF5-binding Faces Important for Multifactor Assembly and AUG Selection. *Journal of Biological Chemistry* **283**: 1094–1103.

Saini AK, Nanda JS, Lorsch JR, Hinnebusch AG. 2010. Regulatory elements in eIF1A control the fidelity of start codon selection by modulating tRNA(i)(Met) binding to the ribosome. *Genes Dev* **24**: 97–110.

Seong BL, rajbhandary UL. 1987. Mutants of Escherichia coli formylmethionine tRNA: a single base change enables initiator tRNA to act as an elongator in vitro. *Proceedings of the National Academy of Sciences of the United States of America* **84**: 8859–8863.

Shih WM, Gryczynski Z, Lakowicz JR, Spudich JA. 2000. A FRET-Based Sensor Reveals LargeATP Hydrolysis–Induced Conformational Changes and Three Distinct States of the Molecular Motor Myosin. 1–12.

Shoji S, Abdi NM, Bundschuh R, Fredrick K. 2009. Contribution of ribosomal residues to P-site tRNA binding. *Nucleic Acids Research* **37**: 4033–4042.

Simonetti A, Marzi S, Myasnikov AG, Fabbretti A, Yusupov M, Gualerzi CO, Klaholz BP. 2008. Structure of the 30S translation initiation complex. *Nature* **455**: 416–420. http://eutils.ncbi.nlm.nih.gov/entrez/eutils/elink.fcgi?dbfrom=pubmed&id=18758445&retmode=ref&cmd=prlinks.

Singh CR. 2004. Efficient Incorporation of Eukaryotic Initiation Factor 1 into the Multifactor Complex Is Critical for Formation of Functional Ribosomal Preinitiation Complexes in Vivo. *Journal of Biological Chemistry* **279**: 31910–31920.

Singh CR, Curtis C, Yamamoto Y, Hall NS, Kruse DS, He H, Hannig EM, Asano K. 2005. Eukaryotic Translation Initiation Factor 5 Is Critical for Integrity of the Scanning Preinitiation Complex and Accurate Control of GCN4 Translation. *Mol Cell Biol* **25**: 5480–5491.

Taylor DJ, Devkota B, Huang AD, Topf M, Narayanan E, Sali A, Harvey SC, Frank J. 2009. Comprehensive Molecular Structure of the Eukaryotic Ribosome. *Structure/Folding and Design* **17**: 1591–1604.

Trauner A, Bennett MH, Williams HD. 2011. Isolation of Bacterial Ribosomes with

Monolith Chromatography. *PLoS ONE* 1–6.

Valasek L, Nielsen KH, Zhang F, Fekete CA, Hinnebusch AG. 2004. Interactions of Eukaryotic Translation Initiation Factor 3 (eIF3) Subunit NIP1/c with eIF1 and eIF5 Promote Preinitiation Complex Assembly and Regulate Start Codon Selection. *Mol Cell Biol* **24**: 9437–9455.

Walker SE, Fredrick K. 2008. Preparation and evaluation of acylated tRNAs. *METHODS* **44**: 81–86.

Walker SE, Zhou F, Mitchell SF, Larson VS, Valasek L, Hinnebusch AG, Lorsch JR. 2013. Yeast eIF4B binds to the head of the 40S ribosomal subunit and promotes mRNA recruitment through its N-terminal and internal repeat domains. *RNA* **19**: 191–207.

Wei Z, Xue Y, Xu H, Gong W. 2006. Crystal Structure of the C-terminal Domain of S.cerevisiae eIF5. *Journal of Molecular Biology* **359**: 1–9.

Weisser M, Voigts-Hoffmann F, Rabl J, Leibundgut M, Ban N. 2013. brieF communications. *Nature Structural & Molecular Biology* **20**: 1015–1017.

Wrede P, Woo NH, Rich A. 1979. Initiator tRNAs have a unique anticodon loop conformation. *Proceedings of the National Academy of Sciences of the United States of America* **76**: 3289–3293.

Yamamoto Y, Singh CR, Marintchev A, Hall NS, Hannig EM, Wagner G, Asano K. 2005. The eukaryotic initiation factor (eIF) 5 HEAT domainmediates multifactor assembly and scanning withdistinct interfaces to eIF1, eIF2, eIF3, and eIF4G. 1–6.

Yatime L, Mechulam Y, Blanquet S, Schmitt E. 2007. Structure of an archaeal heterotrimeric initiationfactor 2 reveals a nucleotide state betweenthe GTP and the GDP states. 1–6.

Yu Y, Marintchev A, Kolupaeva VG, Unbehaun A, Veryasova T, Lai SC, Hong P, Wagner G, Hellen CUT, Pestova TV. 2009. Position of eukaryotic translation initiation factor eIF1A on the 40S ribosomal subunit mapped by directed hydroxyl radical probing. *Nucleic Acids Research* **37**: 5167–5182.

Zhou F, Walker SE, Mitchell SF, Lorsch JR, Hinnebusch AG. 2014. Identification and Characterization of Functionally Critical, Conserved Motifs in the Internal Repeats and N-terminal Domain of Yeast Translation Initiation Factor 4B (yeIF4B). *Journal of Biological Chemistry* **289**: 1704–1722.

Curriculum Vitae

Antonio Muñoz Ph.D.

1101 N Calvert St Apt 604 Cell: (336) 918-1650
Baltimore, MD 21202 autobahntm@gmail.com

EDUCATION

National Institute of Health; Bethesda MD 2013-Present
Graduate Partnerships Program National Institute of Child Health and Human Development

Johns Hopkins University School of Medicine; Baltimore, MD Oct. 2014
Doctor of Philosophy (Ph.D.) candidate in Molecular Biophysics
Department of Biophysics and Biophysical Chemistry
GRE 1310: Quantitative: 790, Verbal: 520; Analytical Writing: 4.0/6.0

North Carolina State University; Raleigh, NC 2005-2009
Bachelor of Science in Biochemistry; Bachelor of Arts in Chemistry
Graduated with Honors in both majors
Minor in Genetics; GPA 3.61/4.00, *Magna Cum Laude*
SAT 1410/1600: Quantitative 750, Verbal 660

Internationales Kulturinstitut; Vienna, Austria June 2008
North Carolina State University Study Abroad; GPA: 4.0/4.0

RESEARCH

Graduate Student Researcher 2009-Present
Johns Hopkins University School of Medicine; Baltimore, MD
Department of Biophysics and Biophysical Chemistry - Advised by Dr. Jon Lorsch

- Dissertation**:** Examining the role of $tRNA_i$ in transmitting the start codon recognition signal
- Determined distinct mechanisms by different regions of the tRNA for control of start codon recognition signaling within the Ribosome
- Established an improved protocol for the production of active yeast ribosomes by anion exchange column purification
- Developed assays to test thermodynamic and kinetic characteristics of protein synthesis
- Managed ordering through SAP program for 6-10 person laboratory

Summer Research Intern May-Aug. 2007
North Carolina State University; Raleigh, NC
Department of Biochemistry – Advised by Dr. Paul Agris

- Received $4k stipend for full time summer research project resulting in a poster presentation
- Identified errors (now corrected) in a nationally used database of modified nucleotides

Undergraduate Researcher 2006-2009
North Carolina State University; Raleigh, NC
Department of Biochemistry – Advised by Dr. Paul Agris

- Computationally modeled modified RNA molecules to examine energetics of base pairing
- Assisted in general lab maintenance, including equipment repair and sample preparation

HONORS AND AWARDS

2013 Bridge to BCG participant, 1 of 20 from the mid-Atlantic region (1000 applicants)

2011 Turock Young Scientist Award, 2 awarded annually among 1000 students, $5000 award, Johns Hopkins University

2006 Phi Etta Sigma Honor Society Member, Outstanding first year student, North Carolina State University

2005 Aubrey Lee Brooks Scholarship Recipient, Top 7% of ~250 applicants; Half tuition scholarship valued at $50,000, North Carolina State University

2005 Deans Scholarship $2000, 1 award among 849 considered, NC State

2005 Awarded Chancellor's Leadership Scholarship $2500(declined), top 1% of 4500 admitted students, North Carolina State University

FUNDING

2010 NIH R01 Research Supplement to Promote Diversity in Health-Related Research, Johns Hopkins University

2009 NIH Molecular Biophysics Predoctoral Research Fellowship-Training Grant, Johns Hopkins University

PUBLICATIONS

Hussain T, Llácer JL, Fernández IS, **Munoz AM**, Martin-Marcos P, Savva CG, Lorsch JL, Hinnebusch AG and Ramakrishnan V. Structure of a eukaryotic translational preinitiation complex reveals a key intermediate in start codon recognition. *Cell* (in press)

Dong J, **Munoz AM**, Kolitz SE, Saini AK, Chiu W-L, Rahman H, Lorsch JR, Hinnebusch AG. 2014. Conserved residues in yeast initiator tRNA calibrate initiation accuracy by regulating preinitiation complex stability at the start codon. *Genes Dev* **28**: 502–520.

Nanda JS, Saini AK, **Munoz AM**, Hinnebusch AG, Lorsch JR. 2013. Coordinated

Movements of Eukaryotic Translation Initiation Factors eIF1, eIF1A and eIF5 Trigger Phosphate Release from eIF2 in response to Start Codon Recognition by the Ribosomal Pre-initiation Complex. *J. Biol. Chem.* 2013, 288:5316-5329.

Vendeix FAP, Munoz AM, Agris PF. Free energy calculation of modified base-pair formation in explicit solvent: A predictive model. *RNA* 2009, 15(12), 2278–2287

PRESENTATIONS

Muñoz, **A. M.,** Dong, J., Hinnebusch, A.G., and Lorsch, J.R. Examining the role of $tRNA_i$ in transmitting the start codon signal. Presented poster at EMBO Conference Series on Protein Synthesis and Translational Control, Heidelberg, Germany (Sept. 2013)

Muñoz, **A. M.,** Dong, J., Hinnebusch, A.G., and Lorsch, J.R. Examining the role of $tRNA_i$ in transmitting the start codon signal. Presented poster at 9th Annual NICHD Fellows Retreat, Washington, D.C. (May 2013)

Muñoz, **A. M.,** Dong, J., Hinnebusch, A.G., and Lorsch, J.R. Examining the role of $tRNA_i$ in transmitting the start codon signal, Presented poster at 21st Annual Institute for Biophysical Research Retreat, Baltimore, MD (Sept. 2012)

Muñoz, **A. M.,** Dong, J., Hinnebusch, A.G., and Lorsch, J.R. Examining the role of $tRNA_i$ in recognizing and perpetuating the start codon signal. Presented poster at EMBO Conference Series on Protein Synthesis and Translational Control, Heidelberg, Germany (Sept. 2011)

Vendeix, F.A.P., **Muñoz, A.M.**, Graham, W.D., Agris, P. Predictive Modified Anticodon-Codon Base Pair Formation in Explicit Solvent, Presented poster at the Symposium on RNA Biology VII: RNA, Tool and Target, Chapel Hill, NC (Oct. 2007)

LEADERSHIP EXPERIENCE

PMB Career Liaison; Johns Hopkins University 2013

- Organized career panel review feedback to help fellow students
- Initiated student feedback for career panels to improve usefulness in the future (90% response rate)

Vice President of Graduate Student Association; Johns Hopkins University 2011-2012

- Managed $10k fund to improve networking and community events (10-750 students)
- Increased student involvement by 50% from previous year
- Initiated and implemented $5k grant competition for students through an international biotech company in 6 months
- Supervised $30k budget on a 5 member council (representing 1000 graduate students at the School of Medicine) for research travel awards, invited speakers, and student groups
- Hosted monthly meetings and aided student career development through new career panels

- Served on multi-school committee to increase communication between various Johns Hopkins schools, budgeting $20k for quarterly student functions
- Organized novel safety classes targeted towards women, international students, and new Baltimore residents (100 attendees in 1st semester; reoccurring course)

Johns Hopkins Business and Consulting Club Member 2012-2013
- Competing in Johns Hopkins Case Competition (May 3rd, 2013)
- Practiced case interviews in front of the group and in small teams at monthly meetings

Biophysics Rep. to Grad. Student Association; Johns Hopkins University 2011-2012
- Improved parking accessibility by communicating student concerns monthly to committee
- Initiated biannual department soccer game for students, and faculty (~30 attendees)

Professional memberships: American Heart Association 2012

VOLUNTEER WORK
- Mentored high school student from Biophysics Research for Baltimore Teens (Jun.-Aug. 2012)
- Taught a lesson on microbes to ~30 local 5th graders attending the Johns Hopkins Community Science Education Program: Fun with Science Summer Camp (Jun. 2011)
- Community outreach and brand awareness for Inaugural Baltimore Grand Prix (2010-2011)